Dynamic modelling and nonlinear model predictive control of a reversible solid oxide fuel cell

for grid-tied power tracking

R.A. Schotman

Master of Science Thesis

TU Delft Delft University of Technology

Delft Center for Systems and Control

Dynamic modelling and nonlinear model predictive control of a reversible solid oxide fuel cell

for grid-tied power tracking

Master of Science Thesis

For the degree of Master of Science in Systems and Control at Delft University of Technology

R.A. Schotman

December 20, 2019

Faculty of Mechanical, Maritime and Materials Engineering (3mE) · Delft University of Technology

Delft University of Technology
Department of
Delft Center for Systems and Control (dcsc)

The undersigned hereby certify that they have read and recommend to the Faculty of Mechanical, Maritime and Materials Engineering (3mE) for acceptance a thesis entitled

Dynamic modelling and nonlinear model predictive control of a reversible solid oxide fuel cell

by

R.A. Schotman

in partial fulfillment of the requirements for the degree of

Master of Science Systems and Control

Dated: December 20, 2019

Supervisor(s):

Dr.ir. E. Steur

Dr.ir. Y.S. Hajimolana

Reader(s):

Dr.ing. S. Grammatico

Dr.ir. C. Smith

Abstract

The primary objective of this work is to research and develop a dynamic model and an advanced control strategy for a reversible solid oxide fuel cell in a grid to ensure load tracking whilst maintaining fuel utilisation and temperature dynamics within a safe range. This report presents the successful development of the dynamic model and corresponding controller. To do so, modeling and control are discussed in two separate chapters where model requirements, specifications and conception are presented followed by the control techniques, control objectives and controller synthesis.

First, background information is given on the topic this research is focused on. A brief history of fuel cells is provided, giving several types of fuel cells that are being studied and commercialised up to today. An in depth description is given on the technology with its build structure and materials, a foundation is provided on the main acting chemical reactions with their corresponding thermodynamical relations and the workings of solid oxide fuel cells (SOFC) and solid oxide electrolyser cells (SOEC) are discussed with the role of polarisation losses during fuel cell operation. An overall system description is given including auxiliary systems required for RSOFC operation.

In this work a RSOFC model has successfully been developed and thoroughly validated against other literature. To do so, a set of fitting parameters has been distilled from literature to create a good overlap with other studies and are combined in a manner that they can be implemented in other work. Steady state dynamics and the transient dynamics have shown a good match to the available literature. Additionally, the model offers useful insights into RSOFC (transient) dynamics with relation to temperature effects, fuel composition and cell support structure, which have not been documented before. At last the RSOFC stack, together with the developed model has been built in a plug-and-play manner that it can be implemented and adjusted by others, to be used in combination with other models.

From a performed literature review, it was concluded that MPC control seems very favourable for RSOFC control. MPCs have proven to show superior performance compared to other control methods when it comes to handling multiple constraints and nonlinearities. No specific control model was found to take transition speeds into account of RSOFC systems and constraints on temperature, temporal temperature gradients and hardware dynamics; proving this is of interest to study.

As result, in this study an output-feedback adaptive nonlinear model predictive controller has been developed, which is an advanced version of the well established (non)linear model predictive controller. The development of the temperature controller is given wherein the structure of the MPC is presented together with its trajectory, adaptive constraints and tuning variables. After completing the development of the controller, the controller was simulated together with the dynamic model as part of a micro-grid. The simulations were split up into short and long term scenarios and showed satisfactory results as all the set control objectives were achieved.

Table of Contents

List of Figures

List of Tables

Acknowledgements

I would like to thank my supervisors Erik Steur and Yashar Hajimolana for their kind assistance and support during the writing of this thesis. I can truly say the meetings very enjoyable yet informative and having the possibility to receive feedback from both during the writing of this report has proven to truly be of great value.

Thank you.

Delft, University of Technology
December 20, 2019

R.A. Schotman

"I have never tried that before, so I think I should definitely be able to do that."
— *Astrid Lindgren, Pippi Longstocking*

Chapter 1

Introduction

1-1 Motivation

With world population ever growing, the demand for energy has only increased over the last decades. With finite reserves of fossil fuels available and concerns growing over pollution and global warming, both private and public sectors are intensifying research done on finding effective and clean alternatives for energy generation. Until now several potent technologies have emerged for the production of clean power such as tidal wave generators, solar panels and wind turbines. The arrival of these new energy sources has come with a broad scala of challenges that are to be taken on to fully incorporate them into today's energy grid.

One of the main challenges with renewable energy sources is that they are highly intermittent and hard to predict. Solar irradiation on the surface of a solar panel is dependent on the weather quality and day time for instance and so are windmills dependent on harsher weather circumstances. Another factor that complicates power demand and supply dynamics is that power demand varies with time as people and industries tend to demand more energy at 5pm than 5am. To compensate for the surplus or deficit of energy on a electricity network, also known as a grid, it is required to install giant, or a great number of, systems that are able to store and supply energy to compensate for the imbalances between the renewable power supply and overall energy demand.

This research focuses on a promising technology that is capable of doing just that at a large scale: reversible solid oxide cells (RSOFC). RSOFCs are capable of producing hydrogen from water and electricity, and doing vice-versa by generating electricity from air and hydrogen. RSOFCs hereby combine two readily available technologies, solid oxide fuel cells (SOFC) and solid oxide electrolyser cells (SOEC). At this moment, SOFCs are promising to be among the most efficient methods of turning hydrogen into electrical energy and the possibility to combine this technology with SOECs to efficiently store hydrogen too, renders RSOFCs as potent clean and high efficiency energy storage units. RSOFCs have the capability of combining the functionalities of the two different systems into one, resulting in reduced cost of hardware using the same device for both functions. Combining both SOFC and SOEC

technology, allows the RSOFC to operate continuously between both states, hereby removing lengthily start-up times. In addition, compared to other readily available energy storage units such as batteries, RSOFC systems promise longer operational life-times and superior scalability.

1-2 Problem statement and research goal

Reversible solid oxide fuel cell systems have a high potential to be implemented as energy storage devices in the future as it has a high efficiency, low/zero emissions and almost no noise. As with all emerging technologies, RSOFCs suffer from a number of technical barriers that have to be considered and overcome, such as material durability, safety, commercial viability and efficient connection with conventional utility grids. Therefore, research is done on the development of a dynamic RSOFC model that can realistically simulate RSOFC performance. Furthermore this model is made to be combined with the development of a controller to study RSOFC characteristics and assist research on control possibilities for RSOFC-Grid connection.

As not much research has been done on dynamic RSOFC modeling and control until today, this report will cover the development of a dynamic RSOFC model that complies with the following requirements. The model must:

1. be parametric to enable scaling and easy adjustment for later use;
2. provide continuous simulation of RSOFC dynamics during and between SOEC and SOFC states;
3. justify temperature changes due to electro-chemical reactions;
4. provide an input and output interface to dynamically control RSOFC model behaviour;
5. be able to be coupled to an AC utility grid;

In addition to modelling, a literature review has been done on advanced control strategies for a reversible solid oxide fuel cell in a grid, to ensure load tracking whilst maintaining fuel utilisation and temperature dynamics within a safe range. To do so a control scheme will be proposed to be able to:

1. maintain required power output to its desired level;
2. keep the cell temperature between maximum and minimum operating limits;
3. keep temperature change of stack below 2 degrees Celsius per minute;
4. keep temperature difference between fuel inlet and air inlet within 20 degrees Celsius;
5. keep the fuel utilisation within optimal operating limits of 0.7 and 0.9 for all power outputs.

1-3 Outline of thesis

Following the introduction and motivation to research this topic, the remaining part of this thesis is structured as follows:

Chapter 2: Background information Background information on reversible solid oxide fuel cells, ranging from its history, comparable fuel cell types, RSOFC design and geometries, working principles, theory on thermodynamics, balance of plant description and power conditioning.

Chapter 3: Modelling Focus on definition and need of modelling, model assumptions and constraints, methodology, modeling of reversible solid oxide cell elements, such as polarisation losses, thermal dynamics and grid integration. Validation of developed model to other literature and parameter selection.

Chapter 4: Control Focus on the control of a reversible solid oxide cell when being submitted to varying load requests and demands, control objectives and constraints, types of control, review of written literature on control of (solid oxide) fuel cells, proposed controller, development of model predictive controller and adaptive constraint synthesis.

Chapter 5: Simulation results Focus on simulation results, with the controlled system being simulated in multiple different scenarios.

Chapter 6: Conclusion Final remarks on developed model and model predictive controller, recommendations for future work.

Chapter 2

Background information

Research done in the coming thesis will primarily be focused on RSOFCs. To get a better understanding of this system, firstly the systems from which an RSOFC is deduced will be explained to give the reader a better understanding of the underlying theory. The two systems from which an RSOFC is deducted are the SOFC and the SOEC. An SOFC is a device with electrochemical conversion capabilities to produce electricity directly from oxidising a fuel. SOFC fuel can consist out of hydrogen but also carbon based fuels such as methane, butane and other fossil fuels. An SOEC is a solid oxide fuel cell working in a reversed principle, this by having the capability to perform electrolysis of water with a solid oxide to produce oxygen and hydrogen gas. After giving a historical context on fuel cells, the next sections will offer a deeper elaboration of the solid oxide systems, starting with the fuel cell, followed by the electrolyser cell and both combined. Next an overall system description is provided including auxiliary systems required for RSOFC operation. Next to the balance of plant another crucial subsystem for grid connection is introduced, namely the power conditioning unit and its workings.

2-1 The fuel cell

2-1-1 History

The history of the fuel cell starts in 1839 when a "gas voltaic battery" was conceived by Sir William Robert Grove. By mixing hydrogen and oxygen in the presence of an electrolyte he was able to produce electricity and water effectively creating the first hydrogen fuel cell [12]. The device consisted out of two separate platinum coated electrodes in oxygen and hydrogen gas submerged in a dilute sulphuric acid solution acting as electrolyte. The device, which was was only later to be known as a fuel cell did not generate enough power to be of any significance for a long time until Ludwig Mond and Charles Langer improved the design in search of a working fuel cell [13].

From 1932, Francis Bacon began development of an alkaline fuel cell (AFC). What made his fuel cells unique was that they used potassium hydroxide instead of acid electrolytes such as

sulphuric acid. These cells performed as well as acid electrolytes and more importantly were not as corrosive to the electrodes [14]. Francis Bacon continued his research for many years and was able to demonstrate a practical 5 kW fuel cell system in 1959, with Harry Karl Ihrig improving his design fitting a 15 kW Bacon cell to a US Allis-Chalmers tractor the same year.

Next a research surge took place during the early 1960s when NASA, in collaboration with industrial partners, began researching and developing fuel cell generators to be used in manned space missions. William Grub first invented a low temperature proton-exchange membrane fuel cell (PEMFC) at General Electric in 1955 which was later used in the NASA Gemini space program [15].

Fuel cell research diminished until the late 1970s when energy shortages, environmental concerns and higher oil prices made research more interesting again for large companies and governments to develop efficient forms of energy storage and generation. One could say a result of this was the invention of the phosphoric acid fuel cell (PAFC) by the United Technologies Company (UTC). UTC also managed to produce the first commercially available fuel cell system by 1991 and built several experimental large stationary PAFC plants, but no commercial success was made. The company has installed and operated over 245 of 200 kW units in 19 countries worldwide and as of 2002, these units have successfully logged over five million hours of operation with 95 % fleet availability [16].

From the 1990s forward concerns increased over energy security, efficiency, and carbon dioxide (CO2) emissions forcing governments and companies to focus more on fuel cells as one of the potential technologies capable of delivering energy efficiency and CO2 savings whilst reducing dependence on fossil fuels. This can also indirectly be seen from Figure 2-1 from a review written by N. Mahato in which one can observe that the amount of research done on FCs has drastically increased over the last three decades.

To summarise: in the last 20 years, the fuel cell technology has undergone several stages of development from AFC, PAFC, MCFC to SOFC and PEMFC. Today, the market shares for the type of fuel cells are: PAFC-6%, PEMFC-65%, MCFC-3%, and SOFC-4% respectively [17]. Combined to their total share is about 78% of the whole fuel cell applications market. Among all fuel cell types, PAFC technology currently is the most advanced and matured, without any significant technical barriers [18].

Nowadays fuel cell development and commercialisation has lead to research being done on fuel cells over a broad range of end-use possibilities. These possibilities range from transport, such as cars and buses to portable military purposes, stationary household storage systems or even grid-bound fuel and infrastructure systems. As R.J. Braun mentions in his review; SOFCs, which are considered as a third generation fuel cells, are approaching commercialisation in a big pace, especially in stationary applications and distributed generation markets [19]. A report by Cihat Polat even mentions an annual average market growth rate of 24% [20]. So far the SOFC technology has demonstrated satisfactory efficiency and life performance and successful SOFC installations have been produced with the capability of producing more than 250kW and most development efforts for SOFCs are focused on reducing manufacturing costs and reducing operating temperatures [21].

One of SOFCs biggest competitors considering stationary household storage systems and distributed generation is the PEMFC. PEMFCs have successfully developed to a promising energy storage technology due to to technical breakthroughs which have increased cell power

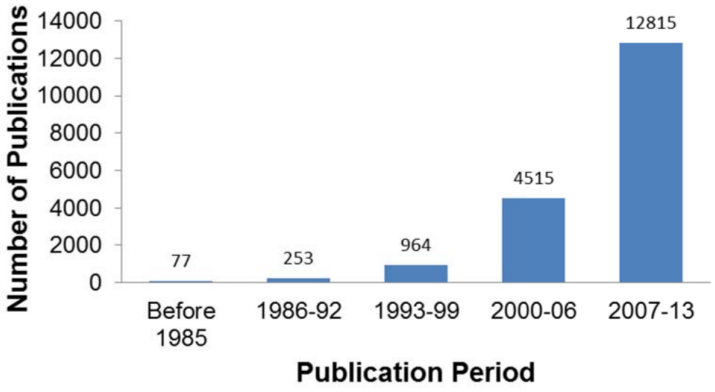

Figure 2-1: Publications on SOFCs over the last 30 years [1].

density in an order of magnitude and have resulted in substantial cost reductions of the cells. Furthermore many major car manufacturers such as Nissan, Volvo and Ford have shown great interest in PEM fuel cell powered vehicles. It is therefore expected that the potential dual market (transportation and stationary power) for PEMFCs will drive the rapid improvement of PEMFC technologies even further.

2-1-2 Fuel cell types

To summarise, 6 specific types of fuel cells have been developed until today, which can be primarily classified by the type of electrolyte being used. Electrolytes are substances that can produce an electrically conducting solutions if dissolved in polar solvent, such as water or a solid ceramic electrolyte, such as zirconium oxide. Electrically, such a solution is neutral and when being placed between a positively charged anode and a negatively charged cathode it allows positively charged hydrogen ions (protons) to move between the two sides. Different electrodes require different kinds of fuel, catalysts and working temperatures, hereby creating the following classes of fuel cells [22, 23]:

- **PEMFC** - Proton exchange membrane fuel cells are a water-based with an acidic polymer membrane as its electrolyte and platinum-based electrodes. What furthermore characterises PEMFCs are that they operate at relatively low temperatures below 100 degrees Celsius.
- **MCFC** - Molten carbonate fuel cells use molten carbonate salts infused in a porous ceramic matrix as the electrolyte. Salts used in these type of cells usually are lithium, potassium and sodium carbonates. Furthermore they operate at high temperatures around 650 degrees Celsius.
- **DMFC** - DMFC are very comparable to PEMFCs as it uses a polymer membrane as an electrolyte. Where this type of cells differs is that another type of anode is used with a platinum-ruthenium catalyst, enabling the cell to directly use liquid methanol as hydrogen source. DMFCs usually operate between 60 to 130 degrees Celsius and are used in applications with modest power requirements up to 1.5kW.

- **AFC** - Alkaline fuel cells use potassium hydroxide in water electrolytes and are generally fuelled with pure hydrogen. Being invented by NASA affiliates in the 1950s, much progress has been made in improving the working temperatures of this cell, now being able to work at temperatures below 80 degrees Celsius.
- **PAFC** - Phosphoric acid fuel cells have an anode and a cathode made of a platinum catalyst on a carbon and a silicon carbide structure that embodies the phosphoric acid electrolyte. PAFCs operate at around 180 degrees Celsius.
- **SOFC** - Solid oxide fuel cells use a solid ceramic electrolytes, such as zirconium oxide stabilised with yttrium oxide, instead of a liquid or membrane. What makes these cells special is that they operate at extremely high temperatures of 800 to 1000 degrees Celsius.

Taking further practicalities into account from [22, 23, 24], the different types of fuel cell systems offer varying possible power outputs and efficiencies when in operation. A summary of their specifications and capabilities is given below.

Type	Operating temperature [°C]	Typical stack size [kW]	Efficiency %
PEMFC	<120	1-100	55
MCFC	600-700	300 - 3000	50
DMFC	<130	0.5-1.5	50
AFC	<100	1-100	60
PAFC	150-200	5-400	40
SOFC	500-1000	1- 2000	60+

2-1-3 Fuel cell comparison

For this research, SOFCs will be used to generate electricity. It is important however to point out why it is of interest to use SOFCs for the research whilst plenty other fuel cell technologies are readily available to generate and store energy too. In the following paragraphs a deeper evaluation will be done of the current state of art of the solid oxide fuel cell and comparisons will be made with other fuel cell technologies.

As mentioned before, two of the most important characteristics that define solid oxide fuel cells is that they operate at high temperatures and with ceramic solid oxide electrolytes. Focusing on these points, several key perks and disadvantages can be found compared to other fuel cells but also challenges can be distinguished for future research and commercial development.

Because SOFCs operate at high temperatures, they do not require expensive platinum catalyst materials, as is currently necessary for lower temperature fuel cells such as PEMFCs. Furthermore other materials needed for building fuel stacks are readily available reducing the costs even more compared to other fuel cells. Currently SOFC technology is not the cheapest technology on the market as the ceramic construction needed to provide stability and reliability is costly. As production of SOFCs is expected to increase many commercial developers believe the future of cheaper fuel cell technology lies with SOFCs systems, due to lower construction costs thanks to production scale and optimisation [25].

Another advantage of fuel cells operating on high temperatures is improved thermal conversion efficiency of PAFCs, MCFCs, and SOFCs and compared to other fuel cells. High operating temperatures enable fuel cells to operate in combined heat and power (CHP) fuel cell systems. CHP systems can be used used to generate both electricity and heat for homes, office buildings or even factories. As SOFCs generate electricity they produce hot air and water which can also be recycled in heat exchangers, to preheat fuel, air and steam inlets. Co-generation SOFC systems have been found to be able to reach efficiencies of 85%, of which 40 to 60% is electric and the remainder as thermal [26]. CHP for SOFCs is still in it's early stage, but according to UTC Power, PAFCs comprise the largest segment of existing CHP products worldwide and can even provide combined efficiencies close to 90% [27].

Lastly, due to high operating temperatures, SOFCs have broader fuel possibilities. Just like many other fuel cell types, SOFC systems can run on fuels other than pure hydrogen gas. Unlike with PEMFCs or DMFCs, SOFCs and MCFCs have the ability to internally reform light hydrocarbons such as methane (natural gas) into hydrogen, thus requiring no fuel reforming systems to be added next to the fuel cell.

Because the electrolyte can be made of solid ceramic material, the fuel cells of an SOFCs can be shaped into several forms. This can bring several design advantages to battle flooding in electrolytes during operation, pressure leaks or greater amounts surface for oxidation. In the next subsection these forms will be briefly covered.

Currently, lifetime, reliability and durability of fuel cells are one of the largest limiting factors for full commercialisation [28]. In research done by Hawkes and Stafell et al. [29], it is estimated that under normal operation PEMFC and SOFC stacks are expected to lose power at a rate of 0-5 % per 1000 operating hours. According to Elmer [28], industry standards are currently set a a target of 40,000 hours for stationery applications, which translates to approximately 10 years. Due to their build materials, SOFCs are expected to operate slightly longer without any significant changes in output or stability as long as temperature gradient inside the cells are kept to a minimum [30].

One of the major disadvantages of an SOFC technology is the start-up time. Reaching the operating temperature has proven to take considerably more time than other fuel cells such as PEMFCs, as the build materials can only handle a small temperature gradient over time; hereby rendering SOFCs less suitable for mobile applications. Although much research is done to decrease start-up times of SOFCs it is expected to stay behind other fuel cell start-up times [31].

To give the reader a final comparison of current fuel cell technologies. a Table 2-1 has been formulated where-in an overview is given of the before-mentioned fuel cells rated along 6 categories, namely efficiency, combined heat and power, catalyst price, start-up time reversibility and durability. These categories have been chosen as they have proven to be the most dominant factors in determining whether fuel cells are of interest for stationary energy storage and distributed generation [22, 26, 18].

If we study the table and count the amount positive and negative tallies per category, one could conclude that PEMFCs and SOFCs appear to come out as victors. This can more or less be seen in today's fuel cell markets with PEMFC being implemented for transportation and smaller stationary power systems and SOFC for large stationary systems. With all the fuel cells covered, a more in depth description will be given of the solid oxide fuel cell used in this research.

Table 2-1: Fuel cell comparison table.

Type	Efficiency	CHP	Catalyst price	Start-up time	Reversibility	Durability
PEMFC	+	0	-	+	0	+
MCFC	-	+	0	-	-	-
DMFC	–	0	0	-	-	0
AFC	0	0	0	+	-	+
PAFC	–	+	-	0	-	+
SOFC	+	+	+	-	+	0

2-2 Solid oxide fuel cells

Operating characteristics of RSOFCs have a significant impact on the performance of the energy storing system that is going to be explored in this research. To inform later discussions and calculations on RSOFC modeling and control in the next chapter, an introduction into the of operation of solid oxide fuel cells in different operating modes will be given here. As the principles of operation of a reversible solid oxide cell are directly analogous to a conventional solid oxide fuel cell, firstly SOFCs will be discussed to later define its SOEC counterpart followed with a distinction between differences found in RSOFC's two different operation modes. The following subsections will therefore cover operation principles related to solid oxide cells with a focus in design and geometry, reaction chemistry, current-voltage relationships and internal losses.

2-2-1 Design and geometry

As mentioned above, SOFCs have a solid electrolyte which make it possible to build the fuel cells in different geometries. The two most common forms are planar and tubular. In tubular fuel cells, the elements of the FC are built in a tubular manner e.g. concentrically hereby forming a hollow cylinder and in planar FCs the elements are stacked in a layered form. The two different forms are given below in Figure 2-2 [2]. Planar SOFCs are most commonly used an will also be used in this research.

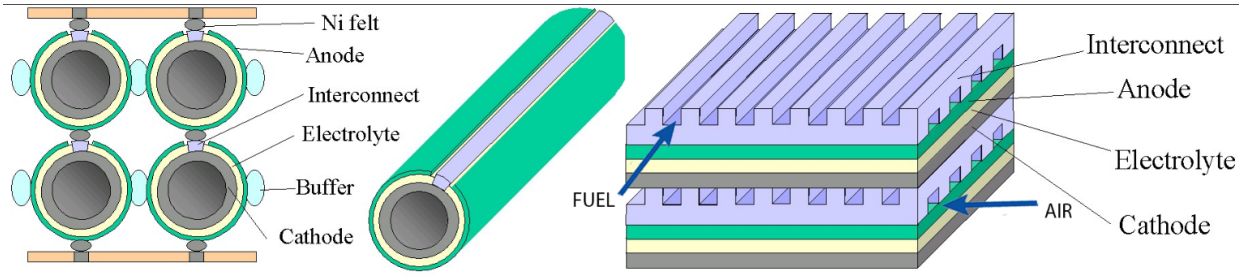

Figure 2-2: Left, a Tubular SOFC - Right, a Planar SOFC [2].

As can be seen from Figure 2-2, the planar SOFC consists of several layers. One layer is an electrolyte membrane that is sandwiched between the two electrodes to physically separate the oxygen an fuel that are being pumped into both sides. The current generated by the electrolyte via electron diffusion is collected by the top anodes (current collectors). The

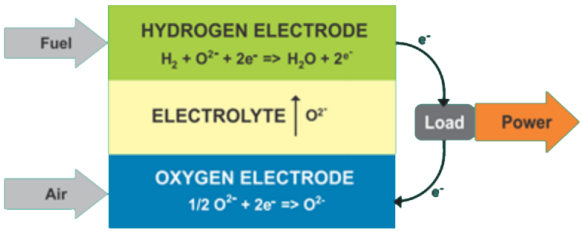

Figure 2-3: Representation of SOFC reactions [3].

current collectors, also known as interconnectors, make it possible to layer multiple cells on top of each other creating a series connection and are shaped in such a manner that they form channels. The channels function as inlet and outlet of the fuel and oxygen gases for the FC.

Looking at Figure 2-3, one can observe that during operation an SOFC, oxygen molecules are adsorbed, dissociated, and reduced on at the cathode interface to ionic oxygen. Next they are infused into the lattice as oxygen ions, which then move through the electrolyte to the anode and combine with fuel molecules to form water and if a hydrocarbon cell is used monoxide/dioxide. Outside the cell, electrons move from the anode to the cathode through an external circuit, completing the process of converting chemical energy into electrical energy [32].

As stated above: SOFCs consist out of four essential elements, namely the fuel electrode, oxygen electrode, electrolyte and current collector that all have their own specific build requirements. The requirements are briefly given next:

- Fuel electrode (anode): It is important that ceramic anode layer of an SOFC must provide thermodynamic stability from room temperature to working temperature, have a high electronic conductivity and must be very porous to allow the fuel to penetrate to the electrolyser layer. Further more the anode must consist out of a combination of a ceramic and metal and which can be achieved with the commonly used mixture of nickel and yttrium stabilised zirconia (NiYSZ), also known as NiYSZ Cermet.

- Oxygen electrode (cathode): The cathode is a thin porous layer where oxygen reduction takes place. Just like the anode the cathode must have a high electronic conductivity and must be very porous to allow the fuel to penetrate to the electrolyser layer. Depending on the type of fuel being used, this layer commonly is made out of lanthanum strontium mangenite, lanthanum strontium cobalt ferrite or lanthanum strontium chromium. manganite).

- Electrolyte: The electrolyte commonly is made of YSZ and has a high ionic conductivity but low electronic conductivity. Furthermore it functions as a layer to prevent oxygen and fuel mixing and is desirable to because it relatively cheap to build. Important to note is that YSZ only has sufficient ionic conductivity above 600 degrees Celsius, hereby setting the lowest possible operating temperature of an SOFC.

- Current collector / Interconnector: This element is required to have high electronic conductivity and low permeability of gaseous materials and can be either made of a metallic or ceramic compound.

2-2-2 Working principles

The chemical reactions taking place at the anode and cathode of an SOFC are called half-cell reactions. To give the reader an overview of what chemical (sub)reactions take place with its product as result, the reactions are given in equation (2-1).

$$\begin{aligned} \text{Anode:} \quad & 2\,H_2 + 2\,O^{2-} \rightleftharpoons 2\,H_2O + 4\,e^- \\ \text{Cathode:} \quad & O_2 + 4\,e^- \rightleftharpoons 2\,{O_2}^{2-} \\ \text{Overall:} \quad & 2\,H_2 + O_2 \rightleftharpoons 2\,H_2O \end{aligned} \tag{2-1}$$

It is important to realise that these reactions can work in either ways. In an SOFC the hydrogen and oxygen form water as product, but in an SOEC the water will be split up into hydrogen and oxygen. For the research done, it is essential to have an understanding of electrochemical and thermodynamical quantities present in the working of an SOFC. In other words: one must know what kind of chemicals are needed in what quantities or ratios to produce a certain amount of product and energy. Further more, for the thermodynamic part, one must have an understanding of the heat, temperature and pressure and their relation to the amount of energy and work that is needed or created during a reaction. An example of this is that from the reaction in equation (2-1) we can conclude that two moles of H_2 and one mole of O^2 is required to create a mole of H_2O. With this information we can look further into thermodynamics to calculate the amount of energy that will be released or required for this to occur.

In thermodynamics the total amount of energy in a system is defined by the amount of enthalpy. The enthalpy of a thermodynamic system is defined as [33]:

$$H = U + pV \tag{2-2}$$

where: H : the enthalpy of the system [kJ/mol]
U : the internal energy of the system [kJ]
p : the pressure of the system [N/m^2]
V : the volume of the system [m^3]

A negative change of enthalpy in a system means that energy is released during a reaction, in other words: the reaction is an exothermic reaction. A reaction with a positive change in enthalpy is called an endothermic reaction and indicates and the reaction can only take place when energy is provided, hereby "consuming" energy [34].

What is of interest next is the Gibbs free energy; also known as free enthalpy. The Gibbs free energy is the maximum amount of non-expansion work that can be extracted from a thermodynamically closed system i.e. one that can exchange heat and work with its surroundings, but not matter [35]. This quantity, which is given by equation (2-3), is essential to be able to calculate the amount of energy released by an SOFC.

$$\Delta G = \Delta H - T\Delta s \tag{2-3}$$

where: ΔG : the Gibbs free energy of the system [kJ/mol]
ΔH : the enthalpy energy of the system [kJ/mol]
T : the temperature of the system [K]
Δs : the change in entropy of the system [J/mol K]

Entropy is known as a thermodynamic property of systems used to determine the amount of energy available for useful work in a thermodynamic process. A low entropy means that a system is relatively in order and a high entropy corresponds to a more disordered system, resulting in lower quantity of energy that can be used for work. The change in entropy is defined as:

$$\Delta s = \frac{\Delta Q}{T} \tag{2-4}$$

where: ΔQ : the the change in heat of the system [K]

For the overall equation given in equation (2-1), 572 kJ of heat is generated when two moles of hydrogen gas react with one mole of oxygen gas to form two moles of liquid water. This makes the enthalpy of the reaction: $\Delta H^o_{298K} = -285.8\ [kJ/mol]$. Please take note that reactions are given using universal standard conditions. e.g. a pressure of 1 bar and a temperature of 298K. For entropy we take following relation from equation (2-1) and fill in the standard entropies for H_2, O_2 and H_2O where: $2\,\mathrm{H_2} + \mathrm{O_2} \rightleftarrows 2\,\mathrm{H_2O}\,||\,\mathrm{H_2} + \frac{1}{2}\mathrm{O_2} \rightleftarrows \mathrm{H_2O}$ and thus the total entropy:

$$\begin{aligned}\Delta s &= S^0_{H_2,gas} + \frac{1}{2}S^0_{O_2,gas} - S^0_{H_2O,liquid}\\ &= -130.68 + -\frac{1}{2}205.15 + 69.95\\ &= -163.305\ \text{[kJ/mol K]}\end{aligned}$$

The Gibbs free energy can now be calculated using equation (2-3), giving us:

$$\begin{aligned}\Delta G &= \Delta H^o_{298K} - T\Delta s\\ &= -285.8 - (298 \times -163.305)10^{-3}\\ &= -237.14\ \text{[kJ/mol]}\end{aligned}$$

During the research done, the amount of Gibbs free energy will be expected to be lower because the water will not be in liquid form but gaseous due to the high heat. Calculations adjusted to this scenario will then be done accordingly.

Knowing the amount of Gibbs free energy is important as it enables one to calculate the electric potential of a cell. The cell voltage, also known as the reversible potential, can be calculated using Faraday's law:

$$E_0 = -\frac{\Delta G}{nF} \tag{2-5}$$

where: E_0 : Reversible potential [V]
ΔG : the Gibbs free energy of the system [kJ/mol]
n : Number of electrons transferred per mole of hydrogen, see equation (2-1)
F : Faraday's Constant

Next, the reversible voltage equation is altered as it does not meet the requirements for the system used in the coming research. As mentioned earlier, the actual temperature will be much higher in the SOFCs than used now in the calculations. In addition the controller of the SOFC has the possibility to change inputs to the system. One of these inputs is the flow rate or the amount of pressure put on the inlet fuel. To compensate for this Walter Nernst derived the following equation:

$$E_{rev} = E_0 + \frac{RT}{nF}\ln(Q) \tag{2-6}$$

where: E_0 : Reversible potential [V]
R : Gas constant 8.314
Q : Thermodynamic reaction quotient

The thermodynamic reaction quotient can be also be used to effectively incorporate knowledge of the amount of fuel or air consumed in the reactions during operation, in other words: the fuel utilisation. For FCs the fuel utilisation corresponds to concentrations of hydrogen and oxygen. Since the concentrations of these gasses are equivalent to the pressures in the system as they are at the same temperature in the system, the Nernst equation can also be written in another way. The concentrations and/or partial pressures of fuel and air and their effect on the Nernst equation are given below in equation (2-7).

$$E_{Nernst} = E_0 + \frac{RT}{nF}\ln(\frac{p_{H_2}\sqrt{p_{O_2}}}{p_{H_2O}}) \tag{2-7}$$

$$E_{Nersnt} = E_0 + \frac{RT}{nF}\ln(\frac{y_{H_2}\sqrt{y_{O_2}}}{y_{H_2O}}\sqrt{\frac{p_{cell}}{p_0}}) \tag{2-8}$$

where: p_{H_2} : Hydrogen pressure [bar]
p_{O_2} : Air pressure [bar]
p_{H_2O} : Steam pressure [bar]
y_{O_2} : Air utilization
y_{H_2} : Fuel utilization
y_{H_2O} : 1 - Fuel utilization
p_{cell} : Cell pressure [bar]
p_0 : Normal pressure [bar]

2-3 Solid oxide electrolysis cells

With the basic workings of a conventional fuel cell covered, the fundamental theory of Solid Oxide Electrolyser Cells have been given too. SOECs are inverted SOFCs, meaning that with a certain amount of applied power SOECs have the capability of splitting up water into

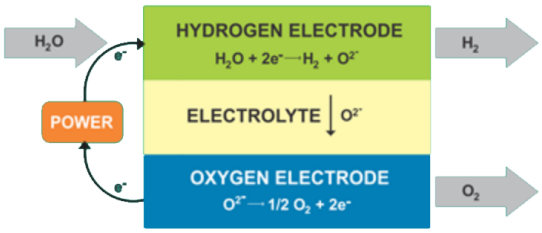

Figure 2-4: Representation of SOEC reactions [3].

hydrogen and oxygen. SOECs have the same structure as SOFCs which is given below in Figure 2-4.

Furthermore, the half reaction will given as:

$$\begin{aligned} \text{Anode:} \quad & 2\,O^{2-} \rightleftharpoons O_2 + 4\,e^- \\ \text{Cathode:} \quad & 2\,H_2O + 4\,e^- \rightleftharpoons 2\,H_2 + 2\,O^{2-} \\ \text{Overall:} \quad & 2\,H_2 \rightleftharpoons O_2 + 2\,H_2 \end{aligned} \tag{2-9}$$

As expected the entropy and enthalpy of the reactions will be the opposite of the exothermic reaction of SOFCs where 572 kJ of heat was generated when 2 moles of hydrogen gas react with one mole of oxygen gas to form two moles of liquid water. This will make the enthalpy of the SOEC reaction: $\Delta H^o_{298K} = 285.8\ [kJ/mol]$ thus rendering it an endothermic event.

The Gibbs free energy can is now calculated as given below, using equation (2-3), giving us:

$$\begin{aligned} \Delta G &= \Delta H^o_{298K} - T\Delta s \\ &= 285.8 - (298 \times 163.305)10^{-3} \\ &= 237.14\ [\text{kJ/mol}] \end{aligned}$$

Resulting too in a positive reversible voltage of around 1.23V. This voltage is needed to get an SOEC to start forming pure hydrogen and oxygen from water. What the differences are in terms of efficiency and working currents will be given later on in Chapter 3 where a deeper elaboration will be given of the system model.

2-4 Reversible solid oxide fuel cells

With the SOFC and SOEC covered, next a deeper explanation will be given of both systems in the form of an RSOFC, a reversible solid oxide cell. RSOFCs have the capability of changing from fuel cell mode to electrolyser mode and vice-versa. The ability to do this makes them very interesting to use as batteries or other storage systems as they have the ability to harness the heat generated in SOFC mode and perform both SOEC and SOFC functions without needing two solid oxide cells. RSOFCs have the same structure as SOFCs and SOECs with electrodes, electrolysers and membranes made from the same materials.

In practice, by reversing the voltage put on the cells one can switch the RSOFC between both SOEC and SOFC modes. This voltage, known as the reversible voltage described was described in the previous sections. In short it is the minimum voltage needed to achieve electrolysis in SOEC mode or current generation in SOFC mode; we calculated this voltage to be the same in both fuel cell modes. In practice this is not true as there are resistances and losses in the cells that require the reversible voltage to be higher or lower depending on which mode it is in. For SOEC mode the voltage needs to be higher and for SOFC it will be lower due to so called polarisation resistances also known as polarisation overpotentials.

2-4-1 Polarisation overpotentials

There are three types of polarisation overpotentials: activation overpotentials, Ohmic overpotentials and concentration overpotentials. Below a short description is given of the polarisation overpotentials from H. Hirschen [36]. Please note, that as literature written on the calculations of polarisation overpotentials tend to differ a lot from each other; a more detailed description of found methods will be given in the following chapter, combined with motivations to why certain calculation methods have been chosen for this research.

- Activation Polarisation: Activation polarisation can be measured when the rate of electrochemical reactions at an electrode surface is controlled by so called "sluggish" electrode kinetics. The electrochemical reactions require overcoming an energy barrier which is called activation energy and results in activation polarisation, which is due to the transfer of charges between the electronic and ionic conductors of a cell. The result of this is that activation polarisation is directly related to the rate of electrochemical reactions occurring in a fuel cell and thus also related to cell temperatures and pressures.
- Ohmic Polarisation: Ohmic losses occur because of resistance to the flow of ions in the electrolyte and resistance to flow of electrons through the electrodes, current collectors and contacts. Dominant Ohmic losses through the electrolyte can be reduced by decreasing the amount of separation between cell electrodes and by improving the ionic conductivity of the electrolyte. Because both the electrolyte and fuel cell electrodes obey Ohm's law, the Ohmic losses are usually expressed expressed by the equation from Hauck et al [37]. Later on in this literature survey an adapted version of this equation will be introduced:

$$V_{ohm} = j(r_{ohmic,el} + r_{ohmic,const}) = j(\frac{\sigma_{el}}{\delta_{el}} + r_{ohmic,const}) \tag{2-10}$$

where:
- j : Current density $[A/cm^2]$
- $r_{ohmic,el}$: Ohmic resistance of the electrolyte layer $[\Omega cm^2]$
- $r_{ohmic,const}$: Resistance of interconnectors and wires $[\Omega cm^2]$
- σ_{el} : Ionic conductivity of the electrolyte $[\Omega^{-1}m^{-1}]$
- δ_{el} : Electrolyte layer thickness [m]

- Concentration Polarisation: As a fuel cell operates, hydrogen is consumed at the anode of the fuel cell. A result of this is that there is a loss of potential in the cell due to the inability of the surrounding material keep a constant concentration of bulk fluid. Next the concentration of hydrogen fuel at the reactive surface of the anode decreases resulting in a concentration gradient being formed. The gradient causes a diffusion of hydrogen from the bulk concentration back to the reactive surface of the anode. This phenomenon is also called diffusion polarisation.

When operating in fuel cell mode the RSOFC outputs power to a load e.g. a network, thus the current is positive, in electrolysis mode the RSOFC generates hydrogen and absorbs power which results in a negative current. According to equations (2-11) and (2-12) the terminal cell voltage is the reversible voltage plus all of the voltage drops in electrolysis mode due to activation, concentration and Ohmic overpotentials. Therefore it is of interest to note that as the current density increases the cell voltage will increase together with the corresponding power input and hydrogen production. This power input can be much more than the power output in fuel cell mode.

$$V_{SOFC} = V_{Nernst} - (V_{activation} + V_{Ohmic} + V_{Concentration}) \tag{2-11}$$
$$V_{SOEC} = V_{Nernst} + (V_{activation} + V_{Ohmic} + V_{Concentration}) \tag{2-12}$$

where: V_{SOxC} : Cell voltage, x=E,F
E_{Nernst} : Nernst voltage [V]
$V_{activation}$: Activation overpotential
V_{Ohmic} : Ohmic overpotential
$V_{Concentration}$: Concentration overpotential

As mentioned earlier, temperature has a large impact on the (maximum) amount of power an RSOFC can deliver or absorb. In a study by Jiangcong Ren [4] on RSOFCs it was proven that output power could be greatly enhanced at higher temperatures, with it having a negative impact in electrolysis mode by reducing the recharging power. Figure 2-5 shows the simulated terminal voltage of a single RSOFC in operation with varying currents (current densities) and temperatures.

2-5 System description

With the workings of an RSOFC covered in the previous section, this section will provide a description the of auxiliary systems of the RSOFC system needed to generate and deliver the energy, other than the fuel cell unit itself. In power engineering these supporting components are usually referred as the "Balance of Plant", BoP. The BoP supports the RSOFC in numerous ways such as supplying the required air and providing fuel at desired temperatures and storage. The BoP thus consists out of compressors, blowers and heaters, but also valves to control the flow of reactions. Figure 2-6 provides a simplistic overview of the RSOFC placed in a system connected to a utility grid for energy storage.

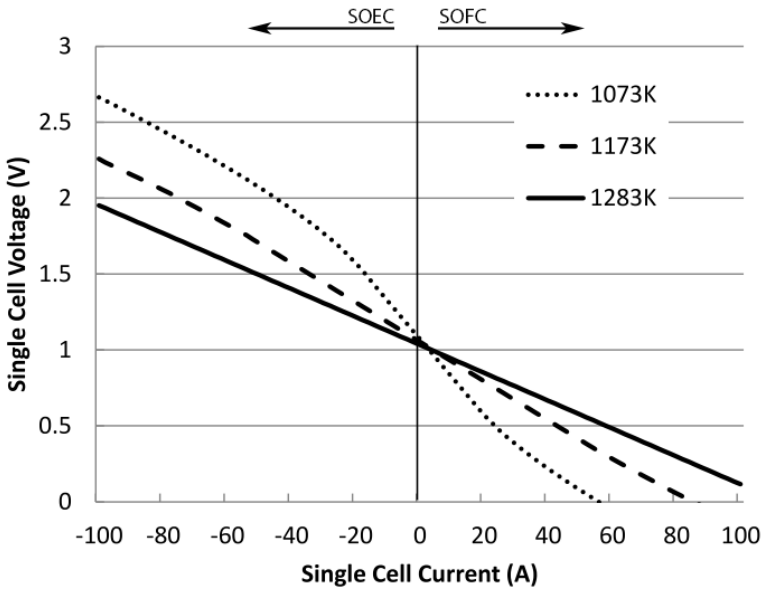

Figure 2-5: RSOFC voltage at 1073K, 1173K and 1283K for a single cell [4].

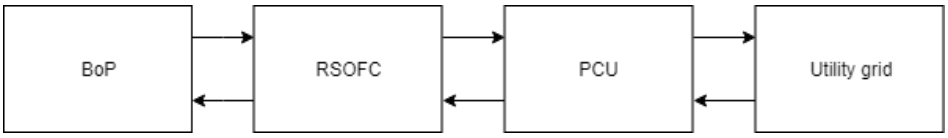

Figure 2-6: Simplistic overview of an RSOFC system.

After discussing the BoP, the power conditioning unit, PCU, will be discussed. PCUs are needed to convert the generated energy by the RSOFC to a format that is compatible with the electrical network it is located in. PCUs generally convert the low voltage DC current supplied and consumed by the fuel cell to and from a higher voltage AC current with help of AC/DC inverters.

2-5-1 Balance of Plant

In this research the RSOFC is a custom built RSOFC at the TU-Delft with key characteristics of being a planar SOC fitted with an anode off-gas circulation system and fuelled purely on hydrogen and air. The supporting BoP system consists of several key components, which are labelled and shown in the model schematic in Figure 2-7. Firstly a brief introduction will be given of the system process followed by more detailed descriptions of the system operation modes.

During normal operation of the RSOFC, hydrogen gas stored in an exhaust tank is expanded from 350 bar storage pressure to 1.1 bar system pressure. Next to hydrogen, water is also retrieved from a separate water tank. The required water which is stored at atmospheric pressure and 363.15 K is pumped off and supplied to an evaporator and superheater unit. *[A-B]* This is to rapidly increase the temperature of the water to super heat steam. During the start-up, the merged stream is sent to an electrical heater to be preheated, but during

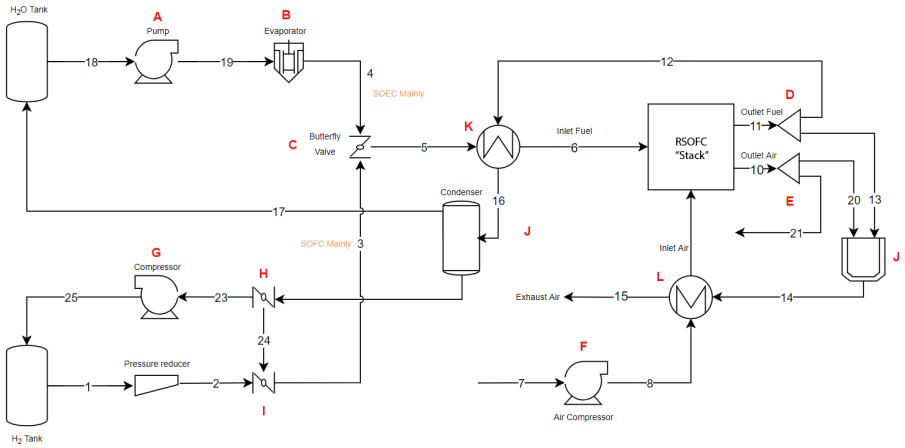

Figure 2-7: RSOFC with BoP used in this research [5].

normal normal operation stream is super heated with the help of heat recovery units supplied by the RSOFC exhaust gas heat. After the water has been heated, the super heated steam is mixed with the hydrogen from the exhaust tank to a set ratio *[C]* and sent to a heat exchanger unit, before entering the fuel cell. *[L]*

Together with the hydrogen-steam mix, the RSOFC is fuelled with air. The air is supplied from ambient temperatures to the system to provide the required oxygen for the SOFC mode. *[F]* At SOEC mode it functions as a gas to flush out the produced oxygen from the electrolysis reactions. A second porpoise of the inlet air is to act as a medium that carries heat to or from the stack to meet the boundary conditions of around 1000 degrees Celsius. The air is preheated in a second heat recovery unit *[M]* that receives it's heat from an afterburner/furnace, placed behind the stack. *[J]*

When the stack is in operation, both hydrogen and air streams exit the stack while a portion of each stream is sent to an afterburner *[D-E]*. In the after burner the hydrogen and air are combusted and the heat created from the exothermic reaction is employed to preheat the air stream in the heat exchanger. After the air has passed through the heat exchanger, the exhaust air is released outside the system. The second part of the outlet fuel portion, not used for the afterburner, is sent to the fuel heat exchanger *[L]* to preheat the inlet fuel stream and the evaporator unit. This portion of the fuel product that bypassed the afterburner, is separated from the steam, to then be compressed and brought to hydrogen storage tank condition *[G]* or to be recirculated back to the stack inlet *[H-I]*. Separated steam is condensed and cooled down to 363.15 K and is sent into the water tank. The outlet air stream from the Stack is sent to the afterburner.

Operation modes

During both SOFC and SOEC operation, nearly all the lines and components are usually in use to provide the stack with its required fuel and air at right temperatures. In Figures 2-8 and 2-9 the model is displayed twice with in addition colours to emphasise the lines and components being used. What stands out is that SOEC and SOFC mode both have one mutually exclusive component, the pressure reducer and the hydrogen compressor. Although

Label	Component	Label	Component
A	Water pump	H	Fuel recirculation valve
B	Evaporator	I	Fuel valve
C	Butterfly valve	J	Pressure reducer
D	Outlet fuel valve	K	Afterburner
E	Outlet air valve	L	Condenser
F	Air compressor	M	Heat exchanger fuel
G	Hydrogen compressor	N	Heat exchanger air

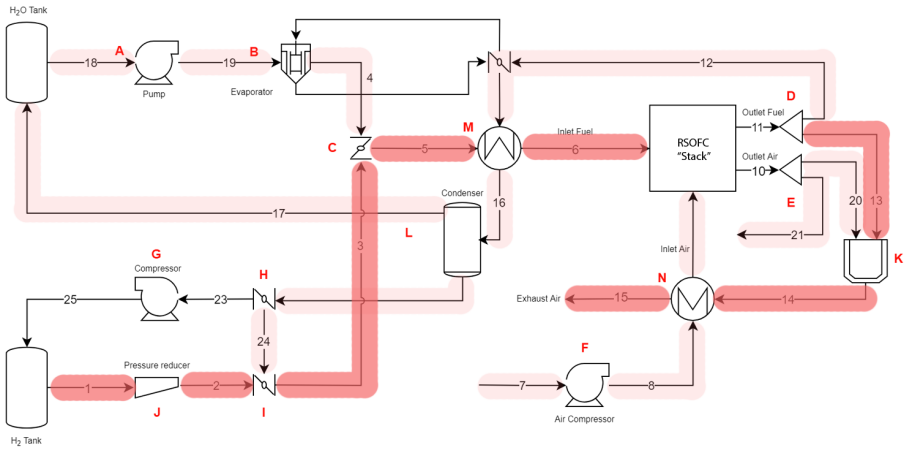

Figure 2-8: System in SOFC mode [5].

all other lines and components are used during both processes, one must know that they are obviously used with different intensities, thus the colours in the figure.

Next to the two SOEC and SOFC modes, the system has four other modes that are important to acknowledge when considering the system operations. These modes are the Start-up, Shutdown and more importantly the transition modes from SOEC to SOFC and vice versa.

- Start-up mode: Unique to the start up mode is that in start-up mode there is no heat recovery possible from the afterburner and outlet fuel from the stack. With no heat recovery, the required air, steam and hydrogen in SOFC and SOEC has to be preheated by electrical heaters. Both heat exchangers and evaporation unit therefore feature electrical heating elements to be switched for use only during start up mode.

- Shut-down mode: As for shutdown mode, there is no use for the outlet fuel heat, therefore the majority is sent to the afterburner.

- SOC Transition modes: The last two states are entered when the stack transitions between SOEC of SOFC mode. What characterises the transition is that in most cases the transitions starts with the decrease of the current ramp and a slow change of stack temperature. After the stack temperature has changed to acceptable operating levels for the new mode, the butterfly valve at *[C]* changes the ratio of hydrogen and steam for the new SOC mode. Usually for SOFC mode to SOEC this will be a decreased amount of hydrogen compared to steam such as 90% H_2 and 10 % H_2O to 10% H_2 and 90 %

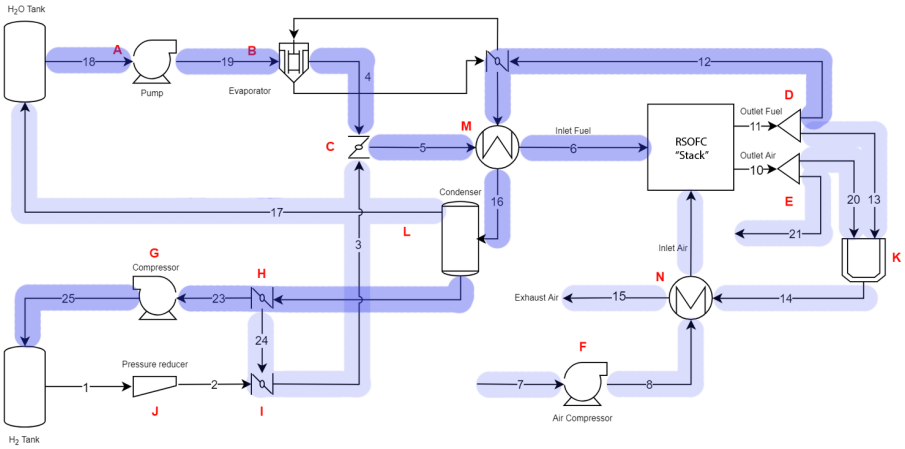

Figure 2-9: System in SOEC mode [5].

H_2O. For control, which will be discussed in Chapter 4, these two states are of great interest and are only found in RSOFCs compared to SOECs or SOFCs. Therefore it is also expected to include the possibility of including these two processes in a model built later on in this research.

2-5-2 Power conditioning

For this research it is required that the RSOFC can be coupled to a utility grid to function as a generator and storage device. To be able to do this power conditioning is required with an AC/DC inverter to be inserted between the two, as the fuel cells generate direct current (DC) and the grid functions on alternating current (AC). An inverter is a device that uses a DC power supply to create an AC supply. As the fuel cell is not only to be used as battery, the inverter is also required to have the ability to generate DC power from an AC source, the grid, during SOEC mode, hereby making it a bidirectional inverter.

Power electronic converters are usually separated into two families: the voltage source converters and current source converters [38]. For fuel cell applications such as PEMFCs and SOFCs, VSCs have proven to be the mostly used sort as the voltage source converter (VSC) is capable of keeping the input voltage constant and whilst the output voltage is independent of load [39].

The main tasks of an inverter are given below, taken from Konrads Mertens book "Photovoltaics: Fundamentals, Technology and Practice" [40] stating that an inverter should be able to, but not limited to:

1. Convert direct current into a possibly sinusoidal-form alternating current.
2. Convert alternating current forms into direct current.
3. Achieve a high degree of efficiency of more than 95 % in partial as well as in peak loads.
4. Feed the current synchronously with the grid frequency

5. Apply maximum power point tracking (More applicable for solar generated power)
6. Monitor the grid for voltage

Next to enabling bidirectional transfer of current, as the power conditioning unit (PCU) is connected to a utility grid, it is also required to supply power in three phases. Next a brief introduction will be given on how an inverter can be constructed that can achieve this requirement.

H-Bridge inverters

A commonly used subarchitecture for inverters is the H-bridge Inverter, illustrated in Figure 2-10. The H-bridge Inverter is widely used in the power electronic industry and known for its simplicity. Furthermore it already has an extensive track record with renewable energy applications and fuel cells.

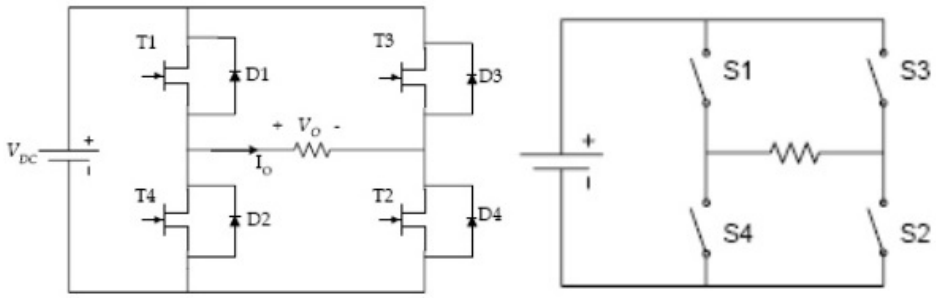

Figure 2-10: Left, single phase H-Bridge model- Right, Equivalent circuit [6].

A H-bridge Inverters consist out of self-commutated electrical components such as the insulated gate bipolar transistors (IGBT) for switching on and off. The electronic circuit enables a voltage to be applied across a load in either direction and duration by toggling the transistors. By carefully switching the transistors on and off, each H-bridge is capable of producing an output voltage of V_{dc}, 0 and $-V_{dc}$. Table 2-2 illustrates the switching with relation to the output voltage of a H-bridge.

Table 2-2: An example of a single phase H-bridge IGBT switching scheme.

	T1	T3	T4	T2	Load Voltage
State 1	Open	Closed	Closed	Open	V_{dc}
State 2	Closed	Open	Open	Closed	$-V_{dc}$
State 3	Open	Open	Closed	Closed	0
State 4	Closed	Closed	Open	Open	0

The resulting waveform of a single phase H-bridge is a square wave form. To synthesise a multilevel waveform resembling more the shape of a sine, the AC output of multiple H-bridge cells can be connected connected in series. This form of connecting H-Bridged is called cascading. The cascaded voltage waveform is the sum of the inverter outputs. The number of output voltage levels that can be generated in a cascaded inverter is defined by [41]:

$$n = 2s + 1 \tag{2-13}$$

where s is the number of DC sources. With these type of multi-level inverters all the outputs from H-Bridges should be quarter symmetric to generate a sin like wave, hereby presenting an output with no even harmonics. The cascaded H-bridge converter has already been proposed as a suitable inverter for photo-voltaic, distributed generation, grid integration such as by Lee et al. [42]. Also Ren et al. [4] mentions that this type of inverter has proven to be suitable for fuel cell grid integration applications thanks to the fact that the cascaded architecture makes it possible generate a multi-level output voltage with high voltage qualities and a corresponding current with a relatively low total harmonic distortion (THD).

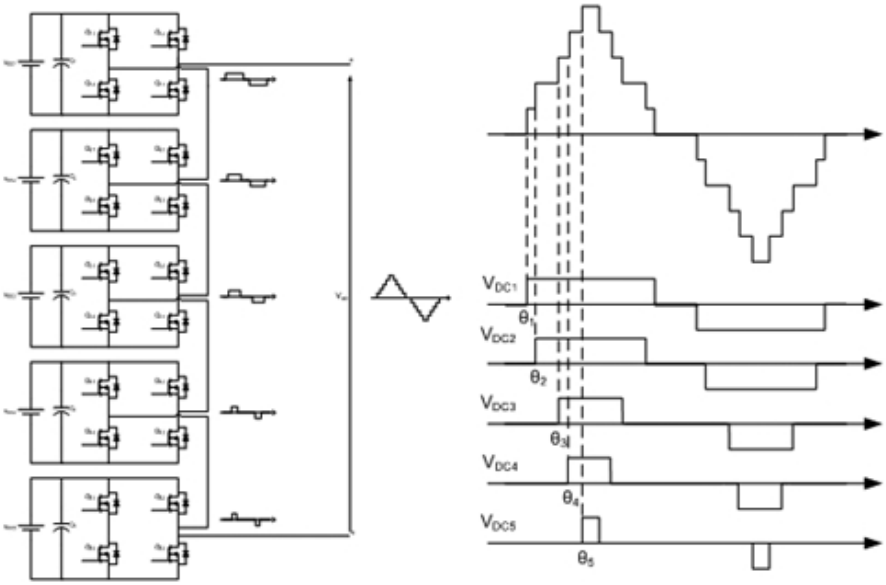

Figure 2-11: Cascaded H-Bridge model [6].

Going back to the initial requirement of the inverter to be able to supply a three phase AC current: we can now construct a suitable three-phase multilevel inverter by simply combining three (cascaded) single phase inverters connected in wye configuration. By doing this, each (cascaded) H-Bridge is connected together hereby supplying one phase to the grid.

Pulse Width Modulation

A voltage source converter normally uses the IGBTs at switching frequency of around 2kHz. This high frequency control of the IGBTs is commonly called Pulse Width Modulation (PWM) and makes fast dynamic response and the independent control of active and reactive power possible [4]. Using a high switching frequency has several advantages. First of all it provides a sufficient spectrum to separate unwanted harmonics from the power frequency, hereby only requiring small sized AC filters to mitigate high order harmonics. The amplitude and harmonic contents of a produced AC waveform can thus be controlled by controlling the rate and

duty cycle of the transistors. There are several types of PWM techniques that can be used, with each having its own advantages and disadvantages, with the most commonly used PWM techniques for three phase power inverters are given below split into two classes; discrete and continuous [7]:

- Continuous PWM
  - Carrier Based PWM Scheme
  - Third Harmonic Injection Carrier-based PWM
  - Carrier-based PWM with Offset Addition
  - Space Vector PWM
  - Artificial Neural Network Based PWM
- Discontinuous PWM
  - Carrier based Sinusoidal PWM

To not go into detail too far, for this research it is chosen to focus on Carrier Based PWM and Space Vector PWM schemes as they have proven the most suitable for our bi-directional 3-phase usage [4]. For these schemes the primary goal is to calculate duty cycles the IGBTs to switch resulting in an output with he desired voltage and current. Secondly, the PWM schemes are used to find the most effective way scheduling the switching processes to minimise undesired THD and switching losses [43].

The main difference between carrier-based PWM (CB-PWM) techniques and space Vector PWM (SV-PWM) is that CB-PWM techniques usually control each phase leg of the converter individually, whilst SV-PWM treats the three inverter phases as a single unit. The SV-PWM is a modulating technique with the objective to output PWM generated voltages equal to a reference voltage vector on average [43]. The SV-PWM vector can be described as follows [7]:

$$V_{-s} = \frac{2}{3}[V_a + e^{j2\frac{\pi}{3}}V_b + e^{j4\frac{\pi}{3}}V_c] \tag{2-14}$$

Where V_a, V_b and V_c are three-phase quantities that can be put as voltages, but also currents or fluxes. The total number of outputs can be displayed as a vector as depicted in Figure 2-12. Here it is shown that the total number of outputs is 8, because $2^3 = 8$ with corresponding states (000, 001, 010, 011, 100, 101, 110, 111)

To illustrate: in Figure 2-12, state 1 (100) denotes the three phase voltage as $V_a = V_s$, with V_b and V_c being equal to zero. From [4], simulation of a inverter based on 400V DC voltage, 0.85 modulation index and 1500Hz modulation frequency using SV-PWM, will yield the following line to line voltage and three-phase currents.

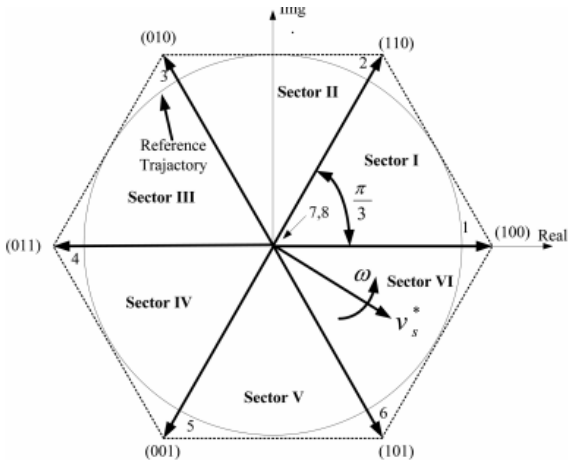

Figure 2-12: Voltage space vector locations corresponding to different switching states [7].

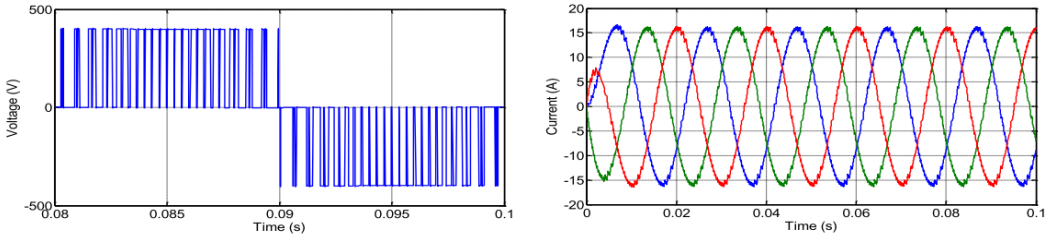

Figure 2-13: Line-to-line voltage and three phase current of SV-PWM modulated inverter [4].

2-6 Summary

In this chapter, background information was given on the topic this research is focused on. A brief history of fuel cells was given, giving several types of fuel cells that are being studied and commercialised up to today, later giving a comparison of the fuel cells with each other and key characteristics that define them and render some suitable for specific applications. After introducing the solid oxide fuel cell, an in depth description was given on the technology with its build structure possibilities and materials. Next, a foundation was provided on the main working principles of solid oxide fuel cells, giving an overview of the acting chemical reactions with their corresponding thermodynamical relations.

With SOFCs introduced, the workings of SOECs and RSOFCs were discussed carefully bringing forward the analogies and differences between the three technologies, also explicating the roll of polarisation losses during the fuel cell operation. With the workings of the systems covered, the way had been paved to introduce the overall reversible solid oxide cell system, including a description of the auxiliary systems required for the RSOFC to operate.

The supporting (sub)systems that enable RSOFCs to supply and absorb energy were separated into two main groups, namely the balance of plant and power conditioning groups. With the BoP, the supporting components were brought forward with relation to the ongoing processes during the fuel cell and electrolysis modes and with the PCU an introduction was given on the workings of inverters and how they can be controlled with pulse width modulation techniques.

Chapter 3

Modeling

With the background information covered, this chapter will focus on the development of a model of the before introduced reversible solid oxide cell and its corresponding dynamics. Before beginning the process of defining ways how to describe and quantify certain physical phenomena prevailing during RSOFC operation; it is important to first understand why it is of interest to model an RSOFC, what is desired to achieve with it, how it is planned to be developed and intended to be used in favour of this research.

3-1 Model description

3-1-1 Definition

A model is a set of rules, formulas, or equations that can be used to predict an outcome based on a set of inputs and other variables. In this research it will be a schematic description of a system that will account for its known or inferred properties and is to be used to further study of its characteristics. By doing so a scientific understanding is to be developed in a form that it can translate into a quantitative expression of current knowledge of the system whilst enabling to test the effect of changes in said system.

According to Dubois [44], in the physical sciences, a traditional (mathematical) model usually contains the following elements:

- Governing equations: The governing equations of a model describe how the values of the unknown variables change when one or more of the known variables change. In other words, the governing equations can be described as the primary formulae that relate input variables to output variables.
- Supplementary sub-models: Next to the governing equations a model might consist out of other models that form subsections of the considered system. Sub-models commonly are models that readily have been researched, are of basic form and are considered as

being of less interest than the main governing equations. In turn, the supplementary sub-models are defined by:

  - Defining equations: Defining equations are equations that define new quantities in terms of base quantities.
  - Constitutive equations: Constitutive equations can be a relation between two physical quantities that is specific to the considered material or substance, and describes the response of it to external stimulae. An example of this can be the electrical conductivity an electrolyte or a spring constant.

- Assumptions and constraints: Lastly, a model usually is based and conceptualised to a certain level to be able to take certain boundary conditions and constraints into account.

  - Initial and boundary condition: For mathematical models, boundaries can be described as regions where a certain (differential) problem are to be solved.
  - Classical constraints and kinematic equations: At last the system is to be held-up upon classical and kinematic constraints. Examples of these can be holonomic constraints which can be time or temperature dependent.

Before the requirements for the model are set, it is important to inspect the previous elements and determine what kind of effects they have on the model to be built. To begin with the governing equations; an example equation of this can be a relation that is required to relate fuel consumption with generated electricity.

From equations such as the Nernst equation (2-6) or from research done by Jiangcong [4], we can expect our model to have one or more objective functions or constraints that are represented with a nonlinear equation, thus rendering the model a nonlinear model. This can also be seen from nonlinear input-output relations depicted in Figure 2-5. As the RSOFC is expected to change between electrolysis and fuel cell modes over time, we will want to model the transition between both states, thus making the model dynamic instead of static.

As the input current is a physical input and model inputs that governs the entire model behaviour, this variable is to be measured, computed and modeled continuously to ensure model credibility. This combination results in the model being continuous and explicit with a deductive and deterministic calculation of the variables and states. Deductive in this case meaning that the governing equations and sub-equations are logically structured and calculated based on a theory.

To summarise: The nonlinear dynamic model will explicitly be described based on continuous modeling of deterministically calculated values based on deductive reasoning.

3-1-2 First principles modeling

Until now, a so-called “first principles” model has been proposed for this thesis. First principles models are often used in engineering to reflect physical laws such as energy balances, mass balances or heat transfer relations. These kind of models are based on physical laws or system implementation knowledge, rather than on recovered or generated data as with empirical models.

First principles models typically have a disadvantage that they are to be built from scratch which is time consuming, but on the other hand do not need to be completely rebuilt if changes in the modeled system configuration or operating modes are made. One of the requirements of the model is that the model must be able to be scaled and parameters such as build structure, fuel composition or temperatures must be easily adjusted for later use. If one were to use an empirical model this would be very time consuming. Another disadvantage of using an empirical model is that, while they are capable of representing some of the same knowledge as first principles models, the model will generally not be explicit, and hence will not easily be inspected for accuracy or completeness.

If a first principles model proves to be too complex, due to inexplicable errors or computational demands, it generally is always possible to distil a more compact version of the model through consolidation of certain model elements. These type of models are called compiled or semi-empirical models and are simplified versions of first-principles models. Although being a respectable back-up plan for first principles models, a problem with compiled models is that simplifying a model generally implies a certain amount of irreversible loss of information contained in the model.

3-1-3 Requirements

With the elements and classifications of the model described, the requirements of the model can be discussed. Requirements of a model can cover a broad spectrum of topics and can be formulated with questions such as "Why do we need a model for this problem?" and "What do we want from it?", further more requirements can be set on the format or even what kind of units are to be used.

A very general answer to the first question might be that studying processes in reality suffer from several disadvantages such as being, expensive due to labour and material costs, time consuming, hard to measure, hard to manipulate or even not ethical such as with experiments with infectious disease spread in human populations. A more specific answer to the question why a model is needed for this problem requires careful consideration to the purpose of this entire study. For this study we want to be able to design an advanced control strategy for a reversible solid oxide fuel cell connected to a utility grid to ensure load tracking within its operational limits. We thus need a platform to accurately model RSOFC dynamics under varying required outputs over time.

In general, model complexity involves a trade-off between simplicity and accuracy of the model. In this case complexity of the model and also the computational intensity can be greatly increased by increasing the modeling resolution with relation to time. In other words: by modeling the system in smaller time steps, the amount of needed computational power rapidly increases. For this research a resolution of half a second seems reasonable as time constants of related processes and systems are expected to be longer. Hereby neglecting the very small time constants from concentration polarisations [45].

To enable easy editing and distribution of the model at the Technical University of Delft the RSOFC system is to be developed in the Simulink/Matlab environment. Use of the Simulink environment has more advantages as it has extensive libraries to enable modeling of AC power network dynamics with the *SimPower* package and other electrical components.

To conclude the before mentioned considerations, a list of requirements for the model is given below:

- The model must:
    1. Be parametric to enable scaling and easy adjustment for later use.
    2. Provide continuous simulation of RSOFC dynamics during and between SOEC and SOFC states.
    3. Justify temperature changes due to electro-chemical reactions.
    4. Provide an input and output interface to dynamically control RSOFC model behaviour.
    5. Be able to be coupled to an AC utility grid.

3-1-4 Methodology

When designing a model with the goal to simulate or measure a certain phenomenon, a preferred method of designing is done in four steps: Conceptualisation, Realisation, Simulation and Evaluation. During the conceptualisation phase of the model design process the scope and boundaries of the model are described and the questions desired to answer with the model are defined. Sometimes this phase also leaves room to introduce expected behaviour and pinpoint which factors are thought to play a key role in the process. During the realisation phase the concepts and their relations from the conceptualisation phase are translated in an unambiguous way to a set of governing equations that can be constrained with certain numerical and logical boundaries. During the evaluation phase, the model is computed with the given inputs and scope to generate a certain behaviour which is measured. In the final evaluation phase it is verified whether the simulations are in line with expectations from step one, leaving the possibility to re-iterate the process and adjust the model.

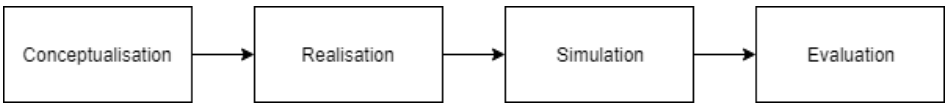

Figure 3-1: Chronological steps in creating a model.

During the work in this thesis project a literature study has been written. Therefore the model is not to entirely generated from scratch, as it is derived from comparison of written literature. That said, the literature survey functioned as a preliminary research to aid with the first two phases of the design process, namely conceptualisation and realisation. The last two steps, simulation and evaluation, will be covered later on in this report and further conclusions in Chapter 6.

During the future analysis of the system assumptions have to me made for the model and are to be considered as being true. However, the results of such an analysis are only as valid as the assumptions themselves. For this model several assumptions are made to support the model in sake of simplicity, scope and realism. These assumptions are given below and were derived from comparable studies such as [8, 11, 46, 47].

Model assumptions:

1. All gases are ideal gases.
2. The Nernst equation is applicable and applied at inlet conditions.
3. The channels that transport gases along the electrodes have a fixed volume, but their lengths are small, so that it is only necessary to define one single pressure value in their interior.
4. Isothermal system, temperatures and pressures are assumed to be homogeneous.
5. The system is assumed to be reasonable well insulated in a rectangular box.
6. Each cell is considered to operate identically.
7. Co-flow configuration, which assumes a uniform distribution of gas flow.
8. Fuel and air inlet can be heated to system temperature
9. Gas-diffusion coefficient is not to be considered constant.
10. Influence of the oxygen side diffusion losses can be neglected.
11. Fuel input, temperature and stack voltage can accurately be measured.
12. Current changes are assumed to occur instantaneously during the simulations.

With conceptualisation finalised and with the assumptions set for the overall system; the next section will focus mainly on the realisation of the model. Together with results of the literature study, giving an in depth review of literature written on the dynamic modeling of RSOFC power calculation elements such as Nernst equations, polarisation losses and thermal dynamics.

3-2 Model dynamics

This section starts with discussion of the source of energy conversion, followed by a short analysis of various losses of the energy which have been brought forward in the background information chapter. From these the dynamics that influence energy generation and losses will be given together with the review of written literature from which derived models were proposed.

3-2-1 Partial pressures

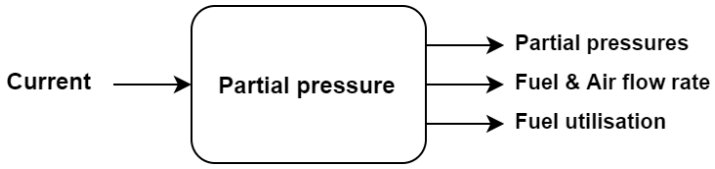

Figure 3-2: The partial pressure block.

For more than 20 years, extensive research has been done on SOFC modeling and behaviour. With a model formulated by Padulles et al. [8] in 1999 being widely accepted as a benchmark model. The model is shown in Figure 3-3 and shows parameters such as the hydrogen and oxygen input flows, $q_{H_2}^{in}$ and $q_{O_2}^{in}$, and stack current I being used to contribute to the calculation of the Nernst voltage covered in the previous chapter.

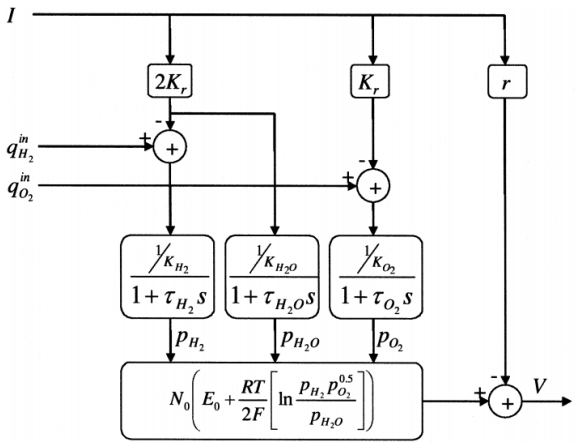

Figure 3-3: SOFC stack dynamic model [8].

As can be seen from 3-3, the partial pressures of oxygen, steam and hydrogen, respectively $p_{O_2}, p_{H_2O}, p_{H_2}$, are needed to calculate the Nernst voltage. To start the calculation of the partial pressures, the ideal gas law, also called the general gas equation, is used as it performs well in approximating behaviour of many gases. The equation is given as follows:

$$p_{H_2} V_{an} = n_{H_2} RT \tag{3-1}$$

where: p_{H_2} : partial pressure
V_{an} : volume of the anode $[m^3]$
n_{H_2} : number of hydrogen moles in the anode channel
R : universal gas constant $[(latm)\dot{(}kmolK)]$
T : absolute temperature [K]

By working out the equation for p_{H_2} and taking the time derivative of the expression such that the hydrogen molar flow, q_{H_2}, is obtained from incoming or outgoing n_{H_2}, the following relation for the partial pressure of hydrogen can be derived [8]:

$$\frac{d}{dt}p_{H_2} = \begin{cases} \frac{RT}{V_{an}}(q_{H_2}^{in} - q_{H_2}^{out} - q_{H_2}^{r}) & SOFC\ mode \\ \frac{RT}{V_{an}}(q_{H_2}^{in} - q_{H_2}^{out} + q_{H_2}^{r}) & SOEC\ mode \end{cases} \tag{3-2}$$

where: $q_{H_2}^{in}$: input hydrogen flow [kmol/s]
$q_{H_2}^{out}$: output hydrogen flow [kmol/s]
$q_{H_2}^{r}$: reacting hydrogen flow [kmol/s]

Next by making use of the known electrochemical relationships from 2 we can rewrite the reacting hydrogen flow $q_{H_2}^{r}$ as $\frac{N_0 I}{2F} = 2K_r I$. Here, N_0 is the number of cells in the RSOFC stack, I the current and F Faraday's constant so that following relation can be created:

$$\frac{d}{dt}p_{H_2} = \begin{cases} \frac{RT}{V_{an}}(q_{H_2}^{in} - q_{H_2}^{out} - 2K_r I) & SOFC\ mode \\ \frac{RT}{V_{an}}(q_{H_2}^{in} - q_{H_2}^{out} + 2K_r I) & SOEC\ mode \end{cases} \tag{3-3}$$

where: K_r : constant defined for modeling purpouses
$\frac{q_{H_2}^{out}}{p_{H_2}}$: K_{H_2}
τ_{H_2} : $\frac{V_{an}}{K_{H_2}RT}$, Response time for hydrogen flow, such that:

$$p_{H_2} = \begin{cases} \frac{\frac{1}{K_{H_2}}}{1+\tau_{H_2}s}(q_{H_2}^{in} - 2K_r I) & SOFC\ mode \\ \frac{\frac{1}{K_{H_2}}}{1+\tau_{H_2}s}(2K_r I) & SOEC\ mode \end{cases} \tag{3-4}$$

The theory and dynamics above is also applicable for the other partial pressures of oxygen and steam. The definition of these partial pressures are given in the following equations:

$$p_{O_2} = \begin{cases} \frac{\frac{1}{K_{O_2}}}{1+\tau_{O_2}s}(q_{O_2}^{in} - K_r I) & SOFC\ mode \\ \frac{\frac{1}{K_{O_2}}}{1+\tau_{O_2}s}(K_r I) & SOEC\ mode \end{cases} \tag{3-5}$$

$$p_{H_2O} = \begin{cases} \frac{\frac{1}{K_{H_2O}}}{1+\tau_{H_2O}s}(2K_r I) & SOFC\ mode \\ \frac{\frac{1}{K_{H_2O}}}{1+\tau_{H_2O}s}(q_{H_2O}^{in} - 2K_r I) & SOEC\ mode \end{cases} \tag{3-6}$$

Next, the derived equations for the partial pressures have to be inserted into the model. Until now, the required information to calculate the partial pressure of hydrogen have been: $K_{H_2}, \tau_{H_2}, q_{H_2}^{in}, K_r$ and I resulting in a relationship where the current I is the only part that has to monitored to calculate the partial pressure continuously.

Fuel utilisation

From literature it was found that it is important to measure the fuel utilisation of the fuel cell. If fuel utilisation drops below a certain level. an unwanted, rapid, rise will occur in the cell voltage. On the other hand, should the fuel utilisation increase far over that that level, the cells may be permanently damaged due to fuel starvation.[8]. The fuel utilisation factor of the fuel cell is defined as u, where u is the ratio of reacting hydrogen and injected fuel flow into the stack such that:

$$u = \frac{q_{H_2}^{in} - q_{H_2}^{out}}{q_{H_2}^{in}} = \frac{q_{H_2}^{r}}{q_{H_2}^{in}} = \frac{2K_r I}{q_{H_2}^{in}} \tag{3-7}$$

Where K_r, the constant defined before for modeling purposes whose value is $\frac{N_0}{4F}$. Hence, with the use of I and $q_{H_2}^{in}$ it is possible to continuously set the fuel utilisation. Levels for u have been defined by Abbas and Murshed to be preferably be between 0.8 and 0.9, rendering the optimal fuel utilisation 0.85. To respect fuel utilisation boundaries of 0.8 to 0.9 for a certain input hydrogen flow, the current of the to be modeled fuel cell system can be restricted as follows [48]:

$$\frac{0.8 q_{H_2}^{in}}{2K_r} \leq I \leq \frac{0.9 q_{H_2}^{in}}{2K_r} \tag{3-8}$$

Using the same formulae, the desired, optimal, hydrogen fuel input is set as:

$$q_{H_2}^{in} = \frac{2K_r I}{0.85} \tag{3-9}$$

Combining all the discussed relationships and inserting them into a readily available simulink template based on [48], successfully a simulink block was created with the input and outputs displayed in figure 3-2.

3-2-2 Nernst voltage

With all the partial pressures calculated, the Nernst voltage can be computed. The derivation for this expression has been done in the background information chapter, but for convenience is given below:

$$V_{Nernst} = E_0 + \frac{RT}{nF} \ln\left(\frac{p_{H_2}\sqrt{p_{O_2}}}{p_{H_2O}}\right) \tag{3-10}$$

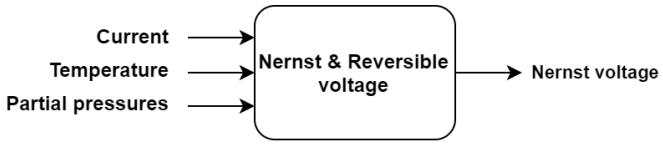

Figure 3-4: The Nernst voltage block.

As stated in the literature review, until now most research done on RSOFCs or even SOFCs has been done on (static) steady-state systems, taking no regard for how the system is to be modeled during the transition from zero voltage condition or the transition between SOFC and SOEC states. The primary complication with the given Nernst voltage equation arises during the transition, where the stack current and partial pressures will become zero. Although in reality both p_{H_2} and p_{H_2O} cannot turn to zero simultaneously as they are fraction of one, the partial pressures do turn to zero equation (3-4) and (3-6) permit them to at zero current. In Section 3-4, the consequences of this are discussed. As p_{H_2} approaches zero, the logarithmic function will expand rapidly to minus infinity, rendering the model useless at that time. Further more a negative partial pressure of oxygen will cause a non existent definition from the square root operation.

To circumvent the numerical complications in the Nernst equation, bi-directional saturations were applied to the model followed by a current controlled logical switch to create a signal that could not pass through zero and with the correct polarity. A saturation zone between 0.05 and -0.05 proved to be sufficient. An example is given below where $\ln \sqrt{p_{O_2}}$ is covered.

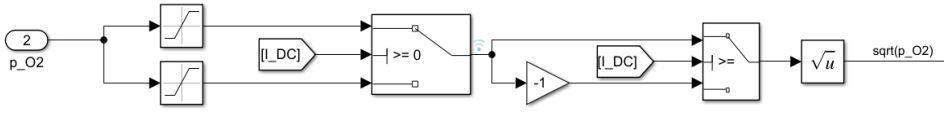

Figure 3-5: Example of bi-directional saturation in Simulink.

From equation (2-5) it is known that the reversible voltage E_0 is highly dependent of the Gibbs free energy of the system and should not be considered as a constant such as in numerous studies such as Padulles et al. [8]. In order to calculate E_0, values for ΔG at different temperatures are to be obtained from literature which results in a cumbersome definition of the voltage. A semi-empirical equation from [49] that encompasses the temperature dynamics of the voltage is therefore used, given below:

$$E_0 = -0.0002809002T + 1.2770578798 \tag{3-11}$$

Using the calculations from the background information chapter and above a Nernst voltage simulink block was successfully created with the following input-output characteristics. The contents of the block are given in the APPENDIX. V_{Nernst} denotes the total voltage of the stack, with V_{cell} being the single cell voltage.

3-2-3 Polarisation dynamics

After the Nernst voltage has been calculated. Voltage losses have to be subtracted from the Nernst voltage to come to the resulting operating voltage of the cells or stack. Although the paper by Padulles introduces useful modeling elements for fuel cells it it primarily comes short with regards to calculating the generated voltage offered to the inverter. The paper only subtracts Ohmic losses and neglects activation and concentration polarisation losses which can be considerably large during fuel cell operation [37, 50]. Further more it uses a set constant for the Ohmic resistance instead of calculating a more realistic resistance that takes the stack temperature into account.

Several papers have been written with different approaches to modeling the cell or stack voltages of fuel cells. In an article written by Li Sun et al. [51], Ohmic, concentration and activation losses are taken into account for instance, but for activation and concentration losses empirical values are used. On the other hand, in [52, 53] activation and concentration losses are modeled and calculated using semi-empirical calculations, whilst keeping the Ohmic resistance static at a predefined value.

Activation polarisation

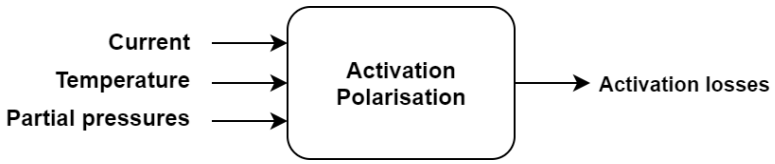

Figure 3-6: The activation polarisation block.

From recent literature it can be found that is customary to express the voltage drop due to activation polarisation by a semi-empirical equation, called the Tafel equation. This equation is explained in full detail by Hirschen [36] and in Chapter 2 furthermore it is widely used in studies on fuel cell modeling [52, 53, 54, 55]. The Butler-Volmer equation is given below:

$$i_{density} = i_0 \left\{ exp(\beta \frac{nF\eta_{act}}{RT} - exp[-(1-\beta)\frac{nF\eta_{act}}{RT} \right\} \tag{3-12}$$

where: β : transfer coefficient of reaction at electrode, usually 0.5
i_0 : exchange current density $[A/m^2]$
η_{act} : activation polarisation [V]
n : number of electrons participating in the reaction

By using the Butler-Volmer equation a semi-empirical expression for activation losses can can be obtained in the form of:

$$\eta_{act} = a + b \log i \tag{3-13}$$

where: η_{act} : activation polarisation [V]
$a = \frac{-2.3RT}{\beta nF} \log i_0$: Tafel constant [-]
$b = \frac{2.3RT}{\beta nF}$: Tafel slope [-]

Although (3-13) has proven to be successful providing activation losses during modeling in [52, 53, 54], it does not explicitly define a difference found in losses during low or high polarisation circumstances depending on the cell current. To adapt the model to this, Ren et al. and Chan [11, 56] managed to define two different activation losses for low polarisation and high polarisation conditions. In their model, the activation loss is switched between two expressions depending on the amount of polarisation defined by:

$$\kappa = \frac{F\eta_{act}}{nRT} \tag{3-14}$$

If the term $\frac{F\eta_{act}}{nRT}$ is less than 1, the primary equation is used in (3-15). If the term is higher than 1, the second equation is used. For this study the equation from their work has been adjusted to account for discontinuity when the expression is equal to 1, therefore the (in)equality is set at "less or equal" instead of "less" in equation (3-13). Furthermore the value of κ is to be calculated each simulation iteration of the model with it's previous value to avoid infinite recursion and continuity of the condition:

$$\eta_{act} = \begin{cases} \frac{RTi_{density}}{nFi_0} & \text{if } \kappa \leq 1 \\ \frac{RT}{\beta nF} \ln \frac{i_{density}}{i_0} & \text{if } \kappa > 1 \end{cases} \tag{3-15}$$

Activation polarisation has been calculated for both sides of the RSOFC as the pressures and gases at those places differ from each other. To do so, two different exchange current densities $i_{o,an}$ and $i_{o,cat}$ are needed which are calculated in the following manner [4]:

$$i_{o,an} = \gamma_{an} \left(\frac{p_{H_2}}{p_{H_2} + p_{H_2O}} \right) \left(\frac{p_{H_2O}}{p_{H_2} + p_{H_2O}} \right) \exp - \left(\frac{E_{act,an}}{RT} \right) \tag{3-16}$$

$$i_{o,cat} = \gamma_{cat} \left(\frac{p_{O_2}}{1} \right) \exp \left(- \frac{E_{act,cat}}{RT} \right) \tag{3-17}$$

where: $\gamma_{an}, \gamma_{cat}$: Pre-exponential coefficients [-]
$E_{an,cat}, E_{act,cat}$: Activation energy of the anode and cathode $[J \cdot mol^{-1}]$

Summing the activation polarisation of the cathode and anode results in the total activation losses of the system. As a side note, it is of interest to know that Kazempoor [50], found in his studies that at high current densities experimental results from his model were not the same as other the experimental data. He concluded that that the cell polarisation in the experimental results increased non-linearly at high current density, mainly due to activation polarisation. These results have also been found in the developed model and are displayed in Section 3-4.

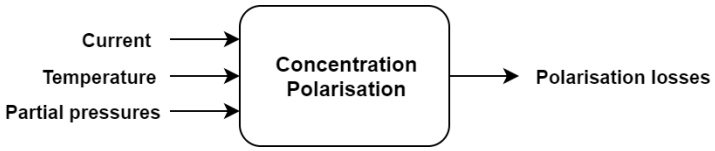

Figure 3-7: The concentration polarisation block.

Concentration polarisation

As mentioned in the journal by Patcharavorachot et al. [57] during operation of a solid oxide fuel cell, concentration gradients develop across the electrodes, resulting in a lower concentration of fuel reactants at the electrode and electrolyte interface called the triple phase boundary. The result of this is a lower concentration overpotential η_{conc}. The most commonly used expression for concentration polarisation losses is [52, 53]:

$$\eta_{conc} = \frac{RT}{2F} \ln\left(1 - \frac{I}{I_L}\right) \tag{3-18}$$

where: I_L : limiting current density $[A/m^2]$

Problems arise as with this expression as the effect of the variation of the gas-diffusion coefficient with a temperature inside a cell is not taken into account. Therefore this thesis uses the concentration overpotential calculations described by Ni Meng [10]. Furthermore Ni Mengs calculations have been used as this paper successfully managed to calculate the losses not only for a SOFC, but for a RSOFC, with the use of readily available measurements such as the steam and hydrogen partial pressures. Furthermore the calculations are fit for a lumped model and do not make use of over complicated, numerically intensive, methods.

A full lengthily derivation of the concentration loss formulae can be found in Ni et al. [58] and won't be fully described in this thesis, a summary is given below.

Concentration losses occur as a resistance to the transport of reactant species such as hydrogen and steam is caused in a fuel cell by entering and exiting the channel and porous media. From this we can expect that the losses are bound to be a function of partial pressures and temperature in the cell, porosity and geometry of the ceramics and the chemicals and at last the physical properties of the reactants.

Using the papers of Ni [10, 58, 9], the concentration the concentration overpotential can be written as given below. It should be noted that the formula for η_{conc}^{SOFC} has been adjusted slightly as it appears to have been written incorrectly in the paper, resulting in the following equations:

$$\eta_{conc}^{SOFC} = -\frac{RT}{2F} \ln\left(\frac{1 - \frac{JRTd}{2FD_{H_2}^{eff} p_{H_2}}}{1 + \frac{JRTd}{2FD_{H_2}^{eff} p_{H_2O}}}\right) \tag{3-19}$$

$$\eta_{conc}^{SOEC} = \frac{RT}{2F} \ln\left(\frac{1 + \frac{JRTd}{2FD_{H_2O}^{eff} p_{H_2}}}{1 - \frac{JRTd}{2FD_{H_2O}^{eff} p_{H_2O}}}\right) \tag{3-20}$$

where: J : current density $[A/m^2]$
R : universal gas constant $[J \cdot (kmol \cdot K)^{-1}]$
T : absolute temperature [K]
d : cathode thickness [μm]
F : Faradays constant [96487 $C \cdot mol^{-1}$]
$D_{H_2O}^{eff}$: effective diffusion coefficient of hydrogen $[cm^2 \cdot s^{-1}]$
$D_{H_2}^{eff}$: effective diffusion coefficient of steam $[cm^2 \cdot s^{-1}]$
p_{H_2O,H_2} : partial pressure [atm]

As mentioned earlier, to ensure a higher amount of accuracy or at least develop a model that sticks close to first principle modeling, diffusion coefficients have to be taken into account. The effective diffusion coefficient $D_{H_2O}^{eff}$ is based on two diffusion mechanisms combined using the Bosanquet formula stated in equation (3-21). The two diffusion mechanisms are the molecular diffusion and the Knudsen diffusion. Depending on the pore size of the cells in relation to the mean free path of the molecular species in the system the prevalent diffusion effect is found.

If the pore size is much larger for instance than that of the free path of the molecules, molecular diffusion will be dominant in the losses. As Ni states [10]: in this incident the molecule-molecule interaction is expected to govern the diffusion process. Vice-versa, if the pore sizes are much smaller than than the mean free path of the species, the molecule-pores interaction will be more prevalent. In other words, the Knudsen diffusion becomes the important mechanism. By using the following formula, the combination of both effects in porous media can be calculated:

$$\frac{1}{D_{H_2O}^{eff}} = \frac{\zeta}{\eta}\left(\frac{1}{D_{H_2-H_2O}} + \frac{1}{D_{H_2O,k}}\right) \tag{3-21}$$

where: $\frac{\zeta}{\eta}$: ratio of electrode tortuosity to porosity [-]
$D_{H_2-H_2O}$: molecular binary diffusion coefficient $[cm^2 \cdot s^{-1}]$
$D_{H_2O,k}$: Knudsen diffusion coefficient $[cm^2 \cdot s^{-1}]$

At last the two different diffusion coefficients from the equation above can be obtained in the following manner:

$$D_{H_2O,k} = \frac{4}{3} r \sqrt{\frac{8RT}{\pi M_{H_2O}}} \tag{3-22}$$

$$D_{H_2-H_2O} = 0.00133\left(\frac{1}{M_{H_2}} + \frac{1}{M_{H_2O}}\right)^{1/2} \frac{T^{3/2}}{P\sigma_{H_2O,H_2}\Omega_D} \tag{3-23}$$

where: r : mean pore radius [μm]
M_{H_2}, M_{H_2O} : molar weight of hydrogen or water $[g \cdot mol^{-1}]$
σ_{H_2O,H_2} : mean characteristic length of species [Å]
Ω_D : dimensionless diffusion collision integral dependent on temperature [-]
: and the Lennard-Jones energy ϵ_{H_2O,H_2} [K]

From Connell, the analytical values of Ω_D and σ_{H_2O,H_2} can be expressed by [59]:

$$\Omega_D = \frac{1.06}{\tau^{0.156}} + \frac{0.193}{exp(0.476\tau)} + \frac{1.036}{exp(1.53\tau)} + \frac{1.765}{3.894\tau} \tag{3-24}$$

$$\sigma_{H_2O,H_2} = \frac{\sigma_{H_2O} + \sigma_{H_2}}{2} \tag{3-25}$$

Where the dimensionless temperature and the Lennard-Jones energy are:

$$\tau = \frac{kT}{\epsilon_{H_2O,H_2}} \tag{3-26}$$

$$\epsilon_{H_2O,H_2} = \sqrt{\epsilon_{H_2O} * \epsilon_{H_2}} \tag{3-27}$$

Finally the values of ϵ_{H_2O} and ϵ_{H_2} are 2.641 Å and 2.827 Å, respectively.

Papers such as Qi et al and a second paper by Ni et al. [9] adopted a comparable calculation using model diffusion along the porous electrodes by describing the mass transfer process along the fuel cell anode as a set of partial differential equations with respect to time and space. By applying Laplace transformations the partial differential equations were converted to sets of dynamic correlations between reaction site and fuel channel concentrations.

To summarise the work done until now; as done by Padulles et al. [8], it is assumed that the modeled SOFC stack can be described as an isothermal, lumped parametered system. In the upcoming research reactant partial pressures are modeled dynamically by means of mass conservation and substituted into the Nernst equation (2-6) to solve for the voltage. For the model the current is given as a dynamic input, which in its turn is directly proportional to the fuel consumption or generation rate of the stack, thus affecting the partial pressures. Padulles research was replicated by Zhu et al. [48] and confirmed the feasibility of lumped dynamic modeling. After successful computation of the Nernst voltage internal losses are to be subtracted to provide the final cell or stack voltage. Until now two of the three losses have been discussed, namely concentration and activation losses, providing the used methods of calculation.

Ohmic losses

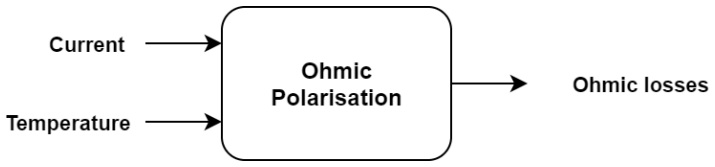

Figure 3-8: The Ohmic polarisation block.

As mentioned in Chapter 2 the Ohmic overpotential of a fuel cell is resistance to the flow of ions in the electrolyte and resistance to flow of electrons through the electrode materials. Hauck et al. [37] introduces a basic framework to calculate the Ohmic resistance of a cell, but recent research has proven that modeling the resistance requires more complex calculations that take temperature into account [60, 11]. Much of the found literature lacks on this account [52, 53, 61, 8, 57], using static parameters for the model. Although Ohmic polarisation

basically obeys Ohm's law, in research done by [54, 62, 9] improvements have been made to model the losses and take temperature into account. The expression for Ohmic losses is given below [62]:

$$V_{ohm} = R_{ohm} i \tag{3-28}$$

$$= \left(\frac{d_a}{\sigma_a} + \frac{d_c}{\sigma_c} + \frac{d_e}{\sigma_e} \right) i \tag{3-29}$$

where: d_a : thickness of anode $[\mu m]$
d_c : thickness of cathode $[\mu m]$
d_e : thickness of electrolyte $[\mu m]$
σ_a : anode conductivity $[(\Omega m)^{-1}]$
σ_c : cathode conductivity$[(\Omega m)^{-1}]$
σ_e : electrolyte conductivity$[(\Omega m)^{-1}]$

The effects of temperature are included in the model by not using static parameters for the component conductivities but using by corresponding electrical and ionic conductivities of the SOFC components found by Tseronis et al. [63]:

$$\sigma_a = \frac{9.5 \times 10^7}{T} \exp\left(\frac{-1150}{T}\right), \quad \sigma_c = \frac{4.2 \times 10^7}{T} \exp\left(\frac{-1200}{T}\right) \tag{3-30}$$

$$\sigma_e = 3.34 \times 10^4 \exp\left(\frac{-10300}{T}\right) \tag{3-31}$$

Furthermore by implementing temperature dependent conductivities the thermal dynamics of the modelled system, e.g. the heat generated by Ohmic losses, is also temperature dependent, rendering the thermal losses later on defined in (3-42) more accurate.

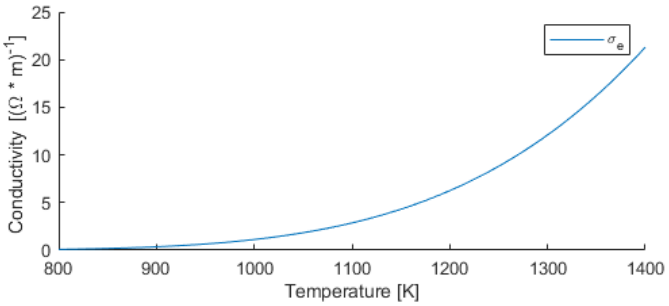

Figure 3-9: Conductivity of electrolyte layer at different temperatures.

3-2-4 Voltage dynamics

The previous sections successfully covered the development of the polarisation losses that occur in the RSOFC model. The primary difference of an SOEC compared to an SOFC is that the polarisation losses are not subtracted, but are to be added to the Nernst voltage of the cell, this voltage will correspond to the voltage needed to produce a desired amount of hydrogen. The relation is given below. With all the losses modeled and brought forward it is now possible to calculate the stack voltage with the following expressions from Chapter 2:

$$V_{SOFC} = V_{Nernst} - (\eta_{act} + \eta_{ohm} + \eta_{conc}) \tag{3-32}$$

$$V_{SOEC} = V_{Nernst} + (\eta_{act} + \eta_{ohm} + \eta_{conc}) \tag{3-33}$$

Equations (3-32) and (3-33) are processed in the operating mode block. Combining the operating mode block with everything covered until now in the modeling chapter the following block diagram could be formulated given below.

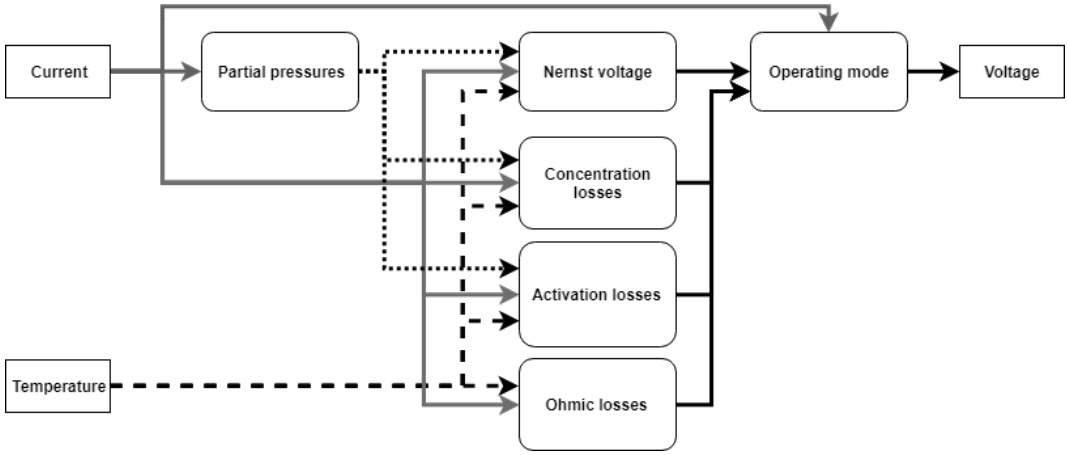

Figure 3-10: Block representation of RSOFC model.

If one were to compare the characteristics of an SOFC with an SOEC, it would be noticed that their internal characteristics such as Ohmic resistance and concentration overpolarisation would be different from each other. This difference stems from the fact that the structures and materials of the solid oxide cells would have been optimised for the consumption or on the other hand production of hydrogen. For RSOFCs this is not possible as they have to function in both fuel cell mode and electrolysis mode using the same cells with thus the same structure with electrodes, electrolysers and membranes. During operation of an RSOFC it is therefore possible to assume comparable Ohmic resistance losses [11, 64]. For SOEC mode and SOFC mode operation, the losses have been specifically adjusted to account for the different currents and pressures.

3-2-5 Thermal dynamics

As mentioned before, and as can be seen in the previous diagram, the dynamics and performance of the RSOFC stack heavily depends on the operating temperature. Therefore it

is needed to incorporate thermal dynamics in the model as the temperature is expected to change considerably during operation and between modes. The heat balance model that is required will consist out of several factors, namely: the enthalpy of the electrochemical reactions, heat generated by Ohmic resistances in the RSOFC and heat losses to the environment in accordance to the heat capacity of the stack. As mentioned earlier, the model will be considered as an isothermal, lumped parametered system, meaning that generated or consumed heat is shared instantaneously with the whole system during operation. The use of an isothermal model also removes several spacial components and dependencies in the system, resulting in relatively less computationally intensive simulations.

During operation in fuel cell mode, reactions in the cell are exothermic, meaning that heat is generated, whereas in the endothermic electrolysis the reaction is endothermic. Is is important to note that it is possible for the SOEC reaction to be exothermic at high current densities at fixed parameters. In the case of a dynamic model with transient thermal behaviour, this will not be experienced as will be discussed in this section. The heat input or output due to the reaction enthalpy change has been discussed in Section 2-3 and will be denoted as Q_e. It is possible to calculate the reaction enthalpy during operation by converting the rate of moles of hydrogen reacted to heat generated per unit time for the RSOFC system. For this it is possible to use a commonly used empirical equation (3-34) given below where:

$$Q_e = N_0 q^r_{H_2}(42.3241T - 4473.97) \tag{3-34}$$

In which the quantity of of heat generated by the reaction depends on the fuel cell temperature. As the goal of this study is to model a stack consisting out over several cells, N_0 denotes the number of cells within the stack with $q^r_{H_2}$ denoting the reacting hydrogen molar flow. Note that, $q^r_{H_2}$ will be positive or negative, depending on the RSOFC operation mode it is in.

Next, the Ohmic heat generation will be calculated. As the fuel cell has an Ohmic resistance, it will produce heat at a rate of Q_{ohm} in both fuel cell and electrolysis modes. As expected the the value of Q_{ohm} depends on the cell-stack current and cell-stack resistance. Note that R_{ohm} has been covered in the voltage loss subsection 3-2-3 and is a variable that also depends on the cell temperature. The Ohmic heat generation is given as:

$$Q_{ohm} = N_0 i^2 R_{ohm} \tag{3-35}$$

At last a the heat loss rate Q_i of the stack to its surroundings has to be calculated. Many research has been done on this, with different stack geometries or even complex 3D FEM models, giving entirely different results. A well known study by Campanari [65], on a working tubular SOFC prototype demonstrates an parametric analysis of the stack working conditions with a corresponding model, but lacks insulation integration. As the heat dissipation depends on the temperature difference between the cell stack and the surroundings, the thermal conductivity and surface area of the vessel. A more simplified model model can be built for heat dissipation that we be more suitable for later adjustment to other RSOFC systems. Ren et al. [11] chose to model the RSOFC as an isothermal cube with a total system volume of $4m^3$. With this assumption, the dimensions of the vessel L_V could be calculated with its corresponding surface area:

$$L_v = \sqrt[3]{2} \qquad A_v = 6L_v^2 \tag{3-36}$$

Under the same assumptions given at the start of this chapter that the insulation is in square geometry. In [11] a high performance insulation is used to insulate the vessel. Furthermore the assumption is made that the all the walls of the RSOFC system have a thickness of 0.15 m. The values for the thermal conductivities were taken from a commercial product Microtherm and its official specification documents. As expected, the thermal conductivity also is proportional to temperature, thus changing the overall insulation of the system:

$$\lambda = aT^2 - bT + c \tag{3-37}$$

where: $a : 2,54132 \times 10^{-9}$
$b : 1,93343 \times 10^{-5}$
$c : 0,0257471$

The outer surface temperature of the insulation T_c, was calculated from a semi-empirical equation (3-38), as a function of the temperature of the hot inner-side of the insulation. As the system is isothermal the inside temperature of the insulation was assumed to be the same as the system operating temperature, therefore in this equation it is represented as T:

$$T_c = 0.0225455T + 279.627 \tag{3-38}$$

Finally it is possible to calculate the the heat flow through the walls Q_i [W] with the help of equation (3-38), which was derived as equation (3-37) being integrated and multiplied by the area from Equation (3-36):

$$Q_i = A_V[(\frac{a}{3l}T^3 - \frac{b}{2l}T^2 + \frac{c}{l}T) - (\frac{a}{3l}T_c^3 - \frac{b}{2l}T_c^2 + \frac{c}{l}T_c)] \tag{3-39}$$

Where l is the thickness of the of the Microtherm RSOFC insulation.

Until now, research done by Ren et al. [11] promises to be very useful for this research as it has many similarities with the the system for this research, being an RSOFC driven on a steam hydrogen mix. One of the main differences of the system in this research with their system is that Ren et al. uses additional heat storage with molten bronze to function as heat reservoir for SOEC mode and that their system is modeled as a pressurised vessel with no controlled gas input. Research done by Ren et al. and Chan [56] have proven that the temperature of an RSOFC system can increase rapidly, rendering heat storage in bronze as a clever method to prevent overheating. For this research heat storage has been chosen to not be an option for the system to be modeled, to not over complicate the thermal dynamics of the model. Furthermore this system, in contrast to the latter, does have controlled gas inputs, making it possible to "flush" out excessive heat with via air through the channels.

To take air cooling into account the sensible heat in a heating or cooling process of air (heating or cooling capacity) can be calculated with the following equation:

$$Q_a = c_p \rho q_{O_2} \Delta T \tag{3-40}$$

where: Q_a : sensible heat [kW]
c_p : specific heat of air [1006 J/kg K]
ρ : density of air $[kg/m^3]$
q_{O_2} : air volume flow $[m^3/s]$
ΔT : temperature difference [K]

As the density of the air also differs as a function of temperature, it can be calculated as follows:

$$\rho = \frac{p}{R_{specific} T} \tag{3-41}$$

where p is the absolute pressure in Pa, T is the absolute temperature in Kelvin and $R_{specific}$ is the specific gas constant for dry air in $J \cdot (kg \cdot K)^{-1}$

With the heat generation and dissipation formulated it is possible to calculate the temperature change of the stack. The rate of temperature change can be determined by dividing the heat output by the cell-stack heat capacity. The equation is given below, in which $M_{stack} CP_{stack}$ denotes the heat capacity of the RSOFC stack:

$$\frac{dT}{dt} = \frac{Q_e + Q_{ohm} - Q_i - Q_a}{M_{stack} CP_{stack} + M_{gases} CP_{gases}} \tag{3-42}$$

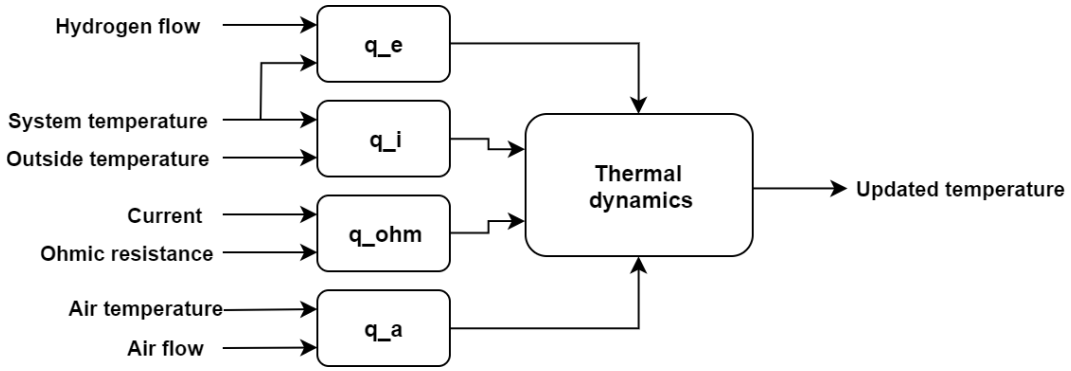

Figure 3-11: Thermal dynamics block diagram.

Equation (3-42) is graphically displayed in Figure 3-11. From the figure it can be seen that next to the system parameters, the thermal dynamics will depend on at least 7 inputs that can vary over time. As it is readily known from literature that the thermal dynamics of a RSOFC system are unstable, or at least unsustainable, temperature control is needed. It is important to study these inputs, as from these the primary control possibilities can be found.

From Equation (3-42) we can see that only Q_i and Q_a can result in a negative temperature change over time. As the insulation or outside temperatures are not easily controllable over time. The equation hints that temperature control will have to be done with the Q_a variable, by modifying the amount of airflow or the temperature of the inserted air.

With the heat dynamics calculated, the previous given model can be updated to account for the generated or lost heat during operation. Note that every iteration of the simulation the temperature block in Figure 3-12 takes on the value of 'New temperature' of the previous iteration.

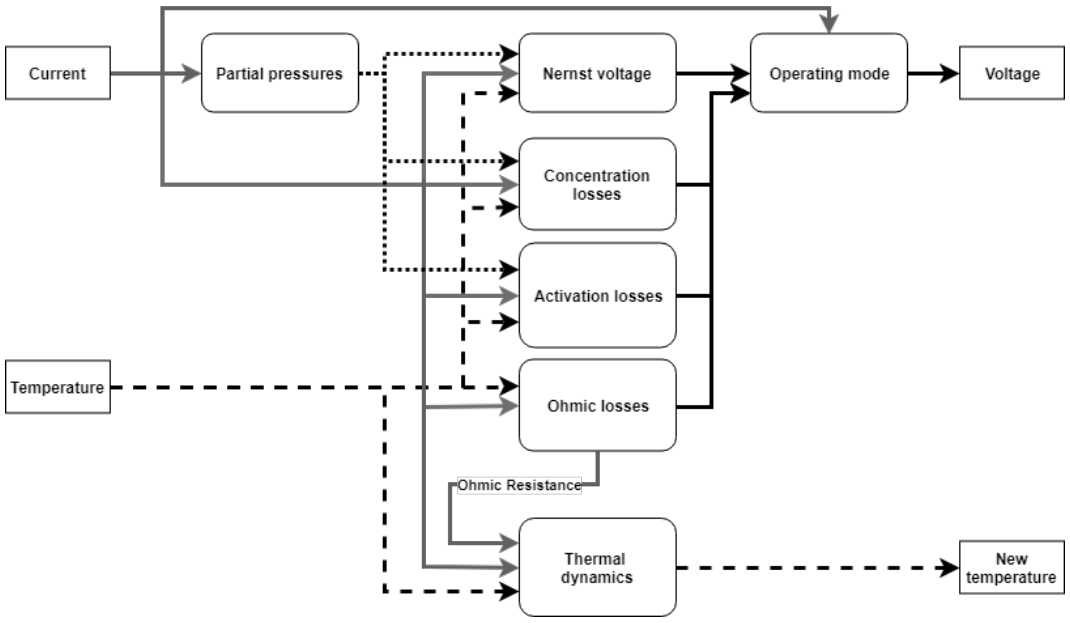

Figure 3-12: Updated block diagram of the developed RSOFC model.

3-3 Power conditioning

For this research it is required that the RSOFC is able to be coupled to a utility grid to function as a power generator and / or as a storage device. To be able to do this an AC/DC inverter is required to convert DC power being generated and consumed by the RSOFC to AC power being offered by the utility grid. In the previous Chapter 2, the workings of an inverter have been introduced, with (cascaded) H-Bridge inverters, proving to be a suitable architecture for power inversion with pulse width modulation as control technique.

As a flexible and controllable energy source and storage, an RSOFC must be able to absorb or fill a power gap on the grid. A grid supply or demand may move over time, caused by two main reasons: firstly the power supply from renewable resources, such photo-voltaic (PV) generation or wind changes because of the weather conditions and daytime. A storm may decrease solar panel power generation or increase wind power supply. Secondly, local loads can be cut in or cut off over the course of the day due to variation of energy demand of consumers.

In a study by Li Sun [51], a model is built of an SOFC to be able to design two basic coordinated control strategies for the power management of an SOFC based in a micro-grid. The literature lacks RSOFC modeling, as it only considers one-way transaction of energy from the SOFC to the grid, but offers a good overview of grid dynamics. For this literature a (micro)grid has been chosen with three local loads and a PV generation unit that is connected to a grid. A schematic of the system is given below. The grid is chosen in such a manner to make it possible to model acute energy demand changes in the grid with local loads, whilst modeling a PV supply that gradually varies over time.

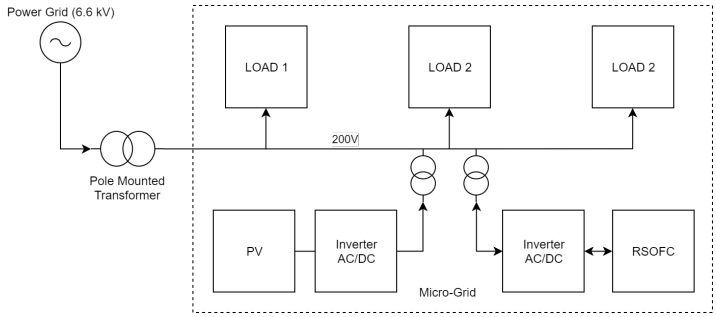

Figure 3-13: Schematic overview of an RSOFC connected to a micro-grid.

3-3-1 Grid integration model

For this study all the model and control work was confined into one single Simulink block and placed into a micro-grid model structure developed by Matlab as part of the Simscape specialised power systems package. The Simulink model was adjusted to suit the work performed in this study and a simplified version is displayed below. From the Simulink model it can be observed that all the variables displayed are in the electrical engineering domains, namely voltage and current. The RSOFC has two outputs, V_{dc+} and V_{dc-} for the voltage, which directly acts as input for the power conditioner that sets the voltage to the micro-grid level of 200V. A feedback loop offered as voltage V_{RSOFC} enters the power tracker that tracks the grid power demand or surplus to generate a current for the RSOFC stack proportional to the power. After the voltage provided to the inverter has been converted to single phase AC, the outputs are fed on the AC load interface. An extensive elaboration of the grid simulation is provided in Chapter 5 Section 5-2 together with the control dynamics to give a comprehensive overview of the overall system dynamics.

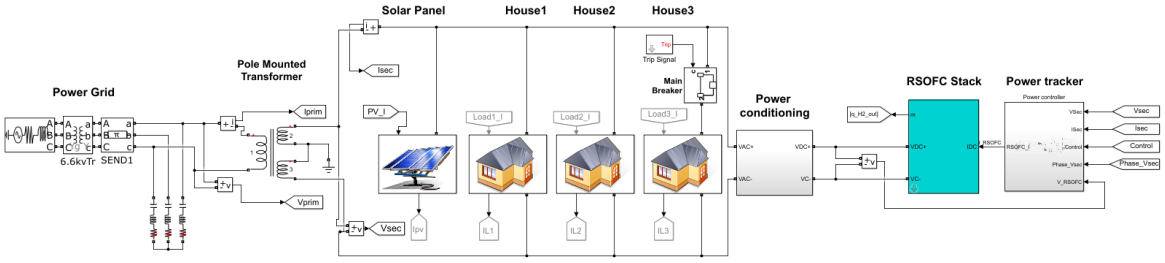

Figure 3-14: Simplified Simulink model of the RSOFC system coupled to a micro-grid.

3-4 Model validation

After and during the development of the model it is important to verify if the model is working properly. To do so, parameters used for validation had to be chosen properly in order to make the developed model comparable to other models developed in referenced papers. The parameters displayed in Table 3-2 were chosen in such a matter that the referenced papers would have as much overlap as possible.

3-4-1 Steady state dynamics

In comparison to dynamic models, there is plenty of work to be found on steady state systems. The model is therefore first validated on its steady state characteristics. As this thesis is based upon successfully developing a parametric model, the steady-state characteristics are not only checked upon relevancy with relation to input current and output voltages, but also with relation to temperature differences, fuel inlet compositions and cell support structures.

The developed model was validated under the steady-state conditions and parameters given in in Table 3-1:

Table 3-1: Steady-state model conditions and parameters.

Specification	**Unit**	**Value**	Ref.
Stack parameters			
Number of cells	[−]	450	[-]
Cell parameters			
Cell length	m	0.042	[-]
Cell area	m^2	0.001764	[-]
Cell density	kg/m^3	6000	[49]
Cell heat capacity	$Jkg^{-1}K^{-1}$	0.4	[49, 66]
Gas conditions			
Pressure	atm	1	[8]
Fuel inlet temperature	K	873 - 1273	[-]
Air inlet temperature	K	873 - 1273	[-]
Steam molar fraction	[−]	0.4 - 0.6	[-]
Hydrogen molar fraction	[−]	0.4 - 0.6	[-]
Inert gases in fuel	[−]	0	[-]
Stack operating conditions			
Current density SOFC	A/m^2	0 - 30000	[-]
Current density SOEC	A/m^2	0 - 30000	[-]
Fuel utilisation	%	0.85	[66]

Table 3-2: Overall model parameters used in this study.

Specification	Parameter	Value	Unit	Reference
Constants				
Faraday constant	F	96487	$C \cdot mol^{-1}$	[–]
Gas constant	R	8314	$J \cdot (kmol \cdot K)^{-1}$	[–]
Molar weight of water	M_{H_2O}	18	$g \cdot mol^{-1}$	[–]
Molar weight of hydrogen	M_{H_2}	2	$g \cdot mol^{-1}$	[–]
Stack parameters				
Stack power	P_{stack}	15	kW	[–]
Stack temperature	T	1073	K	[–]
Number of cells in stack	$N0$	450	[–]	[–]
Cell area	A	0.018	m^2	[–]
Partial pressure parameters				
Constant ($N0/4F$)	K_r	$0.996 \cdot 10^{-3}$	$mol(s \cdot atm)^{-1}$	Padulles et al.[8]
Valve constant hydrogen	K_{H_2}	$8.43 \cdot 10^{-1}$	$mol(s \cdot atm)^{-1}$	Padulles et al. [8]
Valve constant water	K_{H_2O}	$2.81 \cdot 10^{-1}$	$mol(s \cdot atm)^{-1}$	Padulles et al. [8]
Valve constant oxygen	K_{O_2}	2.52	$mol(s \cdot atm)^{-1}$	Padulles et al. [8]
Hydrogen flow response time	τ_{H_2}	26.1	s	Padulles et al. [8]
Water flow response time	τ_{H_2O}	78.3	s	Padulles et al. [8]
Air flow response time	τ_{O_2}	2.91	s	Padulles et al. [8]
Ratio hydrogen to oxygen	r_{H_O}	1.145	t	Padulles et al. [8]
Ohmic polarisation (Anode-supported structure)				
Electrolyte thickness	d_e	500	μm	Ni et al. [9]
Cathode thickness	d_c	50	μm	Ni et al. [9]
Anode thickness	d_a	50	μm	Ni et al. [9]
Activation polarisation				
Anode activation energy	E_{an}	110000	$J \cdot mol^{-1}$	Ren et al. [11]
Cathode activation energy	E_{cat}	120000	$J \cdot mol^{-1}$	Ren et al. [11]
Pre-exponential coefficients	γ_{an}	$7 \cdot 10^8$	$A \cdot m^2$	Ren et al. [11]
Pre-exponential coefficients	γ_{cat}	$7 \cdot 10^8$	$A \cdot m^2$	Ren et al. [11]
Concentration polarisation				
Porosity	η	0.3	μm	Ni et al. [10]
Tortuosity	ζ	6	μm	Ni et al. [10]
Characteristic length of species	σ_{H_2O,O_2}	2.734	μm	Ni et al. [10]
Average pore radius	r	0.5	μm	Ni et al. [10]
Cathode thickness	d	50	μm	Ni et al. [10]
Lennard-Jones energy	ϵ_{H_2O,H_2}	219.78	K	Ni et al. [10]

One of the primary contributors to the parameters chosen for the stack model are papers by Zhu et al. [48] which use several parameters from [8] for partial pressures and time constants for valves. Next to Zhu et al. Ren et al. [11] has been consulted for the calculation of activation overpotentials and thermal dynamics. Lastly research done by Meng Ni [10, 9, 58] has proven to be extraordinarily useful for the validation of concentration polarisation losses in SOEC's, SOFCs, and RSOFCs in relation to temperatures and fuel cell support structures.

Nernst voltage

At the heart of the entire RSOFC model lies the calculation of the Nernst voltage and the standard equilibrium potential E_0. Validation of the Nernst voltage has been found difficult as, perhaps by coincidence, not many results with specific Nernst voltage results have been published on the SOEC - SOFC transition in combination with the partial pressure calculations introduced by Padulles [8]. In a paper by [47] et al. a form of confirmation of the results can be found in a transient response of a RSOFC from 0 to 10000 Am^{-2}, with corresponding voltage levels.

Further more the Nernst voltage has been compared with other studies such as Reznicek et al. [67] and Chen et al. [68]. What is of interest that, next to Botta [47], none of the studies have shown any concrete overlap with each other and the developed model in current density regions close to zero, as the method of partial pressures calculation have proven to be of great impact and different fuel compositions have been used.

If one inspects Figure 3-15 it is noticeable that in broader terms the Nernst voltage increases with an increasing load current and in SOEC mode the voltage increases too with an increasing negative current. At first sight, it may not be immediately clear how the model represented by Equation (2-5) results in the exact voltage levels shown in the equation; this is caused by non-continuities in the logarithmic function of the equation.

Prior explanation in the partial pressures section showed that the mathematical model in this study uses a current dependent calculation of the partial pressures and therefore handles a partial pressure that will approach zero in SOEC-SOFC transition zone. What is of importance is that the partial pressures of hydrogen, steam and oxygen will approach zero at different rates. This exact difference in the rate at which the partial pressures approach zero does not have any effect in real-world experiments. In the model however, it does. The reason for this is that a $\ln(\frac{p_{h_2}\sqrt{pO_2}}{p_{H_2O}})$ is being solved numerically in the simulation environment *Matlab*. The rate difference can therefore result in the logarithmic function exploding to negative

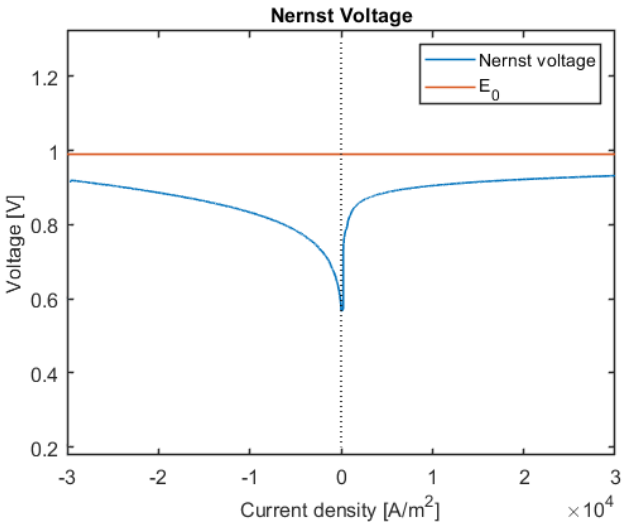

Figure 3-15: Steady-state Nernst and Standard equilibrium potential of RSOFC stack at 1073K.

or positive infinity. In this study the de-
cision has been made to let the function expand to a negative value on both SOEC and SOFC modes, resulting in the spike downwards in Figure 3-15. It is expected that this characteristic will not have any significant effect on the dynamic behaviour of the system as the operational conditions will be outside of this region preferably.

As the current, and thus partial pressures of hydrogen and steam, in steady-state approach zero due to the explicit Laplace definition in Equation (3-4) the logarithmic function will now result in minus infinity. The consequences of the resulting spikes has been mitigated by introducing a saturation for the partial pressures at a minimum of 0.0005 [atm] and more importantly by introducing a tuned median filter on the Nernst voltage in the model. The effects of the saturation and the median filter can be noticed in Figure 3-15 as the Nernst voltage is constant in the areas around zero current density.

After validation of the computed Nernst voltage, verification of the overall system J-V characteristics was done. In Figure 3-16a the composition of system losses are displayed. In other words, the total losses due to activation polarisation, concentration polarisation and Ohmic resistance has been displayed as a summation of each other at 1073K. Figure 3-16a clearly shows the non-linear relationships of the activation and concentration polarisation in relation to the current density of the cells. Just as in Ni et al. [9], the concentration polarisation result in a cut-off region beyond -24500 Am^{-2} and 26500 Am^{-2} resulting the modeled RSOFC to be only suitable for operation between those current densities at 1073 K.

For the validation two studies were taken on (R)SOFCs to check for model accuracy. The first study by Ni et al. [58] is a parametric study on SOFC performance and the second referenced paper is by Zhao et al. [69] where an experimental study has been done. Ni et al. used Zhao's work as well for validation and both the results can be found in Figure 3-16b.

As expected, the model does not show a significant match around the lower current densities as formerly discussed due the the partial pressure calculations. In contrast, the developed model in this study conveniently shows a strong match with a correction of 0.1V with the other two models at higher current densities both in voltage levels and exact current densities.

The model to be developed was required to be easily adjustable to suit different types of solid oxide fuel cells or to be modeled in different working conditions. To do so, the parametric capacity and accuracy of the model has to be validated. Using the before-mentioned parameters the model was simulated in varying conditions to compare its characteristics to other papers. The results will be discussed below on the following 3 subjects: Temperature effects, Support structure and Gas composition.

Temperature effects

Starting with the validation of the temperature dynamics of the system several simulation were done. In Figure 3-17a, 3-17b, 3-17c and 3-17d the total, Ohmic, Activation and Concentration overpotentials are displayed. As one would expect, all the losses show a strong dependency on the operating temperature of the fuel cell with Ohmic overpotentials decreasing drastically at higher temperatures. This is due to the higher oxygen ion conductivity of the electrolyte in the cells.

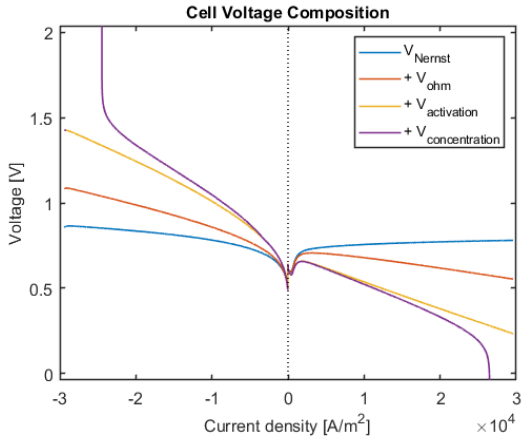

(a) Steady-state composition of cell voltage.

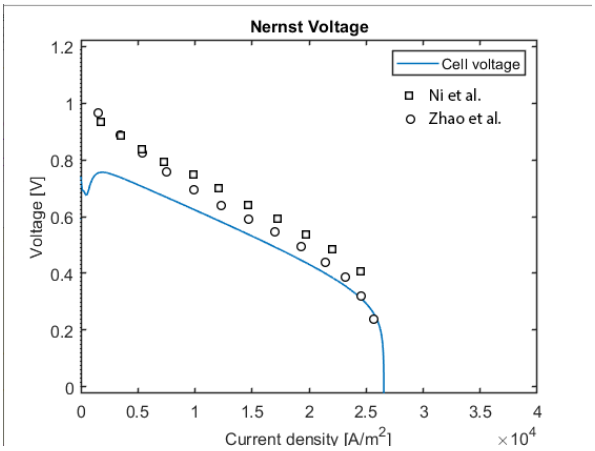

(b) Steady-state SOFC mode cell voltage compared to Ni et al. [9] and Zhao et al. [69].

Figure 3-16: Both simulations were run at 1073K.

Just like the Ohmic losses, the activation overpotential showed decreased values at higher temperatures. Higher operating temperatures cause the electrodes to become increasingly reactive as the "activation energy" is more present in the system, resulting in lower activation overpotentials. Inspecting Figure 3-17c it can be seen that the activation overpotential is very sensitive to temperature with the losses increasing to impractical levels at 873K. Very similar results were found by Ni et al. in [10] for 873K and 1073K in their work, giving credit to the importance of adding temperature dependent elements into current density calculations for the activation losses. The results from this study show a minor, but reasonably and expected difference from the previously mentioned study at higher temperatures and current densities as this work has implemented another way of activation polarisation calculations. The developed model namely uses a modified version developed by Ren et al. and Chan [11, 56] as they managed to define two different activation losses for low polarisation and high polarisation which occur at elevated current densities and temperatures rendering these results sufficient.

Contrary to activation losses, concentration overpotentials show a strong decrease in SOEC mode for the fuel cells and a slight decrease in SOFC mode at lower temperatures. As Ni [10] explains, these results are interesting as one might expect the losses to increase due to a higher binary and Knudsen diffusion rates $D_{H_2-H_2O}, D_{H_2O,k}$. However the gas density will relatively decrease stronger at higher temperatures due to the $\frac{RT}{F}$ terms in Equation (3-19). Although Ni [10] implemented concentration losses for the oxygen electrode complementary to the hydrogen side, these losses were found to be very small and negligible. The model results from this study at this point have not shown a full overlap with other studies as data is very scarce with these exact model parameters. The model, however, does show a very strong match with Ni's work at 1073K and 50% hydrogen mix and a cathode thickness of 50 μm, which will be discussed in the upcoming sections.

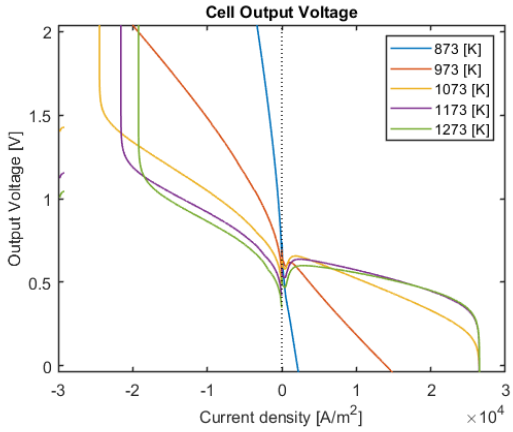

(a) Steady-state effect of temperature on output voltage. (Nernst Voltage fixed at 1073K for readability)

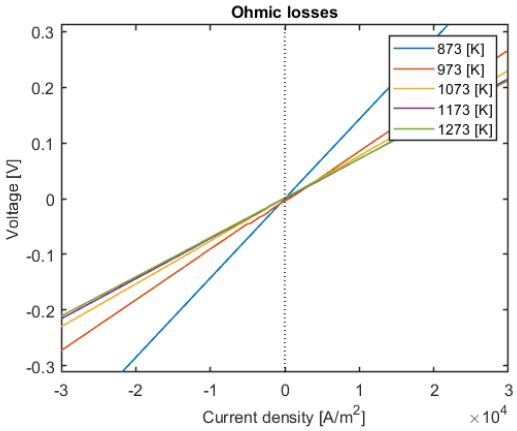

(b) Steady-state effect of temperature on Ohmic losses.

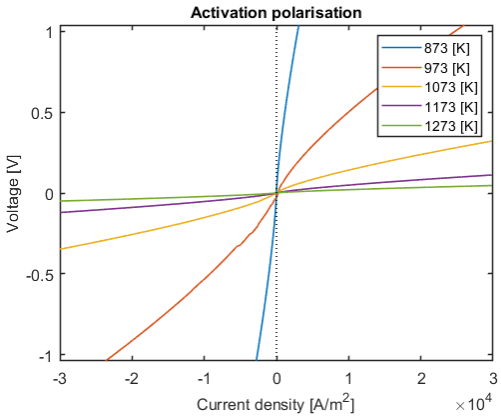

(c) Steady-state effect of temperature on Activation polarisation.

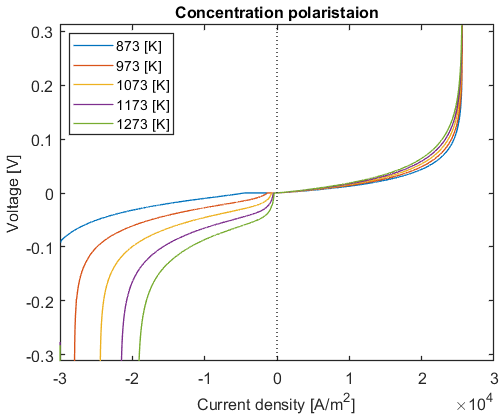

(d) Steady-state effect of temperature on Concentration polarisation ($d_c = 50\mu m$).

Figure 3-17: Simulations ranging from 873 to 1273 K

Fuel composition

The modeling results of the summed total overpotentials of a RSOFC operating under varying molar fractions of hydrogen gas $x_{H_2} = 0.4, 0.5, 0.6$ at 1073K and 1 bar were computed to compare the results with Ni [10, 9]. The results are displayed in Figure 3-18. As expected, different gas compositions did not have any effect on the Ohmic losses, but did have effect on the activation an concentration losses. The activation overpotential showed a considerable decrease as x_{H_2} decreased and with a slight decrease for concentration losses. The concentration losses showed a slight shift of the polarsation spike to higher current densities due to the fact that the limiting current density, at which the hydrogen molar fraction at the electrolyte interface in the cell approaches zero, increases at a higher x_{H_2}. This effect was observed in the developed model, but was not experienced as strong as in [10] at very high or low molar fractions. The model did show good a good fit with other work done by Ni in the $0.4 \leq x_{H_2} \leq 0.6$ zone.

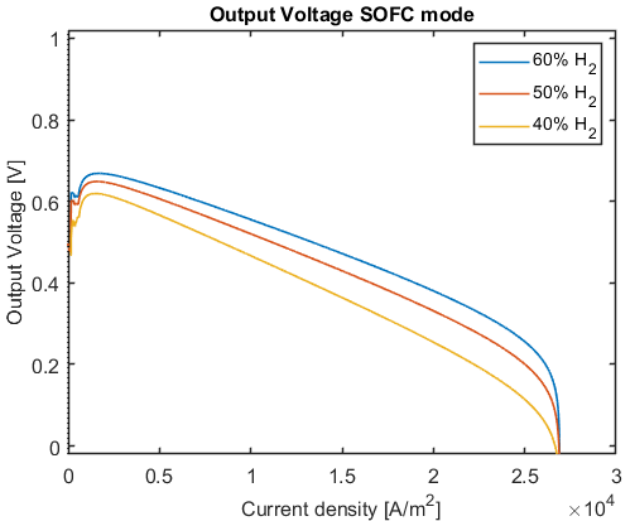

Figure 3-18: Steady-state effect of fuel composition on cell output voltage during SOFC mode (1073 K).

Cell support structure

As mentioned earlier, a RSOFC can be supported in different ways. The three primary distinctions in support structures are anode supported, electrolyte supported and cathode supported cells. For the developed model it was of importance to be able to change the support structure of the cell to compare different performance elements if one were to study or design a RSOFC. Therefore this design feature was implemented and tested. The typical parameters for the different structures are given below in Table 3-3 on which the model was tested and thoroughly checked on concentration overpotentials with work by Ni [10].

Table 3-3: Fuel cell support structure parameters.

Fuel cell support structures			
	Anode-supported:	*Cathode-supported:*	*Electrolyte-supported:*
Anode thickness, d_a (μm)	500	50	50
Cathode thickness, d_c (μm)	50	500	100
Electrolyte thickness, d_e (μm)	50	50	1000

The concentration overpotentials were more intensively investigated as this subject was the only loss on which extensive literature was written with comparable parameters. For this reason it is pleasing that the results in Figure 3-19 show a good match with Ni's model performance in SOEC mode and reasonable comparable results in SOFC mode. The SOFC mode results differ in the lower current density zone as Ni's concentration losses show more of an "s-form" instead of a quadratic curve due to unknown reasons.

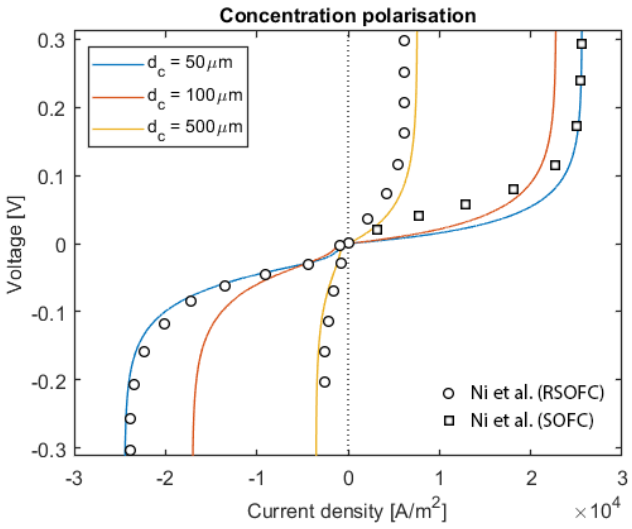

Figure 3-19: Steady-state effect of cathode thickness on Concentration polarisation at 1073 K (SOFC [9], RSOFC [10]).

Remarks

A theoretical model has been successfully developed to model the dynamics of the entire reversible fuel cell from current to partial pressures to polarisation losses and output voltage. The model can perform in both SOFC and SOEC mode and has been verified with help from other models for accuracy. Although the partial pressures show different characteristics in comparison to the most important sources used for validation, the overall voltage dynamics have shown to be accurate within a reasonable broad range of parameters.

To summarise the model has been found to perform most accurate in parameter ranges where the gas composition is modeled between $0.4 \leq x_{H_2} \leq 0.6$, the temperature is close to 1073K and the support structure is anode or electrolyte supported. As the system to be modeled is desired to have a high as possible power rating in both modes, the parameters for transient modeling has been set at 1073K, with 50% hydrogen fuel composition and an Anode support structure. Although this will not result in the largest possible power generation as can be seen in Figure 3-20, these parameters have been chosen to ensure model accuracy.

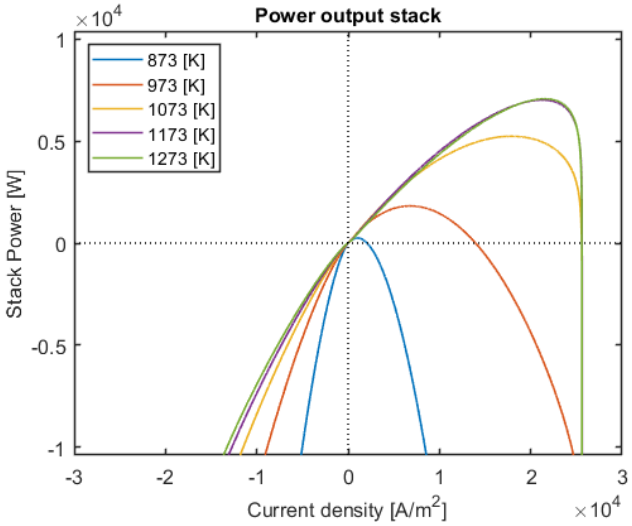

Figure 3-20: Steady-state effect of temperature ranging from 873 to 1273 K on stack power output.

3-4-2 Transient dynamics

Following the validation of the model steady-state characteristics and its accuracy, the model was modified to now run as a function of time instead of solely as a function of e.g. temperature or current density. The model parameters from Table 3-1 were used with a fixed hydrogen molar fraction at 0.5. As stated by Botta et al. [47] Investigating the transient response of a system is required in aid of defining key parameters that influence the the dynamic behaviour of a RSOFC stack. By inspecting the dynamic behaviour of the stack the need of temperature control can be determined which is crucial for the longevity of the stack and efficiency. If the stack is to be used in dynamic operation with intermittent electrical power sources or drains, the temperature variations occurring during transient operation might cause component fractures and degradation. Therefore, the model behaviour is inspected to later define the control parameters for transient operations to avoid these issues.

Temperature development

The background information chapter introduced the exothermic and endothermic behaviour of the RSOFC system. To recap; the modeled system is expected to heat up during SOFC mode due to exothermic reactions and vice-versa is expected to cool down in SOEC mode. To test the system if it showed the corresponding thermal dynamics the model was simulated in a case where the RSOFC stack would switch from a 20000 A/m^2 SOFC mode to a -20000 A/m^2 SOEC mode which corresponds to the current found at maximum SOFC power. The results are displayed in Figures 3-21a and 3-21b. In the former plot the system current and temperature development are displayed and in the latter the 4 existing heating and cooling elements from Equation (3-42) are displayed as a function of time during the mode switch.

Studying the given plots, it is easy to observe that the temperature rises in SOFC mode and cools down in SOEC mode reaching a thermal equilibrium as soon Q_{tot} approaches 0. What is of importance to note is that Figure 3-21b shows that the heat generated due to the electrochemical reactions increases at a higher temperatures, together with the heat due to Ohmic losses and insulation losses which cannot clearly be seen.

To quantify: at 1073K the rate of temperature change, e.g. the slope of the blue line in Figure 3-21a, has been calculated to be 1.4 K/min upwards and 2.6 K/min downwards, whilst experimental research on SOFC by Bujalski [70] suggests a maximum rate of temperature change of 2 K/min. This results in the RSOFC destroying itself over time, requiring some sort of cooling and temperature control to keep the system temperatures within thermal-temporal bounds. Note that the rate of temperature change is also a function of the mass and thermal capacity of the RSOFC stack, the rate of change can thus be increased by decreasing the mass of the stack. One can consider SOFC temperatures to be stable as the temperature cannot continue to rise quadratically as the stack temperature will eventually reach a temperature at which the combined insulation losses Q_a and air cooling will match the Ohmic and reaction heat generation Q_e and Q_{ohm}. This temperature however will commonly not be at an optimal or safe temperature that will fluctuate as a function of current, thus requiring a form of temperature control.

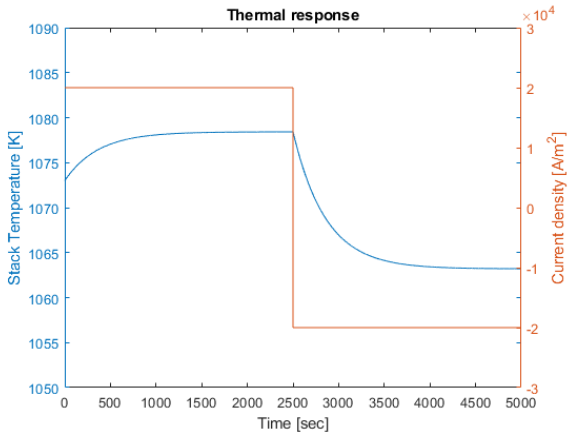

(a) Temperature and current during switch from SOFC to SOEC mode.

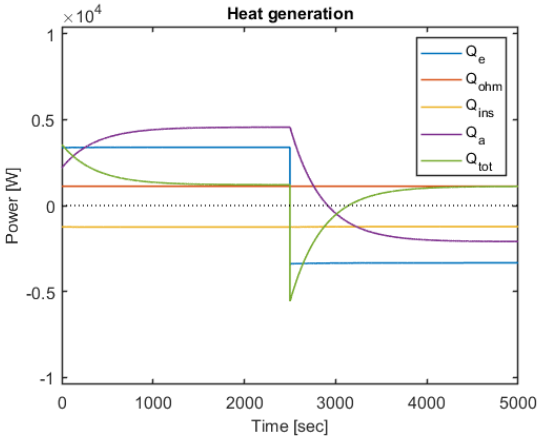

(b) Power of heat consuming or generating elements during switch from SOFC to SOEC mode.

Figure 3-21: Both simulations were run at 1073K.

Load variation

Next to check the voltage and fuel responses to a step input in the input current the dynamic behaviour was validated with research done by Sedghisigarchi et al.[54]. Although research done by Sedghisigarchi uses a relatively outdated form of polarisation loss calculations, the work proves to be of considerable value as it uses the same type of partial pressure calculations and comparable thermal dynamics. The results were compared and showed a match with each other, paving the way to start developing a controller to manage the temperature dynamics of the RSOFC stack. To illustrate the effects of the hydrogen, steam and air flow response times, Figure 3-22b is displayed. In the plot one can see the resulting latency in hydrogen flow as a result to a current step input with a 10-90 rise time of 10.76s.

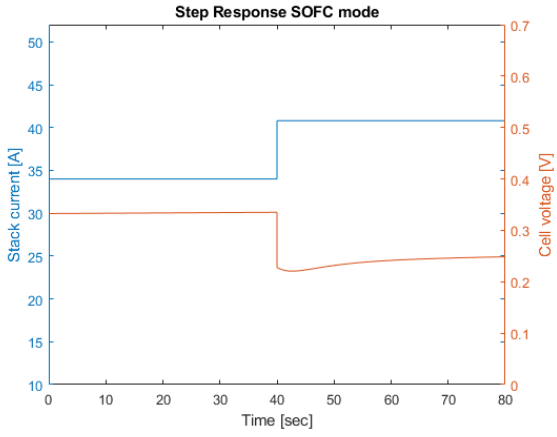

(a) Temperature and current during switch from SOFC to SOEC mode.

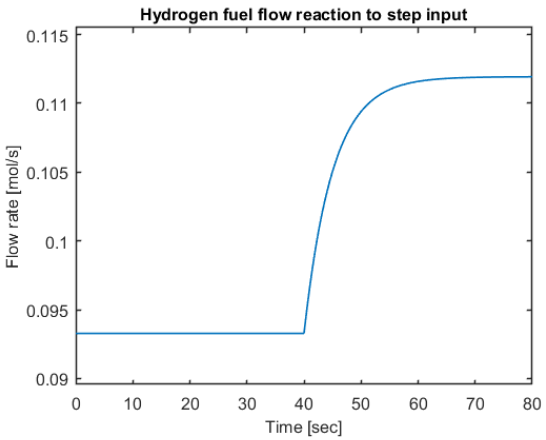

(b) Hydrogen flow rate response to current step input.

Figure 3-22: Both simulations were run at 1073K.

3-5 Conclusion

In this chapter an extensive survey has been done on literature written on the development of models for solid oxide fuel cells. After introducing the need of modeling an RSOFC with a definition of the model and its requirements, a basic path was set for the development of said model and assumptions to be made for system operation. The conceptualisation of the model was followed by a review of model dynamics and research done on solid oxide cells, creating a state-of-the art model. The dynamic modeling was split into several sections consisting out of partial pressure calculations, the Nernst equation and polarisation losses. With those elements, it is possible to model the voltage and thermal dynamics of the system. After the standalone RSOFC was modeled, a layout was given how the system is inserted as an electrical element in a micro power grid.

After the development of the model a validation has been done, comparing the results to other relevant studies. First a set of fitting parameters has been distilled from literature to create as much overlap as possible with other studies, as results, especially on RSOFCs and models in the transient domain are scarce. Steady state dynamics have shown a good match to other studies, with a focus on the verification of the steady state Nernst voltage, temperature effects, fuel composition and cell support structure. Whilst the Nernst voltage is computed using a dynamic form of calculations, a strong match was found with, the relevant, current densities from 5000 A/m^2 and up. Validation on the other subjects showed promising results for the model accuracy with the best results obtained in parameters where the gas composition is modeled between $0.4 \leq x_{H_2} \leq 0.6$, the temperature at 1073K and the support structure is anode or electrolyte supported.

The development of this dynamic model is tailored to purpose as a platform to be exited and controlled by advanced process control strategies. The development of a model based control scheme in it's turn also is very dependent on model it is to be applied on, as the form of the model, whether being a linear or nonlinear, 0D or 3D model, few or many manipulable variables, greatly affects the control possibilities. The next chapter will cover control of a reversible solid oxide cell model when being submitted to varying load requests and demands, together with an in depth specification of how a controller was developed.

Chapter 4

Control

This chapter will focus on the control of a reversible solid oxide cell when being exposed to varying load requests, as a major challenge in RSOFC operation has been found to be to track these variations in load whilst maintaining safe operating conditions. First the control objectives and constraints will be introduced to provide the reader with foundation to why certain types of control are of interest for this study. Next various possible control schemes will be introduced to give an understanding of key control principles. With the given introduction on control schemes and the control objective the chapter will continue with a review of written literature on the control of (solid oxide) fuel cells; concluding with proposed control processes.

4-1 Control objective and constraints

Literature written on the control of SOFCs mainly focuses on solving problems derived from four main issues. The first issue that is commonly found with SOFCs in a grid is that the control schemes have to be capable of regulating disturbances in the output voltage during transient operations. The second issue is that, next to rejecting disturbances like power cuts, the fuel cell has to follow the target load set by the grid. Third, the control scheme has to be able to meet constraints set by the balance of plant and fuel cell considering safe operation limits and fourth: improvement in the operational efficiency is desired in comparison to older control schemes [66].

The first two issues can be handled by designing simple controller such as PID that changes the fuel flow [71], but the last two might prove to be to challenging or even impossible for the scope of a PID. Whilst the first two issues require the control scheme deliver the desired power at optimal efficiency as objectives, the complexity of a control scheme may arise when it is required to operate the fuel cell within certain constraints too.

An example of one of these constraints can be found in the temperature domain. If an RSOFC does not succeed in proper thermal management, the temperature of an RSOFC in fuel cell mode may increase to levels that will induce permanent cell damage. Thus it is of utmost importance that the maximum cell temperature is kept below a certain threshold. Next to

maximum temperature, the cell will experience thermal stresses resulting in fractures if the cell experiences high temporal temperature gradients and if the air and fuel input temperatures are far apart. It therefore is also important to control the temperature gradient over time and the inlet temperature differences in addition to a maximum temperature of the RSOFC.

As mentioned by Murshed [66], aside from the physical constraints of the fuel cell itself, such as temperature, commonly limits are needed on fuel utilisation, fuel and air flow rate and other delimiting factors stemming from the design of balance of plants elements. In papers written by Abbas and Choi [72, 73], it is mentioned that it is desirable to keep fuel utilisation rates stable or even locked, because fuel utilisation is a critical safety indicator considering temperature and current gradients in a fuel cell. Therefore it is claimed that this parameter should be kept within a certain range of 0.7 to 0.9 [47, 66]. If fuel utilisation is controlled by manipulating the molar flow rate of of the inlet air, an override temperature control can be implemented to maintain the cell temperature below its maximum limit. In such case, the override temperature control is to be initiated if the cell temperature has exceeded its higher limit [74, 48].

Considering readily available literature on the control of SOFCs, a proposed control objective for the operation of a fuel cell system has been formulated in the following form [75, 73, 8]. The exact quantities for these targets have been derived from literature and will be elaborated in the following sections.

For the control scheme of the RSOFC it is required that the system is able to:

1. maintain required power output to its desired level;
2. keep the cell temperature between maximum and minimum operating limits;
3. keep temperature change of stack below 2 degrees Celsius per minute [70];
4. keep temperature difference between fuel inlet and air inlet within 20 degrees Celsius [47];
5. keep the fuel utilisation within optimal operating limits of 0.7 and 0.9 for all power outputs [47, 66].

As the design of a controller is absolutely dependent on the control objective, the control objective also dictates what will be the key manipulated variables, also known as inputs, and what will be the controlled variables. From Murshed, an example of this can be that if the control objective of a system is to improve load following capabilities of a system, the stack voltage can be set as the controlled variable, with fuel, steam and air flow rates to the fuel cell acting as manipulated variables for the controller. The flow rates can hereby be controlled by acting upon the compressors, blowers and valves of the balance of plant which in its turn can also be mathematically represented by an ODE model.

With the control requirements set for this research it is also possible to formulate them in the form of a research question in aid of this study:

How can an advanced control strategy for a reversible solid oxide fuel cell in a grid ensure load tracking whilst maintaining fuel utilisation and temperature dynamics within a safe range?

To answer this question, this chapter has been split up into two sections: Control techniques and Control literature. In the control techniques section, univariate and multivariate control techniques will be introduced with a discussion on their relevancy to fuel cell control. In the following section an in depth review will be given on the literature written on (R)SOFC control in addition to control proposals for this research.

4-2 Control Techniques

Controllers exist to make a system follow a certain set point or exert a desired form behaviour by adjusting inputs to a system that drive an actuator, such as a valve or a blower. Although all controllers thus have the same purpose, their design and workings may greatly differ from each other. How the inputs and outputs of a controlled system are manipulated is what makes the difference between different controllers as the specification of controller may dramatically affect the system's behaviour and control possibilities. From (R)SOFC control literature, the two most commonly and successfully applied control techniques are PID or (N)MPC [55]. Next, an introduction will be given of both.

4-2-1 PID Control

In control engineering the PID (Proportional, Integral and Differential) controller is the most commonly used form of feedback control. PID control has proven to be successful in industry automatisation as it allows for a simple control structure can easily be easy designed and is inexpensive.

For a PID controller, the control law is:

$$u(t) = K_p e(t) + K_i \int_0^t e(t')dt' + K_d \frac{de}{dt} \tag{4-1}$$

where K_p, K_i, K_d are the non negative coefficients for the proportional, integral, and derivative terms respectively and $e(t)$ the measured error. The controllers objective is to minimise the error over time by adjusting a control variable denoted as $u(t)$. In practice this can be the stimulation of air blowers, or the opening of a valve for fuel input.

By manipulating current, fuel and air flow rates using PID control, Kandepu et al. [71] showed that power, fuel utilisation and cell temperature in an SOFC-GT system are possible to be controlled. By setting $r(t)$ as a reference (desired) power output, the error signal $e(t)$, could be calculated and fed to a PI(D) controller. The PI(D) controller would translate the power difference to an input signal $u(t)$ in the form of q_{H_2}, which in it turn would increase or decrease the generated power of the SOFC. In their research comparable controllers with rate limiters were developed to maintain fuel utilisation and temperature within the safe operating limits. Just like Kandepu et al., Sorrentino et al.[76] used a PI controller to regulate temperature variation by manipulating air flow rates. A crude example is given below, where a reference power trajectory is to be followed by a fuel cell. Here, $u(t)$ resembles the input hydrogen

molar flow introduced in Chapter 3, such that:

$$e(t) = r(t) - y(t) \tag{4-2}$$

$$\text{[Power control]} \qquad r(t) = [P_{ref}] \qquad u(t) = [q_{H_2}] \qquad y(t) = [P_{out}] \tag{4-3}$$

Other work by Sendjaja et al [77] controlled fuel flow rates to match power demands in case of load changes, but acknowledged that since it is not always possible to know the load (variance) in advance, load changes had to be treated as disturbances to the controller. A decentralised control strategy was made according to the systematic selection of controlled variables in order to facilitate constraint satisfaction for all the key variables in the control problem.

While PID controllers have proven to be very versatile and being applicable to many control problems they do fall short on a couple of things. Although easily being able to provide satisfactorily control in most situations, PIDs lack in control possibilities (and performance) if the process is to be actuated within multiple constraints. Although the "summation" of multiple PID controllers, each with a specific purpose such as fuel utilisation, temperature or power make it possible to control a system it commonly results in mediocre performance. Furthermore a PIDs do not provide optimal control in these situations as their control is tuned for a linearised domain of the process. If the process to be controlled is highly nonlinear, such as with a (R)SOFC, a PID can offer good control in a linearised domain, if the system where to operate outside this domain performance will be immediately compromised.

Another problem that is to be noted with PIDs is that the fundamental difficulty with PID control stems from it being a feedback control system with fixed parameters and no direct knowledge of the process it is controlling. PID control is suitable for a process that is being observed without a model of the process. If one were to be in the situation of having a model of the process on the other hand, it would be possible to achieve better performances by using the available information of the systems characteristics. The next subsection will cover a type of control that enables this.

4-2-2 Model predictive control

As one could expect from the name, model predictive control (MPC) is a type of control based on a model that predicts the behaviour of the system over time. Model predictive control is utilised to find an optimal control sequence for a system over a set time frame called a prediction horizon which is based on a (constrained) cost function. In other words: an optimisation algorithm is used in the control scheme to find the most suitable future track for the control signals. During every iteration of the control model a prediction is made of the behaviour from the model and an optimal control signal is formulated for set prediction horizon. Whilst a PID controller only uses the current and past states of the system to adjust the input signals, a MPC attempts to predict the future using information from the current states and a model of how the system behaves.

Mentioned earlier; the control objective in this research includes several constraints that need to be satisfied due to physical and operating limits of the RSOFC such as temperature and fuel utilisation. Even though PID controllers have proven to be able to achieve control objectives at nominal operating conditions, they showed to be incapable of handling constraints and are prone to failure under these conditions. MPCs do have the capability of taking constraints

into account by formulating a cost function to be optimised based on the constraints and applying it to the control law.

To summarise, (non)linear model predictive control has the capabilities of handling nonlinearities of a system and constraints. Based on actual measurements in steps, an MPC can predict predict future states and the therefore required control actions so that a predefined objective function is optimised over a set prediction horizon.

A MPC can be mathematically be represented in the following form [66]:

$$\min_{u(k|k),u(k+1|k),\ldots,u(k+M-1)} J = \sum_{i=1}^{N} \|\tilde{x}(k+i|k) - x_{ref}\|_Q^2 + \|u(k+i|k) - u_{ref}\|_R^2 + \|\Delta u(k+i|k)\|_S^2 \tag{4-4}$$

Subject to:

$$\tilde{x}(k+1) = f(\tilde{x}(k), u(k), w(k)) \tag{4-5}$$

$$x_{min} \leq \tilde{x}_k \leq x_{max} \tag{4-6}$$

$$u_{min} \leq u_{k+i|k} \leq u_{max} \tag{4-7}$$

$$\Delta u_{min} \leq u_{k+i|k} \leq \Delta u_{max} \tag{4-8}$$

In this formulation $u(k)$ is the input, control action, of the fuel cell which can be fuel, steam or air flow rates. $u(k+1|k)$ denotes the expected control action at i-th step from k, with u_{ref} being the the desired operating point of the input. At last Δu is the incremental control move which states how big of a difference between current time and previous control action can be made. M in this representation is the control horizon over which control actions will be optimised. N is the prediction horizon over which future states are calculated and the objective function is minimised, $\tilde{x}(k+i|k)$ is i-step ahead prediction of the state x, x_{ref} is the reference of the state control variable which commonly is the stack voltage. Please note that the cell temperature a fuel utilisation can be control variables too. The demand current, the fuel and air temperatures are considered as disturbances.

As can be expected, model predictive control also suffers from a few flaws just as PID controllers. Although MPCs are considered to be relatively simple to adjust and tune, a drawback is that the controller easily becomes complex to derive compared to a PID controller [78]. Secondly MPCs are very dependent on the quality of the model it is based on. If the model offers inaccurate intrinsic dynamics, disturbance estimation or much noise, the overall prediction capabilities of the MPC will rapidly decline, resulting in the controller not working properly. Furthermore for systems with large unpredictable disturbances MPCs are considered as a bad choice of controller.

4-3 Literature review

With the basics of control theory covered and control objective and constraints discussed, this section will give a review of written literature on (R)SOFC control. It should be noted that the lettering of "(R)SOFC" was explicitly chosen as the amount of literature written on SOFCs compared to RSOFCs is exorbitant, forcing preliminary research on RSOFC control to be mainly derived from SOFC research.

4-3-1 SOFC research

Early literature on the control and modeling of SOFC stacks commonly is based on the design of coordinated control strategies that mimic the practice of conventional pulverised coal (PC) boiler-turbine units. The advantage of comparing an SOFC cell with pulverised coal boiler turbine (PCBT) units, is that control schemes have proven to be successful in practice and offer sufficient analogies to a fuel cell. In an article written by Lichang [51] it is mentioned that control of SOFC is challenging in terms of providing a fast load tracking whilst maintaining safe operation circumstances with regards to fuel utilisation rates.

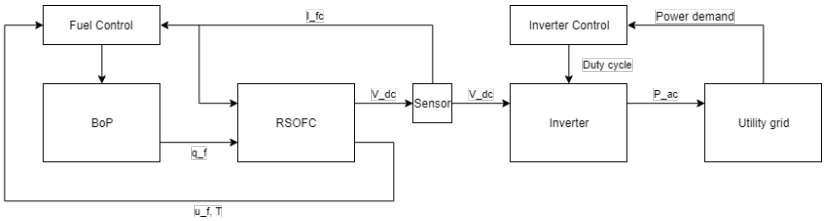

Figure 4-1: Fuel cell follows inverter.

Two coordinated control strategies are made: fuel cell follows inverter (FCFI) and inverter follows fuel cell (IFFC). Both control schemes were proven to be successful, but whether the FCFI or IFFC scheme should be utilised depends on the end use case of the fuel cell. It is shown that FCFI can serve as coordinated control strategy in the case when fast power tracking is preferred of the grid, whilst IFFC is a good option for applications where high safety must be guaranteed. In the paper, Lichang [51] uses the utilisation factor of fuel in the SOFC as performance metric for safety. Although no particular interest has been shown until now into safety in this literature survey, fuel utilisation has been found to be crucial parameter in the control process of fuel cells.

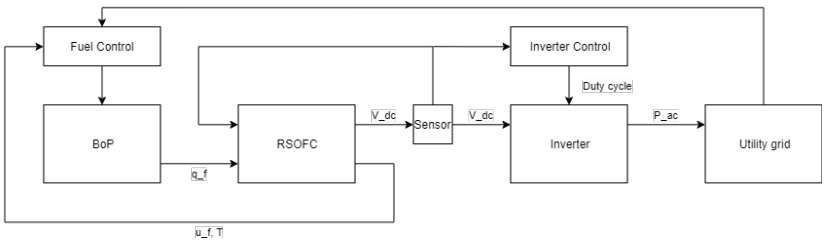

Figure 4-2: Inverter follows fuel cell.

Mentioned earlier in the control objectives; in papers written by Abbas and Choi [72, 73], it is mentioned that it is desirable to keep fuel utilisation rates stable or even locked, because

fuel utilisation is a critical safety indicator considering temperature and current gradients in a fuel cell, because of this it is claimed that this parameter should be kept within a certain range of 0.7 to 0.9. To keep the utilisation factor stable, "Inverter follows fuel cell" control schemes thus seem favourable.

In an article written by Lichang [51] it is mentioned that control of SOFC is challenging in terms of providing a fast load tracking whilst maintaining safe operation circumstances with regards to fuel utilisation rates. Two control (inverter) schemes are proposed.

A paper and report by Ren et al. [49, 79] addresses the integration of the SOFC with a power electronic inverter as a distributed generation device. The SOFC model and power inverter blocks are implemented in MATLAB/Simulink with three competing inverter control schemes. Voltage drive was found to be most suitable and a Randle circuit was discussed for impedance spectroscopy. It can be noticed that the schematics from this research shows a great amount of similarities compared to 3-14 from the last chapter.

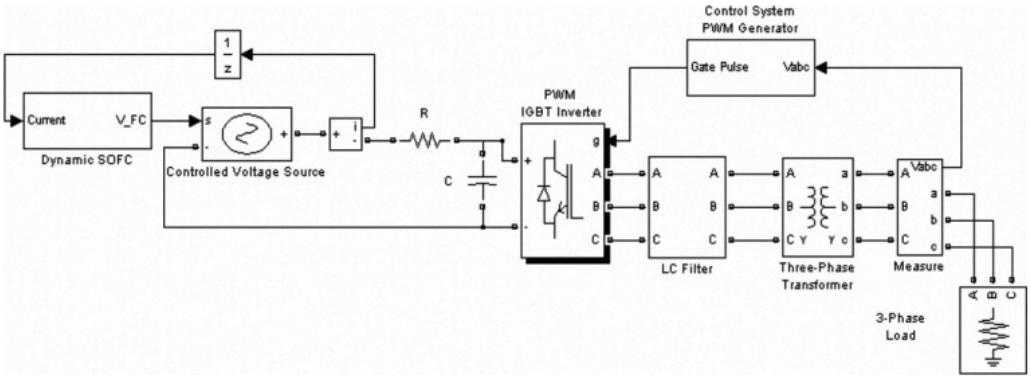

Figure 4-3: Schematic from ren et al [11].

In a paper written by Xi Lin [80], based on an allocation mechanism, the current reference I_{ref} of each stack is calculated. Therefore, the current of each stack is regulated. The allocation of current references can be set to different rules under different load conditions.

Missing in most papers are the recycling of both hydrogen and air streams in the afterburner to preheat the air and fuel stream in the heat exchanger. A second article by Murshed [66] provides two types of control relevant models of planar solid oxide fuel cell system with different details. Dynamic models of system components which include heat exchanger, reformer and after-burner are also provided along with the necessary formulation of a fuel cell connected in parallel with a capacitor.

Stiller et al. [81] analysed the stable region of an SOFC gas turbine system comparable to the earlier mentioned system by Kandepu [71], where a a multi-loop control strategy was developed to control the power output, fuel utilisation, and cell temperature. In this case the power is controlled by manipulating SOFC current, fuel utilisation by manipulating the fuel flow and cell temperature is controlled by adjustment of the air flow. In a paper by Taher, [82], PI control is proposed for control of grid-connected solid oxide fuel cells where active power control was achieved with satisfactory physical/operational constraints. Although the relatively simple PI control achieved reasonable results, the controller lacks short as it does not provide any dynamic constraints on temperature such temporal gradients or air temperature

as input. A comparable model with the same bottleneck was realised by A. Hajimolana [83, 84] with two decentralised proportional-integral (PI) controllers to control cell temperature and voltage.

A. Gebregergis and P. Pillay [85] have written a paper that introduces the development of a solid oxide fuel cell (SOFC) emulator that mimics the behaviour of an actual fuel cell for testing, design, control and optimisation. Their model served as inspiration on how to start the modeling process and shows similarities as their simulations are also based on a lumped isothermal solid oxide fuel cell. The model and is tested for various cell temperatures, flow rate concentrations and load changes to predict the static and dynamic response useful for MPC use.

In paper paper by Carre [86], a feed-forward control for SOFC system with anode offgas recycle was developed. The control strategy requires a limited number of variables and relations and is based on the work done by the earlier mentioned [8], being it one of the most basic models in the field. In strong contrast to [86], complex three dimensional models have been created too. An example is the model by Chaisantikulwat et al. [74] which is a 3D dynamic model of an anode-supported planar SOFC.

Camblong et al. [87], introduces a system that has analogies with an RSOFC, namely an SOFC in combination with a gasturbine, SOFC-GT, just like aforementioned [81]. The research is very comparable to other studies [88, 89, 90] that use a similar system that is connected to a rural micro-grid through a three-level neutral point clamped inverter. Operating strategies that maintain the SOFC power at its rated value were defined, but their discussion mentions durability, e.g. temperature constraints, was not taken into account.

4-3-2 RSOFC research

In an article by Mottaghizadeh et al. [60], a process system model was implemented for a commercially available RSOFC. Generated heat in fuel cell mode is exploited by latent heat storage tanks to enable endothermic operation of reactor in its electrolysis mode. The article proved very useful as it is one of the first to provide an electrochemical model of the system, next to a fuel cell model. Despite promising results, again no regard durability was made and furthermore no regard for concentration and activation losses.

In a paper by Ren et al. [11], which has already been brought forward multiple times, a full RSOFC model is proposed. Next to a full model, voltage control was realised of a pressurised vessel, with help of flow and pressure manipulation. In addition to control of the RSOFC control schemes were introduced for interaction with an inverter and AC grid. Although proving to be very useful the paper also has no regard for temporal temperature gradients. The model also does not allow for control of the fuel utilisation as the system is one vessel also making air inlet temperature control not possible.

A study by Barelli [91], can be of considerable interest as it aims to investigate the behaviour of RSOFC in the two operation modes and in the transition phase. Research on the transition of RSOFCs between modes is scarce as [11, 91] only have been found. Although the paper has a focus on modeling instead of control, it does provide a feasible platform for model based control. The paper has two main objectives, firstly to design and test RSOFC operation in the transition and secondly to develop a dynamic model of temperature and voltage transients under different fuel electrode feeding mixtures.

Srikanth et al. [92] did research on RSOFC modeling and control and has proven to be of great help for literature research as it belongs among one of the few studies to acknowledge that a combined system for electrolysis and fuel cell operation can result in complex system configurations that have to be able to switch between the two modes as quickly as possible. With their system they had been able to fit switching from SOFC to SOEC mode within one minute, respecting a temporal thermal gradient of maximal 15 K/min during switching. Compared to Srikant, Bujalski et al. [70] handled a far more conservative approach to thermal-temporal constraints and used a fraction of the thermal gradient at 2 K/min. As this study is purely experimental and considered more worthy, this value is used for the control objective and constraints.

Huang et al. [55] mentions that there are two main bottlenecks to taking RSOFC to commercial applications: load following ability and durability. Durability mainly is linked to temperature gradients. Zhang [93] researched dynamic modeling and analysis of a 5-kW solid oxide fuel cell system from the perspectives of cooperative control of thermal safety and high efficiency, taking Huangs research into account.

In research done by K. Wei [94], model predictive control is employed in mission of control of distributed renewable generation units that are integrated in an electrical grid, comparable to as proposed for this research. Model predictive control is also successfully deployed in a study by Xiao Wu [95] a centralised energy management system is implemented with MOC, which allows the optimal power release of energy storage units.

Last but not least, Zhang's [75] study presents the application of the NMPC on a planar RSOFC, where care is taken on model accuracy as the states are estimated based on the output of the plant using a MHE method. In this work, the air and fuel flow and current density are taken as variables to control the output power, fuel utilisation and operating temperature.

From the previous section it can be concluded that although sufficient research has been done on SOFCs and modeling with PID and MP controllers: none of the studies show sufficient overlap to be replicated for use in this study. The result of this is that, as expected, a combination is needed to be able to derive a model that: provides transient simulation of RSOFC dynamics during and between SOEC and SOFC states, that justifies temperature changes due to electro-chemical reactions and is scalable in combination with a control scheme that is feasible, controllable and accurate. By taking research on RSOFCs [11, 60, 92] lacking on subjects such as temporal gradient, air flow and nonlinear control and combining it with designed predictive control models capable of filling these gaps [75, 94, 95, 87, 66]. It is possible to develop an accurate model within the scope of this project to achieve the before mentioned control objectives. The controller will be analogue to a FCFI structure as this creates a controlled model that is easier to be implemented in other studies. Furthermore it has a better match with the scope of this study on temperature control, as detailed grid modelling is not of interest.

4-4 Controller synthesis

This section will cover the design process of the controller, starting with a short recap of the thermal dynamic element in the total RSOFC model and its input-output relationships. After

covering the model, the process of synthesising a model predictive controller is given. As the model predictive controller lacks the possibility to define constraints on the rate of change of continuous states $\Delta x_{min} \leq \Delta x_{k+i|k} \leq \Delta x_{max}$, a form of adaptive constraint synthesis is introduced. Resulting the controller to be an output feedback adaptive nonlinear model predictive controller. At last, noise modelling is discussed. Below an overview is given of the developed model. In Figure 4-4, MD stands for measured disturbances such as the current I or Ohmic resistance R_{ohm} being measured and UD for unmeasured disturbances such as noise or plant errors.

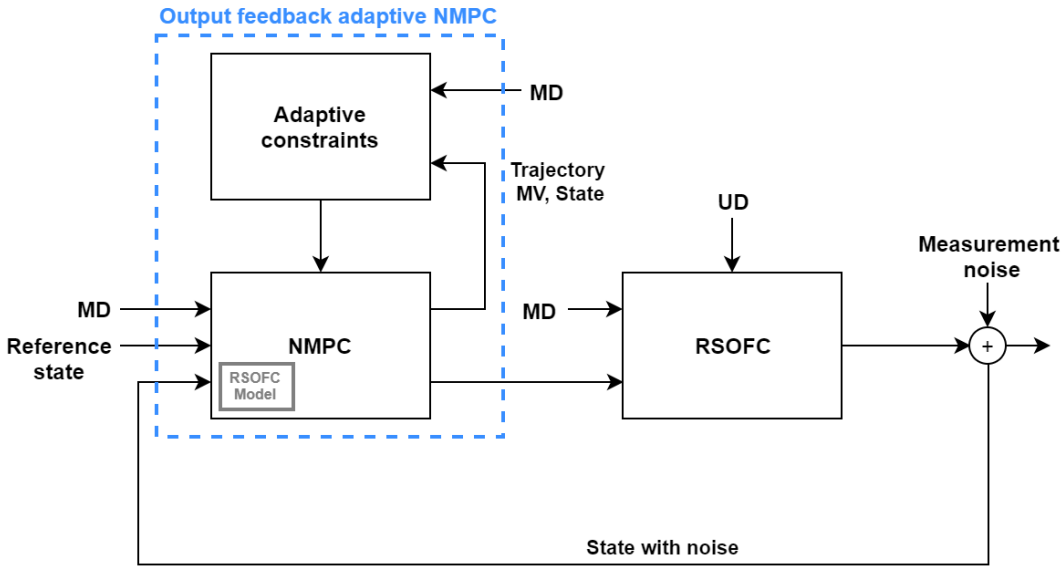

Figure 4-4: An overview of the developed controller system.

4-4-1 Thermal system

As one would expect from the name of the control sort, *model predictive control* requires a *model* to *predict* system behaviour as a function of a number of inputs and a states, to *control* the behaviour of the modeled process. The thermal dynamics of the RSOFC stack are nonlinear, resulting in the need of a nonlinear model predictive controller.

For the thermal dynamics we consider the nonlinear process model as given below. Here the development of the state over time $\dot{x}(t)$ is a function of time, inputs and the state itself. As we are solely interested in the temperature of the system, the output $y(t)$ is presented as the state $x(t)$ itself, resulting in:

$$\dot{x}(t) = f(x, u, t) \tag{4-9}$$

$$y(t) = g(x, t) = x(t) \tag{4-10}$$

$$x \in X, u \in U \tag{4-11}$$

In the equation (4-13), $\sum Q(x,u,t)$ is denoted in Watts and consists out of 4 heat generating or consuming elements which will briefly be discussed later on. For control purposes it is essential to define the variables used in the equations as inputs and states. In the developed model, the state of the model is the temperature of the RSOFC stack and the inputs are I, R_{ohm}, q_{O_2} and T_a. Substituting given inputs with the corresponding state renders the following structure:

$$X = \begin{bmatrix} x_1 \end{bmatrix} = \begin{bmatrix} T \end{bmatrix}; \quad U = \begin{bmatrix} u_1 \\ u_2 \\ u_3 \\ u_4 \end{bmatrix} = \begin{bmatrix} q_{O_2} \\ T_a \\ I_{DC} \\ R_{ohm} \end{bmatrix} \tag{4-12}$$

In this form the first two inputs u_1 and u_2 will be manipulated variables by the developed MPC and the last two, measured disturbances. The measured disturbances can be determined as the current is easily measurable and the Ohmic resistance can be calculated as a function of given parameters and temperature. The entire formulation of temperature control is based upon a controller 'manipulating' the amount of air and its temperature into the system to achieve a cooling or heating effect, hereby steering the RSOFC stack temperature and its rate of change to-and-within the design objective specifications mentioned earlier Section 4-1.

For this study a model was developed to study and control the dynamic behaviour of a RSOFC subject to varying operating conditions. As it is of interest to control the thermal dynamics of the system, the equation given below was studied to find control possibilities. From the modelling chapter 3 we find the thermal dynamics have been defined as:

$$f(x,u,t) = \frac{\sum Q(x,u,t)}{M_{stack}CP_{stack}} = \frac{Q_e(I,T) + Q_{ohm}(I, R_{Ohm}(T)) - Q_a(q_{O_2}, T_a, T) - Q_{ins}(T)}{MCP_{stack}} \tag{4-13}$$

In the previous chapter, the possibilities of cooling a system with air was introduced together with a calculation method but the effects of cooling were not described due to the fact that no controller had been developed yet. The cooling equation is formulated as follows:

$$Q_a(q_{O_2}, T_a, T) = c_p \rho q_{O_2}(T - T_a) \tag{4-14}$$

Where q_{O_2} and T_a are inputs to the system and to be considered as manipulated variables.

Q_{ohm} is an element that will always generate heat, no matter what the current or in which mode the RSOFC is operating. The heat generation is purely reliant on the current and the Ohmic resistance, which in it's turn is reliant on the system temperature and compound thicknesses in the equation given below:

$$Q_{ohm}(I, R_{Ohm}) = N_0 I^2 R_{ohm} \tag{4-15}$$

The heat generated is therefore purely a function of measured values, e.g. measured disturbances that enter the thermal dynamics system and the state $x = T$.

Similar to Q_{ohm}, the insulation and radiation losses Q_{ins} do not change sign during operation no matter what the current or in which mode the RSOFC is operating as the area in which

the RSOFC stack is operating is assumed to be cooler than the system itself resulting in heat loss defined as:

$$Q_{ins}(T) = A_V[(\frac{a}{3l}T^3 - \frac{b}{2l}T^2 + \frac{c}{l}T) - (\frac{a}{3l}T_c^3(T) - \frac{b}{2l}T_c^2(T) + \frac{c}{l}T_c(T))] \tag{4-16}$$

The insulation losses are not a function of measured disturbances and increase quadratically at higher temperatures. At last, Q_e is a function of measured disturbances and the state of the system. unlike Q_{ohm} and Q_{ins}, Q_e can change sign as the chemical reactions are exothermic in SOFC mode and endothermic in SOEC mode. The effects of such a mode switch can be seen in Figure 3-21a and the equation is given below:

$$Q_e(I,T) = \frac{N_0 I}{2F}(42.3241T - 4473.97)) \tag{4-17}$$

4-4-2 Nonlinear model predictive control

As stated before in the literature review, model predictive control has proven to be a good choice for the control of SOFC/SOEC and RSOFC control and has presented itself as the most successful process control technology [55]. In this study a nonlinear model predictive controller, NMPC, has been developed, which is an advanced version of the well established linear model predictive controller. The NMPC can handle process nonlinearities and constraints. After completing the development of the process model in Simulink and implementing a state-estimation with additive noise using an EKF discussed later on, controller synthesis was started.

The model predictive controller is able to combine current-time state estimation and measured disturbances to predict future states and required control actions. The control actions are derived by optimising a predefined objective function over a set horizon. Increasing the horizon, will force the MPC to try to predict states further in the future, but comes with a higher computational load and uncertainties. The (N)MPC algorithm can mathematically be written as deriving a set of future control actions, e.g. manipulated variables, $u(k|k), u(k+1|k), ..., u(k+M-1|k)$ by solving the general optimisation problem given in Equation (4-18):

$$\min_{u(k|k),u(k+1|k),...,u(k+M-1)} J = \sum_{i=1}^{N} \|\tilde{x}(k+i|k) - x_{ref}\|_Q^2 + \|u(k+i|k) - u_{ref}\|_R^2 + \|\Delta u(k+i|k)\|_S^2 \tag{4-18}$$

In the optimisation formulation N is the prediction horizon over which the future states are calculated and the objective function is minimised. M is defined as the control horizon over which the control actions are optimised subject to the following constraints where:

$$\tilde{x}(k+1) = f(\tilde{x}(k), u(k), w(k)) \tag{4-19}$$

$$x_{min} \leq \tilde{x}_k \leq x_{max} \tag{4-20}$$

$$u_{min} \leq u_{k+i|k} \leq u_{max} \tag{4-21}$$

$$\Delta u_{min} \leq u_{k+i|k} \leq \Delta u_{max} \tag{4-22}$$

This block uses the same process model developed earlier except in discrete-time form. To convert the continuous state definitions from equations (4-9) to discrete, the discrete form can be written as follows:

$$x_k = F(x_{k-1}, u_{k-1}, t_{k-1}) = x_{k-1} + \int_{t_{k-1}}^{t_k} f(x(\tau)), u(\tau)), \tau) d\tau \tag{4-23}$$

$$y_k = g(x_k, t_k) \tag{4-24}$$

where $t_k = t_{k-1} + \Delta T$ and ΔT is referred to as the sampling time which is set to 15.5s. This value will be motivated in Chapter 5. All the states and the inputs should satisfy $x_k \in X, u_k \in U$

From Equation (4-18) it can be seen that the are 3 norms to which the cost function is optimised. The norms are Q,R and S which are weighting matrices on the state, control action and control action rate of change. The implementation of the weighting matrices will be discussed later on. Equation (4-18) is the standard form of MPC cost function formulation and for this study another part is added to take constraint violations in account. Next a short introduction will be given of the optimisation problem elements.

With the addition of a constraint violation element, the cost function takes the following form:

$$J(x, x_{ref}, u, u_{ref}, \epsilon) = J_x(x_{ref}, x) + J_u(u_{ref}, u) + J_{\Delta u}(u, u_{ref}) + J_\epsilon(z_k) \tag{4-25}$$

where every J is a function of variables that vary between the next cost elements as a function of the measured output of the plant (the state of the system) and the inputs of the controlled plant (the manipulated variables). The displayed cost function here is a sum of four terms, where each term focuses on a specific aspect of controller goals and performances, namely trajectory tracking, manipulated variable tracking and rate of manipulated variable change.

The first element in Equation (4-25) relates to trajectory tracking. In the case of this study the controller must keep the plant in between specific operating temperatures to improve the efficiency of the plant or to ensure less material degradation over time. This value can be set a constant value, but is chosen to vary as a function of a measured disturbance: the current I_{DC}. When the RSOFC stack is operating SOFC mode the decision was made to set the reference stack temperature to 1073K as this temperature had proven to show a desirable performance in terms of power output and polarisation losses and the best match in terms of model validation. To further challenge the MPC algorithm and improve RSOFC performance, a different temperature was set for SOEC mode at a cooler 1063 K. The reference temperatures are given below:

$$x_{t,k} = \begin{cases} 1073 & \text{for } I_{DC} > 0 \\ 1063 & \text{for } I_{DC} \leq 0 \end{cases} \tag{4-26}$$

In the cost function element for the output trajectory two summing elements can be found. The first element is the output sum, which in this study can be neglected as there only is one output. The second sum is the sum over the prediction horizon of the controller, wherein the deviation function of the output and the trajectories are added together for the optimisation problem. $w_{i,j}^x$ is the most important element for the tuning and definition of the MPC performance and is a scalar tuning weight for the jth plant output at ith predicted

output within the horizon N. The specific choice of weight and motivation will be given later on in the chapter. The cost function element is given as:

$$J_x(x_{ref}, x) = \sum_{j=1}^{n_x} \sum_{i=1}^{N} \left\{ w_{i,j}^{x} [x_{ref,j}(k+i|k) - x_j(k+i|k)] \right\}^2 \tag{4-27}$$

In our application it can be desirable to keep certain manipulated variables at or close to a certain value, because it can result in the controller to be less prone to errors. Furthermore it can be that certain quantities of input to the RSOFC can be more expensive in terms of performance or resources, making it required to set them at a certain level.

For the RSOFC it was found that it was desirable to set the cooling air input of the stack to a lower value in order to make supporting hardware such as the air pump consume less power and provide more control leeway in absolute and relative terms. Therefore the decision was made to let the controller make the air flow fall back down to 7 mol/s, which is 35% of the maximum flow rate of air for the pumps $q_{pump,max}$. Next to the amount of air flow, the temperature of the cooling air was set to a value between the SOFC and SOEC mode trajectory state temperature as it was found to improve controller reactivity. s_j^u is the scale of the input and is of engineering unit order. This is an artefact of MPC controller programming as it has no effect on the control strategy, but has an impact on numerical behaviour of the algorithm. As the air temperature is expected to be around 1070K this value is set to this amount. The MPC controller uses the following performance measure for manipulated variable tracking where similarly to Equation (4-27), the two input-input trajectory deviations are summed together with the predicted states combined with a weight $w_{i,j}^u$:

$$J_u(u_{ref}, u) = \sum_{j=1}^{n_u} \sum_{i=0}^{N-1} \left\{ \frac{w_{i,j}^u}{s_j^u} [u_j(k+i|k) - u_{j,ref}(k+i|k)] \right\}^2 \tag{4-28}$$

.

Next to defining a cost on the difference between target input and actual inputs at current time and at predicted time k. With model predictive controllers it is possible to put a weight on the amount an input may change at each time step. This is called manipulated variable move suppression and often provides useful tuning capabilities for the controller. Usually most applications prefer a low rate of adjustment to manipulated variables, as intuitively sudden large steps can come with a greater risk of exaggerated and unwanted system responses to the inputs. The cost function element is given below with similar variables as before:

$$J_{\Delta u}(u) = \sum_{j=1}^{n_u} \sum_{i=0}^{N-1} \left\{ \frac{w_{i,j}^{\Delta u}}{s_j^u} [u_j(k+i|k) - u_j(k+i-1|k)] \right\}^2 \tag{4-29}$$

For any form of control, in reality it is common for constraints set on the controller to be violated due to a range of numerical or other measurable faults. To handle these kind of situations and in an effort to overcome computational errors it is possible to define soft constraints on the controller in order to allow a feasible quadratic problem solutions. The

MPC controller employs a dimensionless, positive slack variable, ϵ_k in this case that can quantify a worst-case constraint violation:

$$J_e(\epsilon) = \rho_\epsilon \epsilon_k^2 \tag{4-30}$$

Combining all the introduced cost function elements, the total equation stated in Equation (4-31) was formulated and employed in the controller. In Equation (4-31) compared to (4-18), Q,S and R can be seen as a rewritten form of $\frac{w_{i,j}^z}{s_j^z}$, furthermore the first summation term from Equation (4-26) has been removed as there only is one state:

$$\begin{aligned} J(x, x_{ref}, u, u_{ref}, \epsilon) = &\sum_{i=1}^{N} \{w_i^x [x_{ref}(k+i|k) - x(k+i|k)]\}^2 \\ &- \sum_{j=1}^{2} \sum_{i=0}^{N-1} \left\{ \frac{w_{i,j}^u}{s_j^u} [u_j(k+i|k) - u_{j,ref}(k+i|k)] \right\}^2 \\ &- \sum_{j=1}^{2} \sum_{i=0}^{N-1} \left\{ \frac{w_{i,j}^{\Delta u}}{s_j^u} [u_j(k+i|k) - u_j(k+i-1|k)] \right\}^2 \\ &+ \rho_\epsilon \epsilon_k^2 \end{aligned} \tag{4-31}$$

With the cost function defined, constraints can be set on the controller and next controlling weights can be defined to tune it's behaviour. In the next paragraphs the (adaptive) constraint synthesis will be described.

4-4-3 Adaptive constraint synthesis

For the controller to work properly and make use of the model in an efficient way, the to be computed cost function has to be subject to carefully chosen constraints. Commonly in control theory, constraints set on a system are put on the range in which the process model may operate. In our case there is only one state of interest in the model, namely the maximum or minimum temperature of the system. For this study, this state may be considered relatively unimportant as the system may operate in a broad range of temperatures ranging from 800 up to 1200K and is not truly in the scope of the control objectives. Therefore the range for the states has been set to these levels.:

$$x_{min} \leq x_k \leq x_{max} \tag{4-32}$$

$$1000 \text{ [K]} \leq x_k \leq 1150 \text{ [K]} \tag{4-33}$$

What is more of interest are the constraints that will be discussed in the upcoming paragraphs, namely the input, the input rate of change and the output trajectory constraints. To ensure controller stability all the inputs should have constraints properly set to guarantee that the controller asymptotically steers the state to the reference trajectory. [96] To do so, an output-based constraint has been set on the operational range of future control inputs. The constraint in the case of this study is dynamic as the control objective to keep the RSOFC stack within

a set temporal temperature gradient $\Delta\tilde{x}_k$ introduces great complexity into the overall, to be computed, optimal control trajectory. From the control objective section at the beginning of this chapter is is known that for the control objective it is desired to set a constraint on the system as displayed in Equation (4-34):

$$\Delta\tilde{x}_k \leq \Delta x_{max} \tag{4-34}$$

$$-2\ [\text{K/min}] \leq \Delta\tilde{x}_k \leq 2\ [\text{K/min}] \tag{4-35}$$

Problems arise in the formulation of this boundary as it is not possible to explicitly configure this constraint in (N)MPCs. A direct constraint on the rate of change of a state is not possible. It is therefore required to implement the control objective via an alternative method. For this study the decision was made to implicitly include the constraint, by inserting or combining it with another constraint put on the control law. This method resulted in the formulation of $\Psi(\tilde{x}_k, \Delta x_{max}, \tilde{u}_k, d_k)$, which will be elaborated in the following paragraphs. This method has been successfully implemented by inserting the state constraint into the min-max input constraints of the system, resulting in the formulation given below:

$$u_{k,min} \leq u_{k+1|k} \leq u_{k,max} \tag{4-36}$$

$$\begin{bmatrix} u_{1,k,min} \\ u_{2,k,min} \end{bmatrix} \leq u_{k+1|k} \leq \begin{bmatrix} u_{1,k,max} \\ u_{2,k,max} \end{bmatrix} \tag{4-37}$$

$$\begin{bmatrix} 0 \\ \tilde{x}_k - \delta_{inlet} \end{bmatrix} \leq \begin{bmatrix} q_{O_2} \\ T_{air} \end{bmatrix} \leq \begin{bmatrix} \Psi(\tilde{x}_k, \Delta x_{max}, \tilde{u}_k, d_k) \\ \tilde{x}_k + \delta_{inlet} \end{bmatrix} \tag{4-38}$$

where:
q_{O_2} : Coolant air flow rate [mol/s]
T_air : Coolant air temperature [K]
$\Psi(\tilde{x}_k, \Delta x_{max}, \tilde{u}_k, d_k)$: Air flow rate constraint [mol/s]
δ_{inlet} : Maximum temperature difference between fuel and air inlet, 20, [K]

Next, the MPC algorithm was used in advantage of the controller robustness by incorporating the future predicted states and manipulated variables. This was done by tapping the set of future control actions, and predicted state from the MPC controller and combining them together to calculate the maximum air flow and temperature. Next to a scalar constraint, MPC controllers accept vector constraints. In the case of this study the vector length is a function of the control horizon of the controller. In the optimisation formulation N is the prediction horizon over which the future states are calculated and the objective function is minimised. M is defined as the control horizon over which the control actions are optimised subject to the following constraints. In this study the control horizon was set ate the same length as the prediction horizon N, making the constraint vector of size $(n_{mv} \times N) \times 1$. The resulting input constraints could now be formulated as:

$$\begin{bmatrix} 0 \\ 0 \\ \vdots \\ 0 \\ \tilde{x}_k - \delta_{inlet} \\ \tilde{x}_{k+1} - \delta_{inlet} \\ \vdots \\ \tilde{x}_{k+N-1} - \delta_{inlet} \end{bmatrix} \leq \begin{bmatrix} q_{O_2} \\ T_{air} \end{bmatrix} \leq \begin{bmatrix} \Psi_k(\tilde{x}_k, \Delta x_{max}, \tilde{u}_k, d_k) \\ \Psi_{k+1}(\tilde{x}_k, \Delta x_{max}, \tilde{u}_k, d_k) \\ \vdots \\ \Psi_{k+N-1}(\tilde{x}_k, \Delta x_{max}, \tilde{u}_k, d_k) \\ \tilde{x}_k + \delta_{inlet} \\ \tilde{x}_{k+1} + \delta_{inlet} \\ \vdots \\ \tilde{x}_{k+N-1} + \delta_{inlet} \end{bmatrix} \tag{4-39}$$

In Equation (4-39) a new function is introduced to calculate the upper bound of $u_{1,k+1|k}$. The function is given below and stems from the overall thermal dynamics of the system described in Equation (4-13), where the thermal time derivative $\frac{dT}{dt}$ has been exploited for the temporal gradient constraint Δx_{max}. The function ultimately uses predicted values of the stack temperature and control actions of the MPC to calculate, together with measured disturbances the maximum control action regarding air flow. The output dependent constraint is given below:

$$\begin{aligned} u_{1,max} &= \Psi(\tilde{x}_k, \Delta x_{max}, \tilde{u}_k, d_k) \\ &= \begin{cases} \min\left(\left| \dfrac{-\Delta x_{max}\Phi + Q_{e,k}(\tilde{x}_k) - Q_{o,k} + Q_i(\tilde{x}_k)}{c_{p,air}\rho_{air}(\tilde{x}_k - u_{2,k})} \right|, q_{pump,max} \right) & \text{for } I_{DC} \geq 0 \\ \min\left(\left| \dfrac{\Delta x_{max}\Phi - Q_{e,k}(\tilde{x}_k) - Q_{o,k} + Q_i(\tilde{x}_k)}{c_{p,air}\rho_{air}(\tilde{x}_k - u_{2,k})} \right|, q_{pump,max} \right) & \text{for } I_{DC} \leq 0 \end{cases} \end{aligned} \tag{4-40}$$

where:

$\tilde{x}_k$	: Predicted state of system at time interval k [K]
$\tilde{u}_k$	: Predicted control action at time interval k [K]
d_k	: Measured disturbance, such as the current [A]
Δx_{max}	: Maximum rate of change of state [K/min]
Φ	: MCP of system
$Q_{e,k}(\tilde{x}_k, d_k)$	: Heat due to reacting hydrogen as function of state [W]
$Q_{o,k}(d_k)$	: Heat due to Ohmic losses at time interval k [W]
$Q_i(\tilde{x}_k)$	: Heat losses to environment as function of state [W]
$c_{p,air}$	: Heat capacity of air [J/kg K]
$\rho_{air}(\tilde{u}_{2,k})$	: Density of air as function of air temperature [W]
$q_{pump,max}$	: Maximum throughput of air through system, 20, [mol/s]

Lastly, boundaries were set on the constraints of the rate change of the manipulated variables that control the process model. In these constraints consideration is taken of how fast the fuel pumps can or may accelerate the flow of air rate and how fast the heaters can adjust the air temperature. Resulting in the following formulation:

$$\Delta u_{min} \leq \Delta u_{k+i|k} \leq \Delta u_{max} \tag{4-41}$$

$$\begin{bmatrix} -2.5 \\ -25 \end{bmatrix} \leq \begin{bmatrix} \Delta q_{O_2} \\ \Delta T_{air} \end{bmatrix} \leq \begin{bmatrix} 2.5 \\ 25 \end{bmatrix} \tag{4-42}$$

In table 4-1 an overview has been given of the constraints put down on the controller, furthermore the table also presents the values given to the scaling factors s_j^x and the target values of the states and manipulated variables.

4-4-4 Control weights and slack variables

With constraints defined for the optimisation problem, the controller was ready to be implemented in Matlab and simulated. To avoid mediocre performance and inexplicable controller action choices, first the control weights were set. Until now all the variables noted in Equation (4-31) have been discussed, except the weights w_i^x,$w_{i,j}^u$ and $w_{i,j}^{\Delta u}$, next to the scalar value ϵ, a dimensionless, positive slack variable for constraint violations. Bad performance and control

Table 4-1: Initial conditions, constraints, manipulated variable targets and scales of controller.

Input	Variable	Init. cond.	Min	Max	Target	Scale	Unit
x_1	T	1073	1000	1050	$x_t^{[a]}$	1073	[K]
u_1	q_{O_2}	0.1	0	$\Psi(x_k, \Delta x_{max}, u_k)$	7	10	[mol/s]
u_2	T_a	1070	$T - \delta_{inlet}$	$T + \delta_{inlet}$	1070	1070	[K]
Δu_1	Δq_{O_2}	-	-2.5	2.5	-	-	$[mol/s^2]$
Δu_2	ΔT_a	-	$-0.167^{[b]}$	0.167	-	-	[K/s]

[a] x_t is dependent on the operation mode, see Eqn. (4-26), [b] 10 K/min from the control objective equals to 0.167 K/s.

actions can be credited to cases where no weights have been appointed to the cost functions and thus are assumed to be of value 1 by the MPC algorithm.

The weights w_i^x,$w_{i,j}^u$ and $w_{i,j}^{\Delta u}$ are non-negative and correspond to the superscripted variable. The weights are provided to the algorithm in matrix form with $n_y \times n_y$ and $n_u \times n_u$ sizes with the value per state or manipulated variable on the diagonal of the matrix. A smaller $w_{i,j}^z$ indicates the controller should consider the corresponding variable as less important to the overall performance index of the controller. The matrices are given below:

$$w^y = \begin{bmatrix} w^y \end{bmatrix}, w_{i,j} = \begin{bmatrix} w_1^u & 0 \\ 0 & w_2^u \end{bmatrix}, w_{i,j}^{\Delta u} = \begin{bmatrix} w_1^{\Delta u} & 0 \\ 0 & w_2^{\Delta u} \end{bmatrix} \tag{4-43}$$

Output weight

As there is only one output and thus state to be controlled by the controller, the weight for the output is a scalar. The value was set to a high 50 for this research to force the controller to track the reference output as close as possible. It should be noted that a fair amount of the importance of the weight is lost as it commonly also functions as a relative weight to other outputs, something that is not possible in this research.

Manipulated variable weight

Mentioned earlier in this section, it was found that for the RSOFC it was found that it would be desirable to steer the cooling air input of the stack to a lower value when possible. This was done in order to let supporting hardware such as the air pump consume less power and to make it possible to have an absolute and relatively larger increase in cooling air when needed. The manipulated variable weight penalises the difference between the manipulated variable action and the target manipulated variable value. Furthermore the ratio of w_1^u to w_2^u tells the controller the importance of the target value for the corresponding manipulated variables being reached relatively to each other. In this case that was the importance of the air flow settling back to 7 mol/s in comparison to how important it would be for T_a to reach 1070K. The effect of changing the weights is discussed in the next Simulation results Chapter 5, together with the motivation of the following weights:

$$w_{i,j} = \begin{bmatrix} 30 & 0 \\ 0 & 1 \end{bmatrix} \tag{4-44}$$

Manipulated variable rate weight

Also known as the manipulated variable move suppression weight, this weight indicates the implicit cost of the controller changing in the manipulated variables per time increment. A high weight on the on the second input T_a would mean that the controller would consider it unfavourable to quickly change the air temperature within the set air temperature constraints. Although the absolute values of the weights did not offer any value for the control strategy, it did offer significance in relative terms. By carefully tuning the weight relatively to each other it was possible to "suggest" the controller what input has to react more aggressively than the other to disturbances in the system or a change in reference temperature. In the case of this study it was considered that in real-world practice, changing the temperature often and rapidly would be less in favour than more easily changing the rate of airflow. Therefore the following weights were chosen to make the airflow react in a more aggressive manner than the air temperature:

$$w_{i,j}^{\Delta u} = \begin{bmatrix} 1 & 0 \\ 0 & 30 \end{bmatrix} \tag{4-45}$$

Slack variable

Until now in Equations (4-33), (4-37) and (4-40)(5b), the constraints on x_k u_k and Δu_k and have been hard constraints, allowing for no violation of these. Introduced by the cost function element (4-30), it is possible however to introduce a positive slack variable, that relaxes the constraints. By default Matlab sets all input constraints as hard and output constraints are soft. Meaning that for inputs ρ_ϵ is $10e5$. Hard output constraints may cause in-feasibility of the optimization problem [97]. This can happen for example due to an unpredicted disturbance in the system or a model mismatch. As these are likely to happen, an Equal Concern for the Relaxation (ECR) was introduced into the controller. The use of ECR is formulated below where the vectors V_j^z have non-negative entries that represent the concern for relaxing the corresponding constraint. A large V corresponds to a softer constraint. V = 0 thus means that the constraint is hard and may never be violated and is implemented in the following manner:

$$x_{j,min} - \epsilon_k V_j^{x,min} \leq x_k \leq x_{j,max} + \epsilon_k V_j^{x,max} \tag{4-46}$$

$$u_{j,min} - \epsilon_k V_j^{u,min} \leq u_{k+1|k} \leq u_{j,max} + \epsilon_k V_j^{u,max} \tag{4-47}$$

$$u_{j,min} - \epsilon_k V_j^{\Delta u,min} \leq \Delta u_{k+1|k} \leq u_{j,max} + \epsilon_k V_j^{\Delta u,max} \tag{4-48}$$

$$\tag{4-49}$$

In turn the weight, ρ_ϵ, which was first introduced in Equation (4-30) penalizes the made violation of the constraints. Resulting in a larger ρ_ϵ penalising a constraint violation a bigger amount.

4-4-5 Noise modelling

Complexities regarding the physical plausibility of the model and its control structure arise during simulation as the model predictive controller uses the same model as the observed and controlled process. The prediction accuracy will therefore be unrealistically high, causing the controller to be barely challenged in its robustness or operational range. To overcome this, a realistic form of model inaccuracy or noise is to be introduced into the system. A solution for this has been implemented by designing the nonlinear MPC controller to continuously process the temperature augmented by an unmeasured disturbance at every sample time.

The first noise added to the system in the form of average white Gaussian noise. Theoretically, introducing a continuous white noise results in a additive disturbance that has a correlation time of 0 and a total energy of infinity. In practice, physical systems are never disturbed by white noise, but Gaussian noise has proven to be a a useful theoretical approximation if the noise has a very small correlation time relative to the natural bandwidth of the system. For this study a average white Gaussian noise was added to the system with a maximum value of 0.1. Secondly a noise was added to the system to model frequency harmonics. The harmonic distortion was set as a function of the microgrid frequency of 60Hz by adding two small distortions at 120 and 1/60 Hz with an amplitude of 1% of I_{DC} on the stack current I_{DC} itself.

As a recap for the previous sections: Following the steps provided, this study has documented the development of a non-linear model predictive controller that follows a reference temperature subject to several constraints. The model predictive controller is fed a temperature measurement augmented with noise based on output measurements together with several adaptive constraints. Therefore the controller can also be considered to be an output-feedback adaptive nonlinear model predictive controller. With the MPC developed and adaptive constraints set, the next chapter will cover simulation results.

Chapter 5

Simulation results

Until now the control objectives of the the controller, controller techniques, written literature on RSOFC control and controller synthesis have been covered. After specifying the controller synthesis wherein the structure of the MPC controller had been introduced together with its trajectory, output based constraints and tuning variables such as weighting matrices and slack variables; this chapter will finally cover the simulation results that were achieved with the controller developed in this chapter combined the entire model developed in chapter 3.

To inspect the controller performance and to provide useful insights into its behaviour this section is split up into two parts that cover two scenarios. The first scenario is a short-term scenario wherein the MPC controls the RSOFC stack during a time span of 40minutes. During the short term scenario it is easier to view the controller behaviour and the effect of the chosen weights and slack variables. The short-term scenario is again split into smaller sections for further elaboration.

The second scenario is called the long-term scenario wherein the control of the RSOFC stack is simulated during the span of an entire day. As mentioned in chapter 1 and 2, RSOFC technology is of interest as an energy storage to combat the challenges put upon utility grid by intermittent energy sources such as windmills and solar panels. In the long-term scenario the entire model and MPC is tested by inserting them into a micro-grid resembling a neighbourhood with several houses and solar panels connected to a grid.

To reduce the number of pages of this thesis plots have been added of the system where the system is not subject to the complex constraints introduced in section 4-4-3. If interested please refer to Appendix A.

5-1 Scenario 1: Short term

As mentioned above, the short term scenario is a simulation of the controlled system for 2400s. In the first scenario the system is required to switch from SOFC mode to SOEC mode at 500s via a step input, to later turn back to the former SOFC mode following a

ramp function. From Figure 5-1 it can be seen that the current varies between -10000 A/m^2 and -10000 A/m^2, which equals 17.6A and has been chosen as it is at the centre of both operational domains discussed in the model validation Section 3-4. Furthermore for control: the prediction horizon N has been set to 12 for this scenario together with the control horizon at 12 but separated into block moves to increase robustness. These parameters were found to show the best performance and are discussed later on in this chapter. Lastly the weights introduced in section 4-4-4 have been implemented.

5-1-1 Operational mode switch

The entire control related system behaviour when the model is subject to a mode switch is given in Figure collection 5-1. In the first figure, the current dynamics are given. In the second figure the system temperature is plotted together with the reference temperature it is required to track with model predictive control. In the third figure the air temperature is displayed, next to the air temperature, the air temperature bounds defined by $T \pm \delta_{inlet}$ are given and the manipulated variable target of 1060K. In the fourth figure the airflow is plotted together with the adaptive constraint $\Psi(x_k, \Delta x_{max}, u_k)$ for the air flow. In the last figure, the rate of temperature change is displayed. As one of the control objectives the controller and it's constraints are employed to enforce the system to not change more than 2 K per minute. Careful inspection of the figures in 5-1 offers insight into the finer characteristics of the controlled system.

To start with the stack and reference temperature plot, it can be seen that the controller manages to follow the reference signal with a fall time of 200s and a rise time of 230s. The advantage of predictive control can be also seen in the figure. As the current first switches abruptly from positive to negative, the the controller could not predict the abruptly generated difference between the stack temperature but quickly reacts after processing the measured disturbance. During the ramp-up back to SOFC mode, the MPC allows the temperature the deviate from the reference as the model extrapolates the state value from the endothermic to exothermic switch, making more efficient use of it's resources T_a and q_{O_2}. Later a more in depth inspection will be given on effective use of the model prediction horizon.

The figures plotting the air temperature and the airflow are to be inspected next to each other. From t=0 to t=110s the model moves from the initial state and input conditions to an equilibrium resulting in the T_a and q_{O_2} not changing until the current changes due to the step input. After the current step input, T_a and q_{O_2} work in tandem to achieve a maximal responsive action to cool the system to 1068K, but quickly reverse back to a higher temperature and target air flow to avoid a violation of the ΔT_{min} constraint and to dampen the the over cooling effect that could occur if the system gets too aggressively cooled and drops below the reference temperature.

In the last figure the temporal temperature gradient is plotted together with the maximum and minimum allowable temperature change at any moment of the RSOFC. Just as in the figures above, it can be observed that from t=0 to t=110s the model moves from the initial state and input conditions to an equilibrium temperature. What is of interest is that the ΔT makes a considerable step response to the current step response at t=500. Until now this has been found to be the biggest sensitivity in the system. Although it has been found that the temperature gradient will always be pushed back to 0 by the controller, it is possible to

to create an input current step, that will cause a ΔT step greater than 2 [K/min], causing the constraint to be temporarily violated. In order to quantify the sensitivity and gain knowledge into when these violation could occur, a small Matlab function was written that algebraically solved a converted version of $\Psi(\tilde{x}_k, \Delta x_{max}, \tilde{u}_k, d_k)$ for I_{DC} subject to nominal operation conditions and constraints. Computation revealed that if the constraint were to be violated, a step down input of I_{DC} was required of more than 48.8 A.

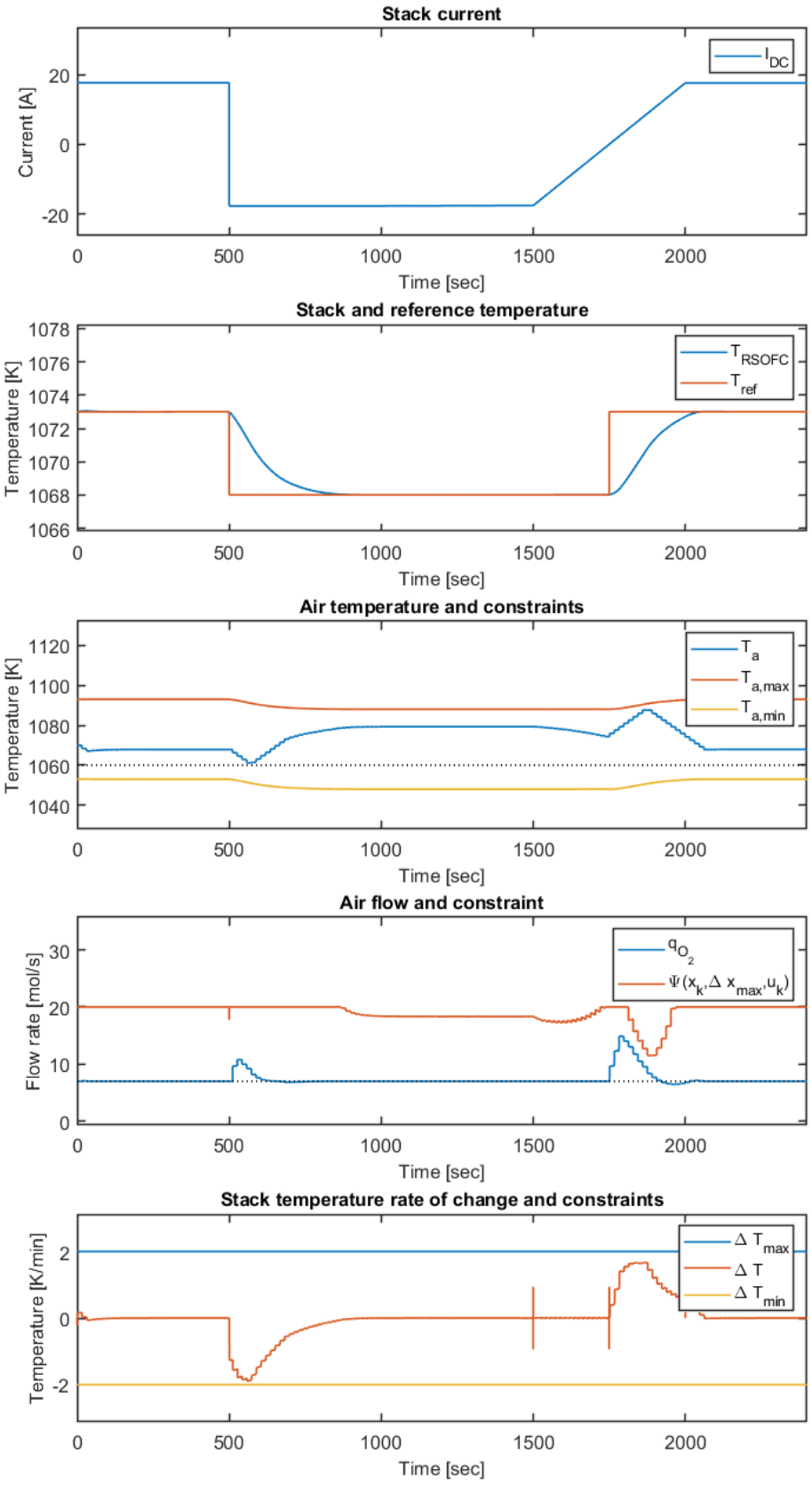

Figure 5-1: Scenario 1: System response to mode switch.

5-1-2 Varying weights

During the work of this thesis, the weighting matrices for the controller were thoroughly tuned to make the control behaviour and actions fit the control objective and personal preferences. As discussed in section 4-4-4, these weights have significant effect on the control dynamics and will be discussed in this section. During the discussion the effects of varying weights will be brought forward together with a justification of the chosen weights earlier on.

With tuning, the primary rule is that a smaller $w^z_{i,j}$ indicates the controller should consider the corresponding variable as less important to the overall performance index of the controller. As mentioned earlier, the cost of changing the rate of air was considered to be lower than that of changing the air temperature. Setting $w^{\Delta u_1} = w^{\Delta q_{O_2}}$ at 1 and $w^{\Delta u_2} = w^{\Delta T_a}$ at 30. Contrary to the manipulated variable change rate, the amount of air entering the stack is desired to be at a lower point if possible, therefore a manipulated variable target was introduced at 7 mol/s to let the controller steer q_{O_2} to that level. To introduce a means of penalising, or intuitively "pressuring", the controller to minimise the difference between a control action and its target; weight $w^u_{i,j}$ was introduced. The collection weights are given below.

From 4-4-4 we have that:

$$w^y = 50, \quad w^u_{i,j} = \begin{bmatrix} 30 & 0 \\ 0 & 1 \end{bmatrix} \text{ and } w^{\Delta u}_{i,j} = \begin{bmatrix} 1 & 0 \\ 0 & 30 \end{bmatrix} \tag{5-1}$$

In the previous paragraphs where the overall system performance was described and inspected, these weights were used. To provide insight into weight variation and to further motivate the choice for these weights, the following paragraphs will illustrate the effect of opposite weighting. In Figure 5-2 two couples of different control actions can be seen for $T_a, T_{a,alt}$ and $q_{O_2}, q_{O_{2,alt}}$. T_a, q_{O_2} are a function of the optimisation problem using the weights in (5-1) and $T_{a,alt}, q_{O_{2,alt}}$ by using opposite weights namely:

$$w^{u,alt}_{i,j} = \begin{bmatrix} 1 & 0 \\ 0 & 30 \end{bmatrix} \text{ and } w^{\Delta u,alt}_{i,j} = \begin{bmatrix} 30 & 0 \\ 0 & 1 \end{bmatrix} \tag{5-2}$$

Note that these weights can swapped with each other without any numerical difficulties in the optimisation problem. This is possible due to the fact that in (4-31) scaling factors had been introduced to pre-scale the weights with each other relative to the sizes of the control actions in engineering units. Upon closer inspection of Figure 5-2 the effects of different weighting can be seen as the second plot shows that during simulation $q_{O_{2,alt}}$ fails to recover back to the steady state target value of 7 mol/s. This is due to the low weight of 1 on target tracking. In its turn, due to the higher amount of air flow, the temperature of the air results in a lower value and slightly returns back to its target value around t=1650.No severe difference can be seen on the rate of change however in both signals, this is due to the fact that although there are weights on the function, ΔT_a and Δq_{O_2} are limited by the physical properties of the cooling and pumping hardware. After laying down the broad aspect into what weight values had to be chosen in relation to each other, finer tuning was done to improve controller reactivity and steer control actions away from higher risk control situations. This process resulted in the weights displayed in (5-1) and has not been documented as it is considered to be highly subjective and simply a result of tedious adjustments of the weight parameters due to trail and error.

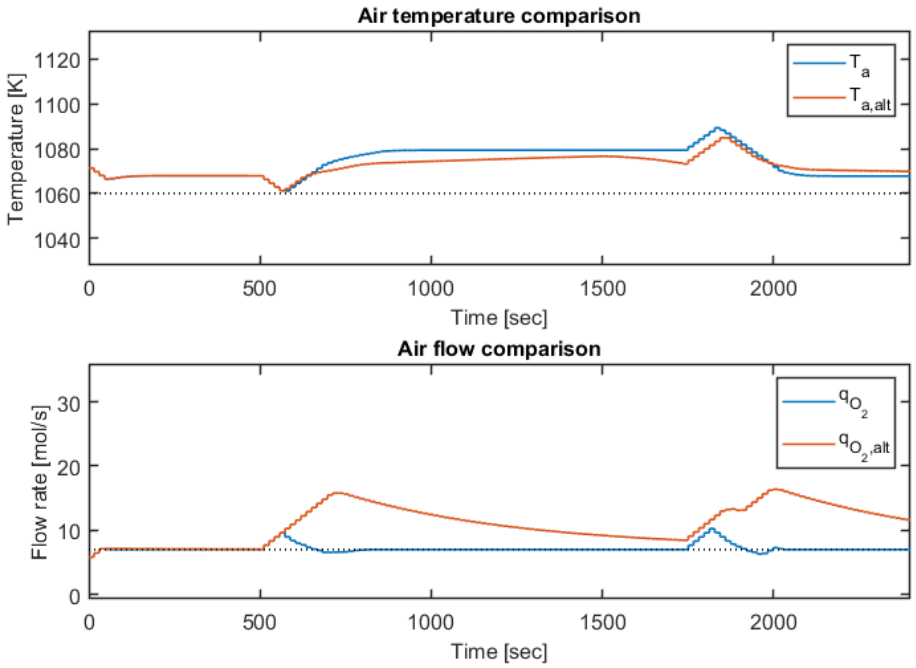

Figure 5-2: Effect of swapping weights on manipulated variables.

5-1-3 Adjustment of prediction horizon

In the centre of (N)MPC performance stands the choice of prediction and control horizons. This section will discuss the differences found in varying the prediction horizons for the MPC and the choice of horizon. For MPC tuning, especially for horizon adjustments it is recommended practice to fist define the control interval duration, analogue to sample time, and then hold it constant as the controller is being tuned. Qualitatively, as the control interval duration decreases the disturbance rejection properties of the controller improves. However, as it becomes smaller the computational intensity of the optimisation problem increases dramatically. Thus, requiring a trade-off between performance and computational effort. Furthermore there is a rule of thumb to set the sample time T_s between 10% and 25% of the required or desired closed-loop response time [98]. Using the set state trajectory specifications from Equation (4-26), the reference temperature will at most change with 5 K as a step input. With the temperature gradient change set at 2 K/min, the optimal response time would be 150s resulting in a $T_{s,10\%}$ value of 15s. For anti-aliasing and error mediation purposes in line with the Nyquist theorem [99], half a second was added, setting T_s to 15.5s. Taking the slow time dynamics of the system into account this value was considered to be more than reasonable, thus taking the minimum 10% into account for accuracy whilst relieving the processor of unneeded computational efforts.

For control the prediction horizon, N, is the number of future control actions the MPC evaluates by prediction whilst optimising the manipulated variables at every control interval k. Correspondingly, the the control horizon, M, is the number of control actions that are optimised at every control interval. The value of $M \leq N$. For MPC a small M and N will result in a smaller amount of variables to be computed in the quadratic problem solver at each control interval, thus improving computation time.

Figure 5-3 gives an overview of the behaviour of the controlled plant subject to different prediction horizons. What immediately can be seen is that the shortest prediction horizon shows the fastest response but has unwanted overshoot characteristics. The longest prediction horizon $N = 24$, shows a much slower response but appears to make more efficient use of the control resources as the temperature gradient is the lowest of all. For brevity, the entire set of plots is not shown here but can be inspected in the Appendix A. Regarding computational load; $N = 24$ proved to be very time consuming with a 2400s simulation requiring more than 15s of computation time. Therefore a shorter prediction horizon was chosen which was $N = 12$ in this case as it showed a desirable response time and no overshoot or under dampening. At last manipulated variable blocking was implemented on the controller as it is documented to have advantages in tuning flexibility, controller robustness.

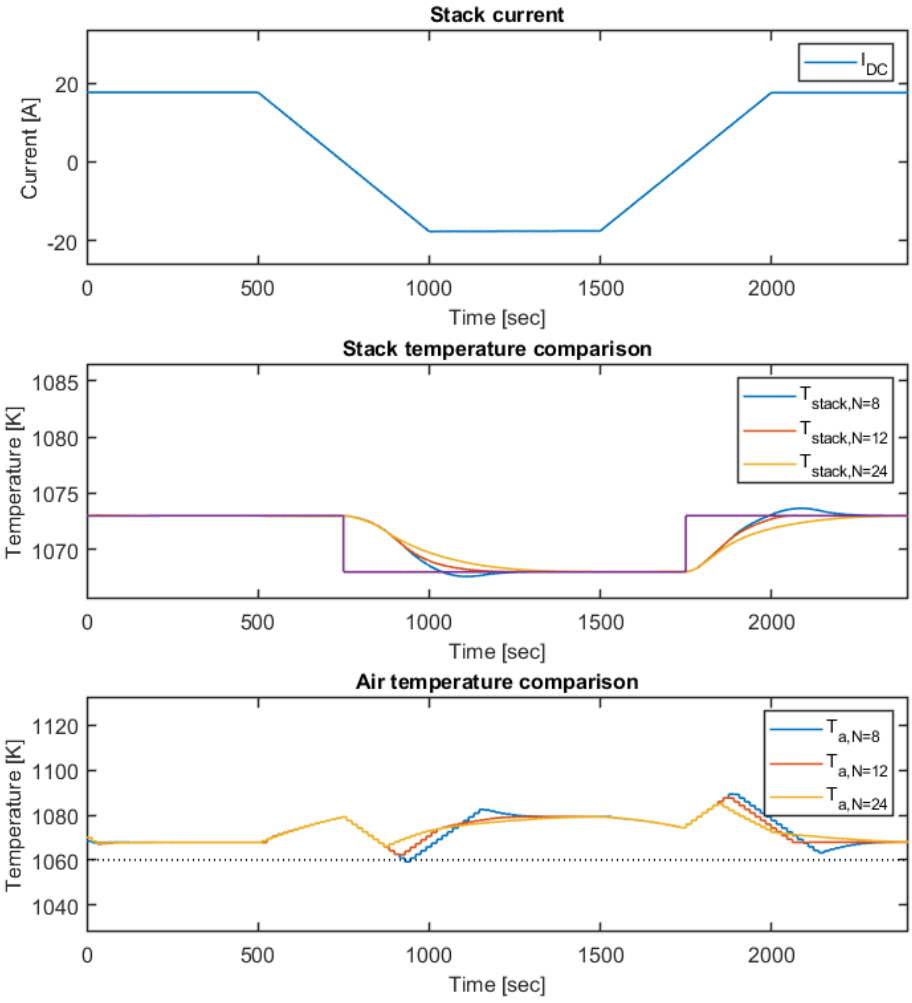

Figure 5-3: Effect of increasing prediction and control horizon.

5-2 Scenario 2: Long term

For the final scenario the entire system was simulated as if it was part of a micro grid. To do so, all the model and control work was confined into one single Simulink block and placed into a microgrid structure developed by Matlab as part of the Simscape specialised power systems package. As depicted in Figure 5-4, the power grid defaultly consists out of 3 loads that resemble houses, a battery and a solar panel connected via a pole mounted transformer to the main power grid. In this system the battery functions as a temporary energy storage of solar powered energy in the micro grid during the day, releasing it back into the surrounding electric loads when it is required during a power shortage. As one might expect, for this study the micro grid was adjusted by removing the conventional battery and replacing it with a RSOFC and a power controller.

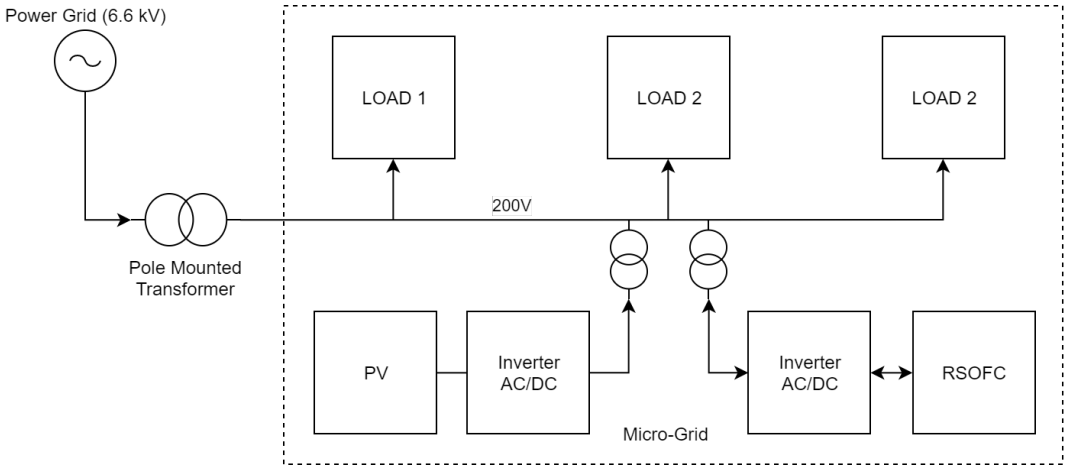

Figure 5-4: Schematic overview of RSOFC connected to a Micro-grid.

5-2-1 Micro-grid simulation

As can be seen in Figure 5-5, the generated amount of solar power varies through the day. The curve represent the common form as illustrated by Vincent [100] and the data is taken from a micro-grid model by Hiroumi Mita [101]. At night, the solar panels generate no power but at 2 to 3pm they reach a peak power generation of nearly 5kW. The houses are simulated to behave and show the typical power consumption over the course of the day. The power demand can be seen spiking in the morning when people wake up and during the evening hours at 8 and 10pm with a consumption of more than 4kW. In the micro-grid, the power controller of the RSOFC performs as an ideal power inverter and converts the output voltage to 200V AC. Furthermore it functions as a tracking control of the micro-grid current so that it can control the amount of current from the main grid entering the system and set it to zero to make the RSOFC supply the total power demand in the micro-grid. As a way of simulating a disturbance, a circuit breaker is toggled at 8am, causing a spike in micro-grid current.

If P_{solar} is subtracted from the total load P_{load} the total energy demand and surplus is derived. In figure 5-6 the amounts are displayed and although not created on purpose, the power curve over the day gives three different operation modii for the RSOFC stack. The first region is

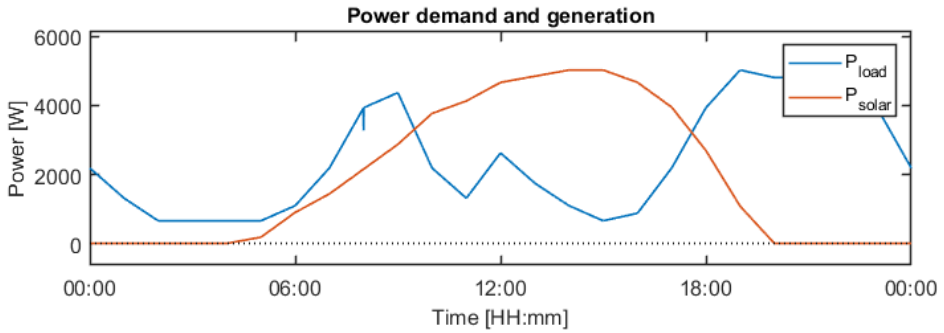

Figure 5-5: Power demand and generation of solar panels and loads.

at night from 0am to 6am where the power demand is low and (nearly) no solar power is generated. If the RSOFC stack is to operate in these hours, it is forced to produce a small amount of power, resulting in the stack needing to be heated in SOFC mode which is not ideal. The second region is from 9:30am to 5:30pm and is coloured green where the RSOFC operates is SOEC mode, with at last region 3 from 5:30pm to 12pm in SOFC mode.

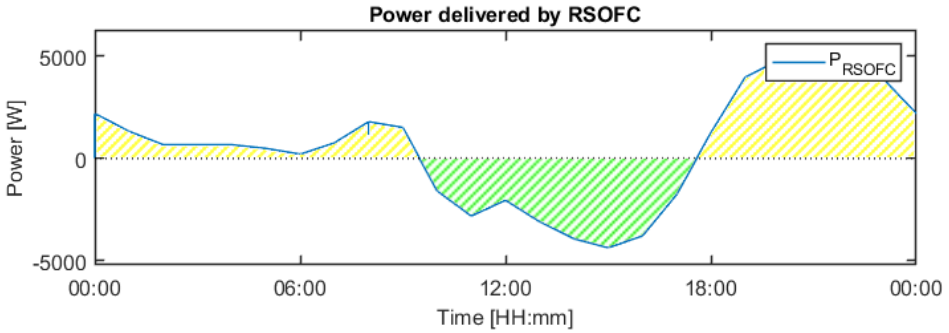

Figure 5-6: Power storage and generation of RSOFC.

In addition to to these plots, similar plots were generated to show the system and controller behaviour over the span of 24hours instead of 2400 seconds. Speaking in more abstract terms, next to the longer duration, the simulation differs from the previous tests as the current does not show any step-input behaviour next to the delta pulse due to circuit breakers at 8am. Furthermore the reference temperature relatively changes less compared to earlier, resulting in the air flow being able to be at it's manipulated variable target of 7 mol/s throughout the day except during the stack operation mode changes. The satisfactory performance of the controller considering the objectives from Section 4-1 on ΔT_{max}, $T_{a,min/max}$ can be inspected in Figure 5-7, showing $T_{a,min/max}$ being achieved at less than 10 K difference instead of the required 20.

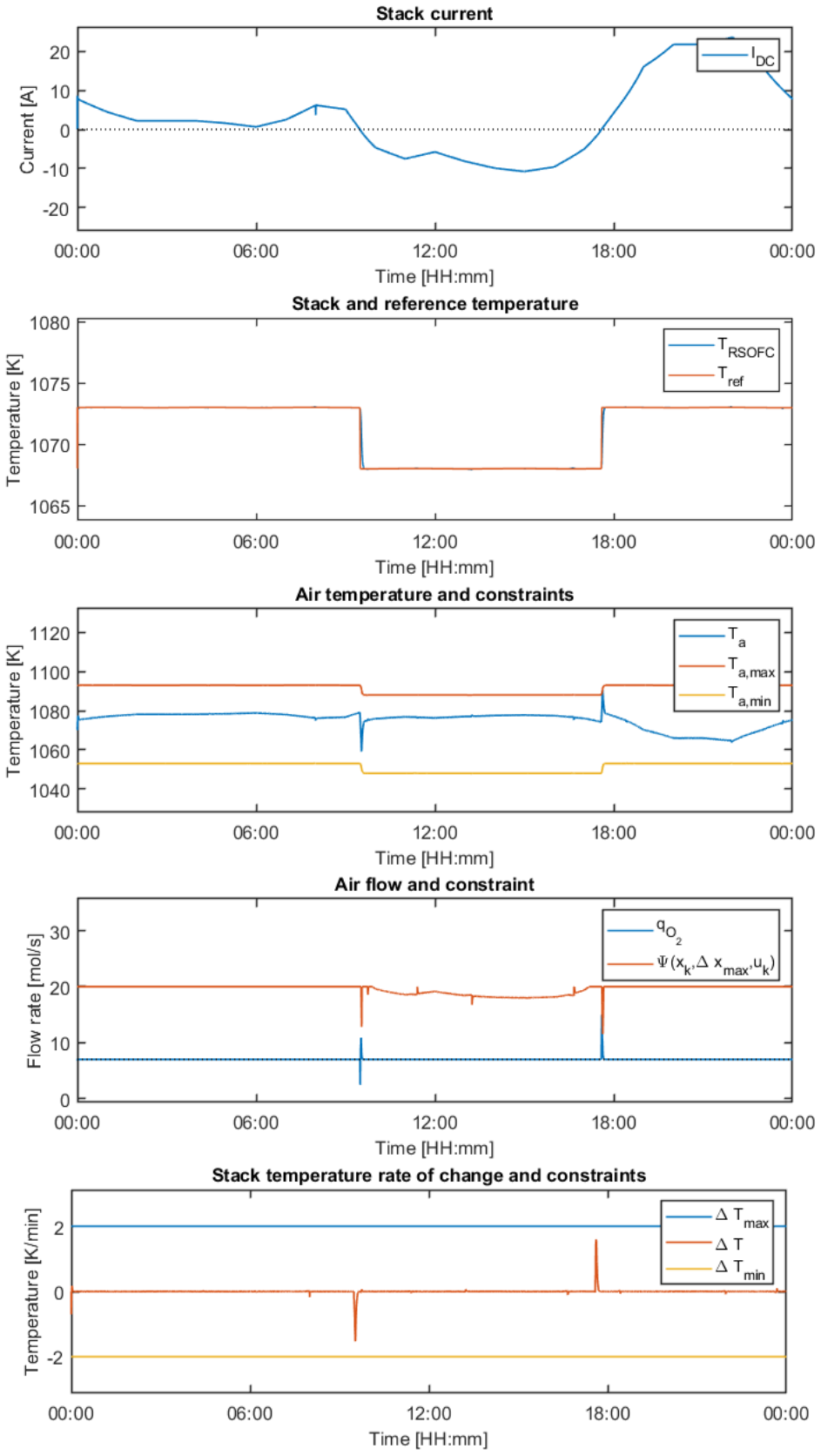

Figure 5-7: Effects of varying the prediction and control horizon.

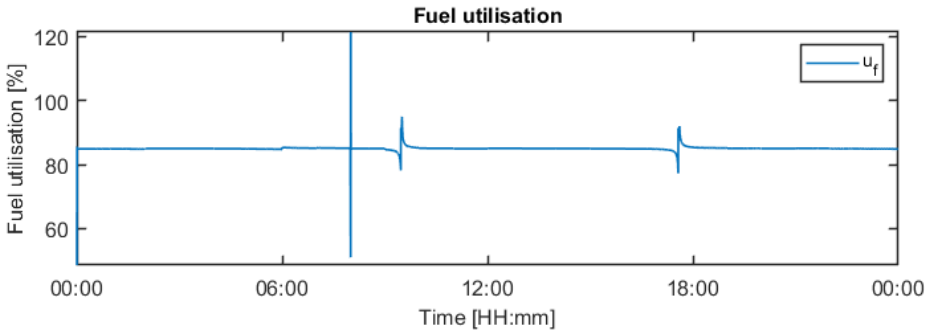

Figure 5-8: Fuel utilisation of RSOFC.

Next to control the objectives on the stack temperature, temperature gradient and air temperature, two other objectives were set on fuel utilisation and maintaining the required power output. In Chapter 3 the fuel utilisation factor of the stack was defined as u, where u is the ratio of reacting hydrogen and injected fuel flow into the stack. Prior to controller synthesis the desired hydrogen fuel input $q_{H_2}^{in}$ was defined as a function of K_r, I and u, rendering the fuel utilisation already set without any control. In Figure 5-8 it can be seen that the fuel utilisation is held at 0.85, 85%, throughout the entire simulation, except for 3 times. The first time the fuel utilisation target is violated is during the moment a load is removed for 10 seconds by a breaker resulting in a spike of $\pm$ 35%. The second and third spikes are due to the current and voltage behaviour that is created by the model when the current approaches and moves away from 0 A. This effect can also be seen in Figure 5-9, but can be neglected in terms of operational safety as fuel flow and current are nearly zero. The peak fuel utilisation peak at 8am, does ask for better fuel utilisation or voltage control however and will be discussed later on.

As a follow-up to a discussion in Chapter 3, Section 3-4 on the differences between the output voltage in this study in comparison to other studies, the result of the use of a dynamic partial pressure calculation can be seen again in the transient behaviour of the voltage in Figure 5-9. To prove that in the voltage drops during the operation mode switching has has no effect, it can be seen that during the drops in Figure 5-9, the power curve in Figure 5-6 is smooth.

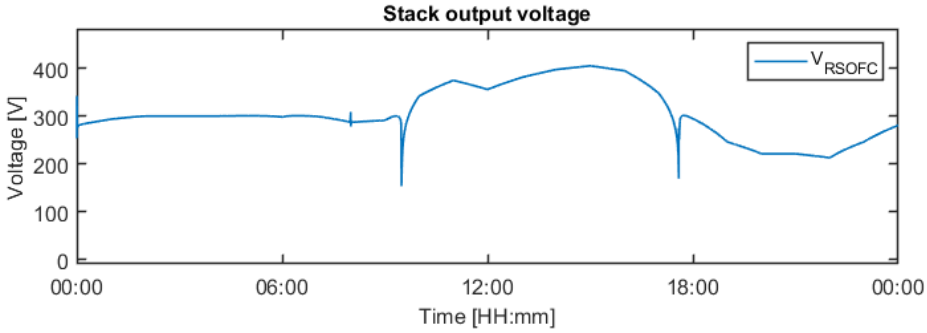

Figure 5-9: Output voltage of RSOFC.

As introduced at the start of this scenario, RSOFC technology has the potential to play a major role in electrical energy storage. By coupling the the fuel producing and power producing modes a stand-alone energy storage system can be developed with the use of

intermediate storage of the hydrogen in tanks. For this study a hydrogen tank was modelled that stores a 1000 moles of pure hydrogen at 25 $°C$ and 300 bar. For the storage a tank of more than 82.6 L is required to store the 2.015 kg of hydrogen. Purely for illustration, in Figure 5-10 it can be seen that initially the tank is filled at 70% of its capacity at 12pm and is slowly filled and depleted over the course of the day. Please note that the values depicted in Figure 5-10, assume that the system is 100% efficient in storing and releasing the hydrogen energy, whilst round trip efficiencies of 60 to 70 % have been reported by other studies [102]. Problems arise as the hydrogen tank does not have the same amount of hydrogen stored at the end of the day as the beginning. As expected, this results in the storage not being feasible to be used as the main power supply of the micro-grid during weekly operation and will require to be scheduled. Scheduling of the RSOFC thus offers a valuable subject of RSOFC modelling and control for future work, together with coupling it to a first principles model of an AC/DC inverter to fully investigate the micro-dynamics of the RSOFC subject to grid fluctuations and discrete power control of IGBT transistors.

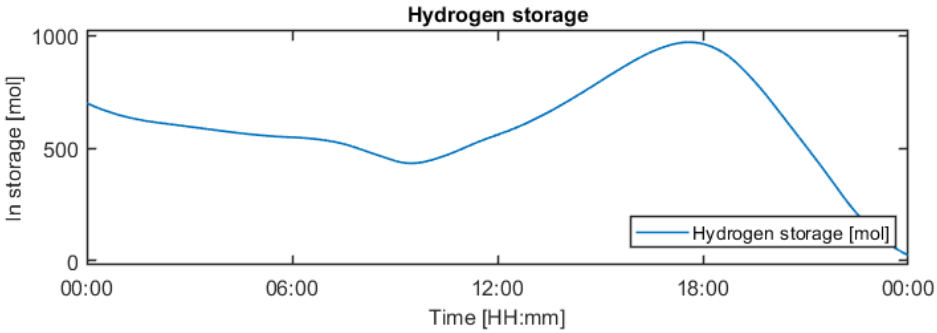

Figure 5-10: Remaining amount of hydrogen in storage.

Chapter 6

Conclusion

In this chapter an overall conclusion will be given on the research done in this study. Furthermore, recommendations will be done together with a discussion on possible improvements or additions to the currently developed model and control schemes.

6-1 Conclusions

This paper provides a comprehensive review of recent developments in RSOFC dynamic modeling and control. The study documentation was structured in such a manner to aid others in the process of creating a model and controller similar to the one presented in this work. First, background information was given on the topic the research is focused on. A brief history of fuel cells was given, giving several types of fuel cells that are being studied and commercialised up to today, later giving a comparison of the fuel cells with each other and key characteristics that define them and render some suitable for specific applications.

After introducing the solid oxide fuel cell, an in depth description was given on the technology with its build structure possibilities and materials. Next, a foundation was provided on the main acting chemical reactions with their corresponding thermodynamical relations. The workings of SOECs and RSOFCs were discussed and the role of polarisation losses during fuel cell operation. An overall system description was given including auxiliary systems, balance of plant, required for the RSOFC to operate. Next to the balance of plant another crucial subsystem for grid connection was introduced, namely the power conditioning unit and its workings.

In the next chapter, Modeling, the need of modelling of an RSOFC with a definition of the model and its requirements were introduced. A path was set for the development of a novel state-of-the-art model and assumptions were listed for system operation. The conceptualisation of the model was followed by a review of model dynamics and research done on solid oxide cells. The dynamic modelling was split into several sections consisting out of the Nernst equation followed by the polarisation, voltage and thermal dynamics of the system. Proposals

were made on how to model certain aspects of the system and the development of said model was documented.

From literature studies it was found that careful consideration should be given to the thermal dynamics of an RSOFC system. Many literature written on RSOFC modeling did not take full account of the effects of temperature on polarisation losses. From SOFC literature solutions were found, which were integrated into the RSOFC. Furthermore no RSOFC model was found to be able to model the temperature-temporal effects of air cooling with a stand alone controller, this was implemented too in the developed RSOFC model.

After the model was developed, thorough validation was done with other literature. To do so, a set of fitting parameters has been distilled from literature to create a good overlap with other studies and are combined in a manner that they can be implemented in other work. As useful results on RSOFCs in the transient domain are rare; the results presented in this study are of considerable value as the steady state dynamics and the transient dynamics have shown a good match to the available literature. Another contribution to literature is the development of a parametric state-of-the-art model of an entire RSOFC stack that can continuously simulate the operation and transition of both SOFC and SOEC modes. Additionally, the model offers useful insight into RSOFC (transient) dynamics with relation to temperature effects, fuel composition and cell support structure, which has not been documented before. At last the RSOFC stack, together with the developed model has been built in a plug-and-play manner that it can be implemented and adjusted by others, to be used in combination with other models such as grid-tied IBGT based inverters.

To recap and compare to the set model requirements in Chapter 3, the developed model is able to:

- ✓ be parametric to enable scaling and easy adjustment for later use. All the equations and relations are parametric, allowing for easy adjustment. Furthermore parameter sets have been given to switch, for example between anode and cathode supported RSOFCs.
- ✓ provide continuous simulation of RSOFC dynamics during and between SOEC and SOFC states. Validation has presented the models capability to move from one mode to the other whilst supplying a smooth power output.
- ✓ justify temperature changes due to electro-chemical reactions. Temperature changes in quantity and in rate have successfully been validated against written literature. Showing temperature increasing by more than 2.6 K/min without control.
- ✓ provide an input and output interface to dynamically control RSOFC model behaviour. Internal components of the model have been created as modules just like the model itself, hereby creating a (Simulink) block that is easily implemented for other studies with current as single input to the system.
- ✓ be able to be coupled to an AC utility grid. The model and controller have successfully been integrated and modeled as part of a micro-grid.

Chapter 4 focused on the control of a reversible solid oxide cell when being submitted to varying load requests and demands. First the control objectives and constraints were introduced to provide the reader with foundation to why certain types of control are of interest for this

study. With the control requirements the main research question was translated from the control objective in aid of the thesis that is to be written during the project:

How can an advanced control strategy for a reversible solid oxide fuel cell in a grid ensure load tracking whilst maintaining fuel utilisation and temperature dynamics within a safe range?

Next various possible control schemes were be introduced to give an understanding of key control principles. Control techniques such as PID or (N)MPC control were given with a discussion on their relevancy to fuel cell control. The chapter concluded with a review of written literature on the control of (solid oxide) fuel cells combined with a proposal on controllers.

From the literature review it was concluded that MPC control seems very favourable for RSOFC control. MPCs have proven to show superior performance compared to PIDs when it comes to handling constraints an nonlinearities. It was found however that if MPC is to be employed, model accuracy combined with proper state estimation is essential for controller realism and performance. No specific control model was found to take transition speeds into account of RSOFC systems and constraints on temperature, temporal temperature gradients and pump dynamics; proving this is of interest to study. The controller implemented was structured in a manner according to a "fuel cell follows inverter" principle as this created a controlled model more easily implemented in other studies and with a scope on temperature control.

As result, in this study an output-feedback adaptive nonlinear model predictive controller has been developed, which is an advanced version of the well established (non)linear model predictive controller. Chapter 4, describes the development of the temperature controller wherein the structure of the MPC is introduced together with its trajectory, adaptive constraints and tuning variables such as weighting matrices and slack variables. After completing the development of the controller, simulations were done together with the model from Chapter 3 to inspect the control performance and to provide useful insights into its behaviour. The simulations were split up into short and long term scenarios and showed satisfactory results as all the set control objectives were achieved in both scenarios, which is presented below with the controlled model being able to:

- ✓ maintain required power output to its desired level. As can be seen from all the plots in both scenarios, the RSOFC follows the reference current.
- ✓ keep the cell temperature between maximum and minimum operating limits.
- ✓ keep temperature change of stack below 2 degrees Celsius per minute: Under various scenarios the temperature gradient does not exceed 2 K/min due to the developed adaptive output-feedback constraints on temperature rate of change.
- ✓ keep temperature difference between fuel inlet and air inlet within 20 degrees Celsius: Within these boundaries the controller achieves the control objective.
- ✓ keep the fuel utilisation within optimal operating limits of 0.7 and 0.9 for all power outputs: Although spikes can be seen, the fuel utilisation is rapidly corrected to 0.85.

6-2 Recommendations

Significant differences between the proposed model and other research have been mainly stemming from choices made in model inclusion. The model proposed for this research for instance includes time delayed dynamics such as pumps starting up, but not residual pressure gradients from compressors shutting down or delays from heat exchangers. With the stack model finished, it is of interest to include the dynamics of more BoP elements introduced in Chapter 2. Further more it might be of interest to include efficiencies and the power consumption of the entire BoP and RSOFC to compute round trip efficiencies of the system and determine optimal operation conditions for the temperature controller.

Considering the model, two hardware additions might be of interest:

The first hardware addition that may be considered is the inclusion of heat storage. Heat storage enables RSOFCs to store excess heat into metal reservoirs for use later on, instead of flushing it away as exhaust. The addition of heat storage also increases the thermal capacity resulting in a lower temporal temperature gradient without control.

Secondly, an ultra-capacitor can be used in parallel with the fuel cell as buffer and auxiliary power source. If there were to be a sudden increase in the demand of current from the grid, the capacitor could step in an share the increase load by releasing its stored energy. Instead of sudden drop in the stack voltage, the voltage would drop more gradually giving the controller more room to to bring the temperature and temperature gradient back to its reference value by increasing air flow rates within its constraints.

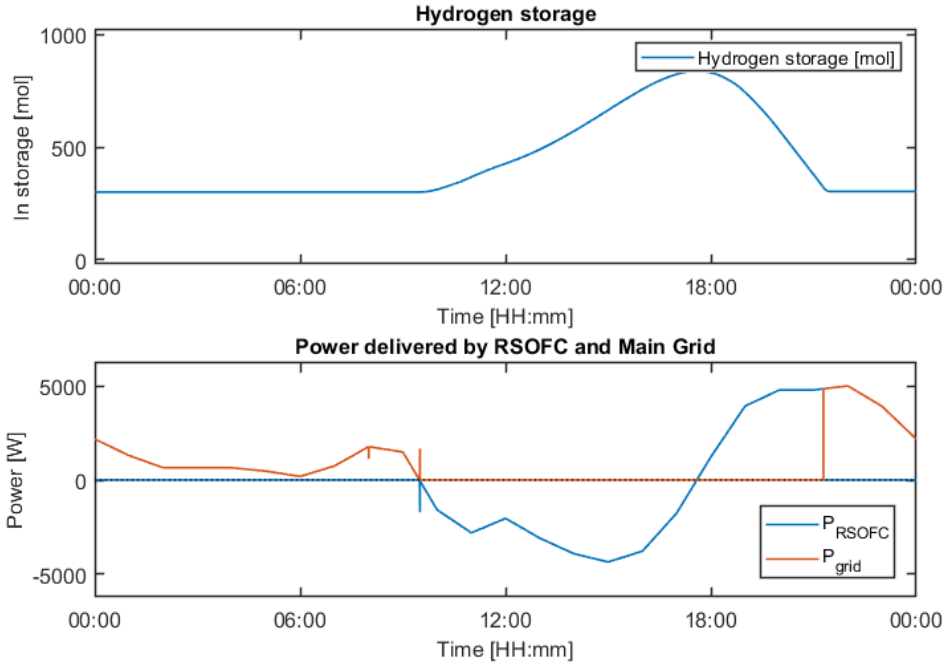

Figure 6-1: Hydrogen storage and power during RSOFC scheduling

The last chapter ended with the illustration of hydrogen storage by the RSOFC stack. It also recommended scheduling the RSOFC storage. To illustrate the potential of scheduling the RSOFC storage, the previous plots show the RSOFC storage being turned on or off

throughout the progress of the day. During the operation over several days, the decision can be made to turn the RSOFC of during night from 12pm to 8am and turn on at SOEC mode to store the excess solar energy. The figures in 6-1 show the hydrogen storage levels being kept stable over the span of the day and the battery power generation and storage taking over the grid power supply. During the time the storage is turned off, the RSOFC stack will be held at 1068K with air or heat storage. In order to make the stored amount of hydrogen stay constant at the end of the day; the RSOFC would subsequently turn off again if the hydrogen storage level depleted back again to its initial storage value at night. These kind of optimisations can be researched, where machine learning with artificial neural networks could provide the improvements.

Appendix A

Complete plot sets

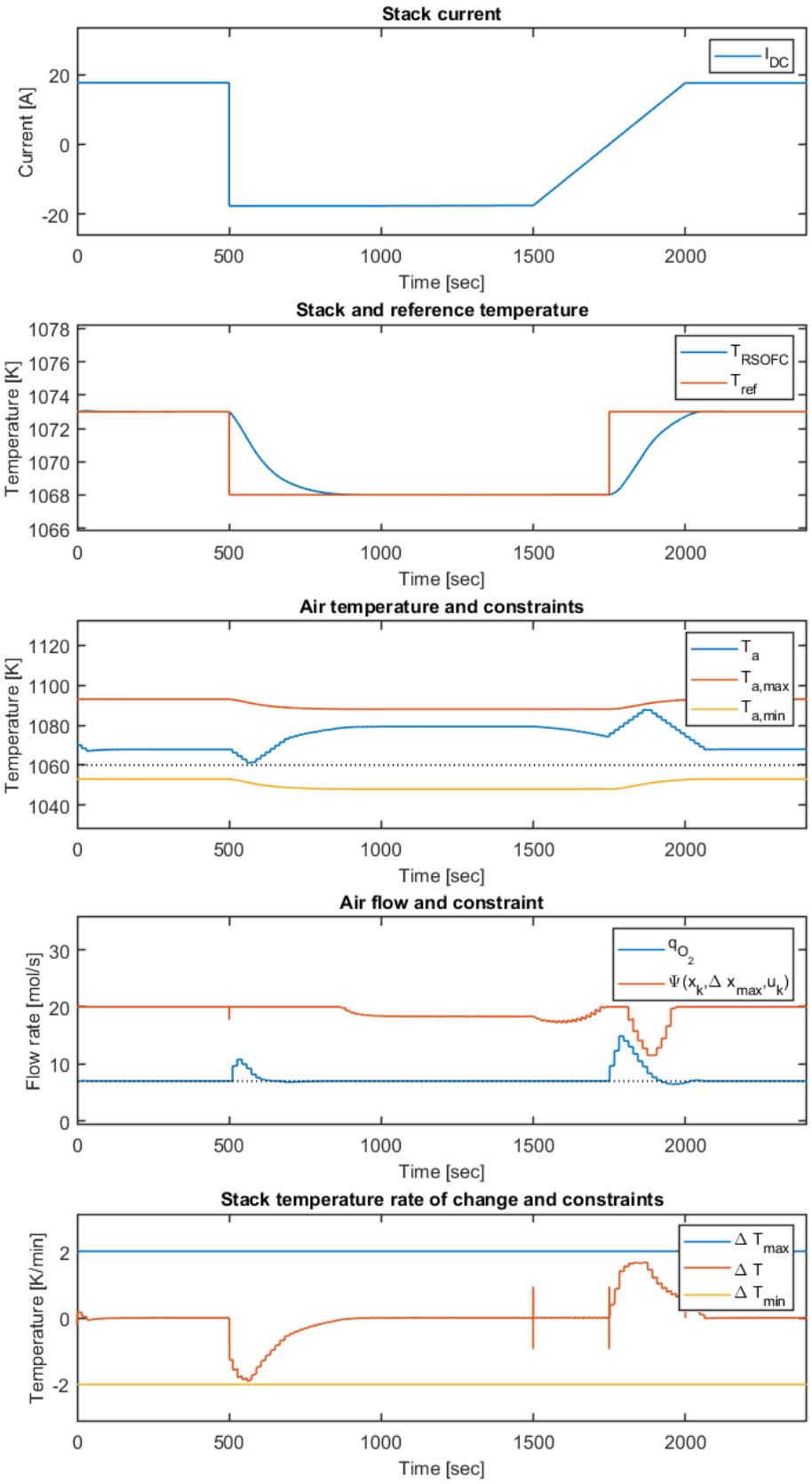

Figure A-1: Chosen, default control results

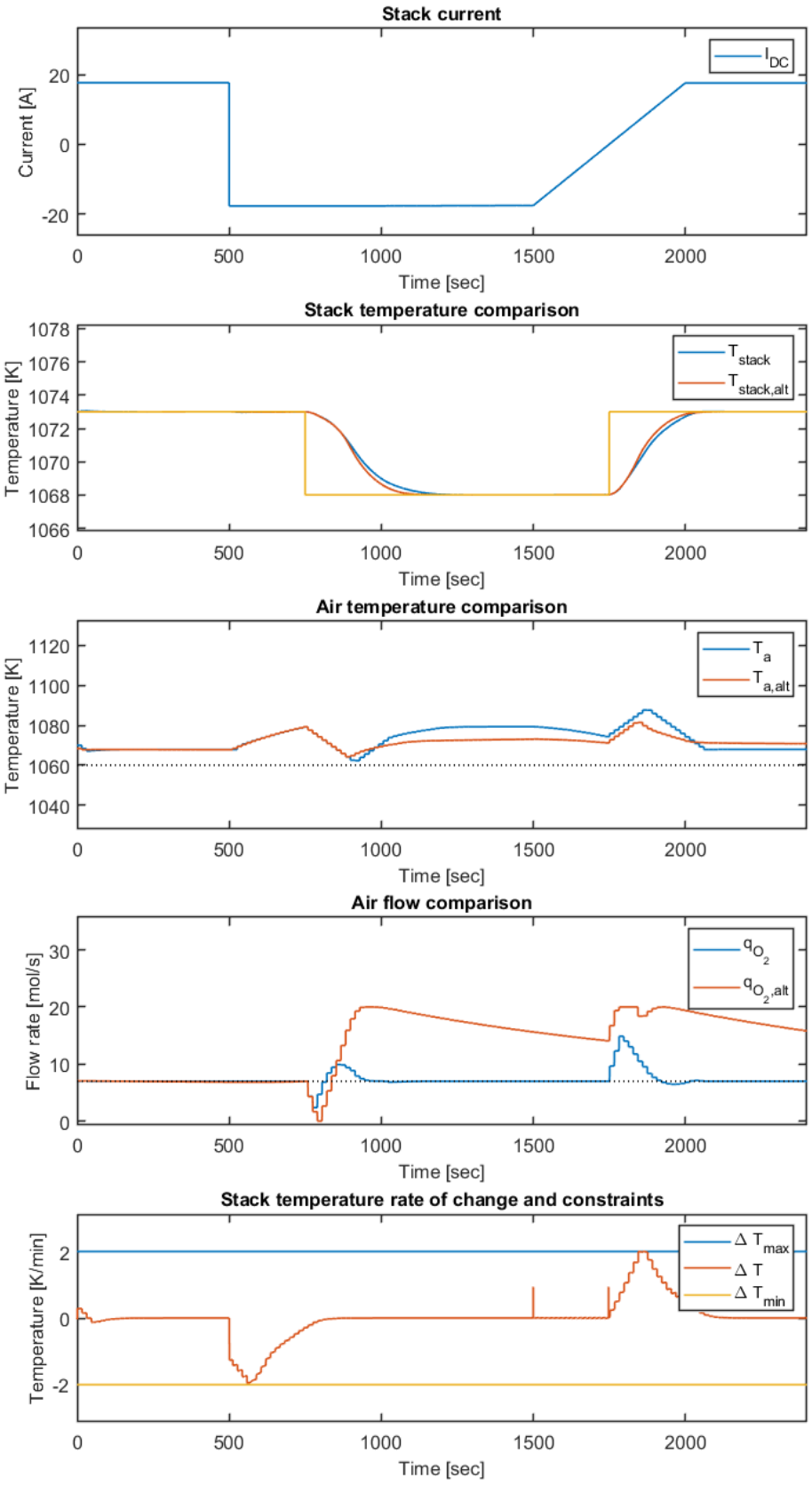

Figure A-2: Control results subject to weight variation

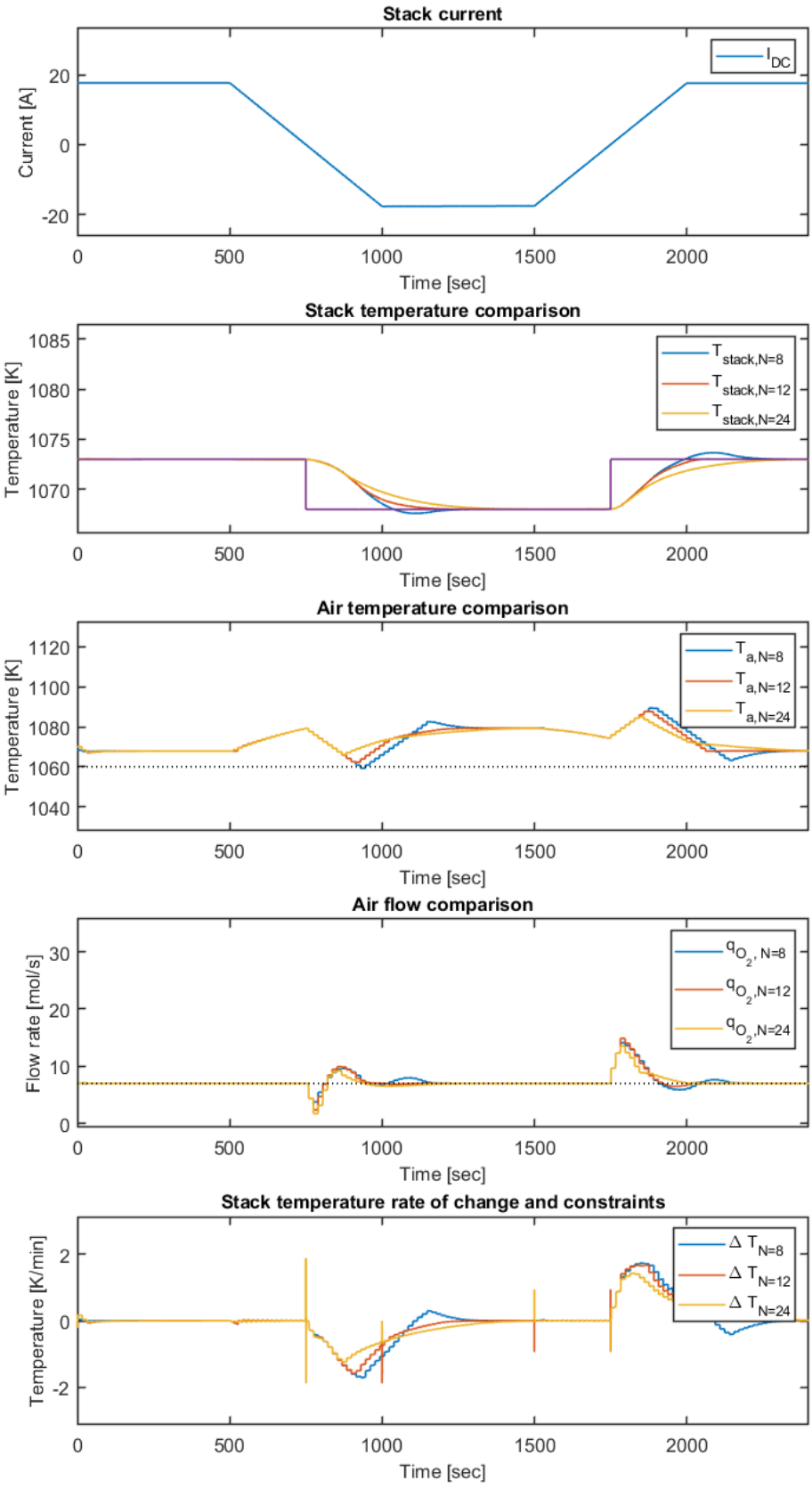

Figure A-3: Control results subject to horizon variation

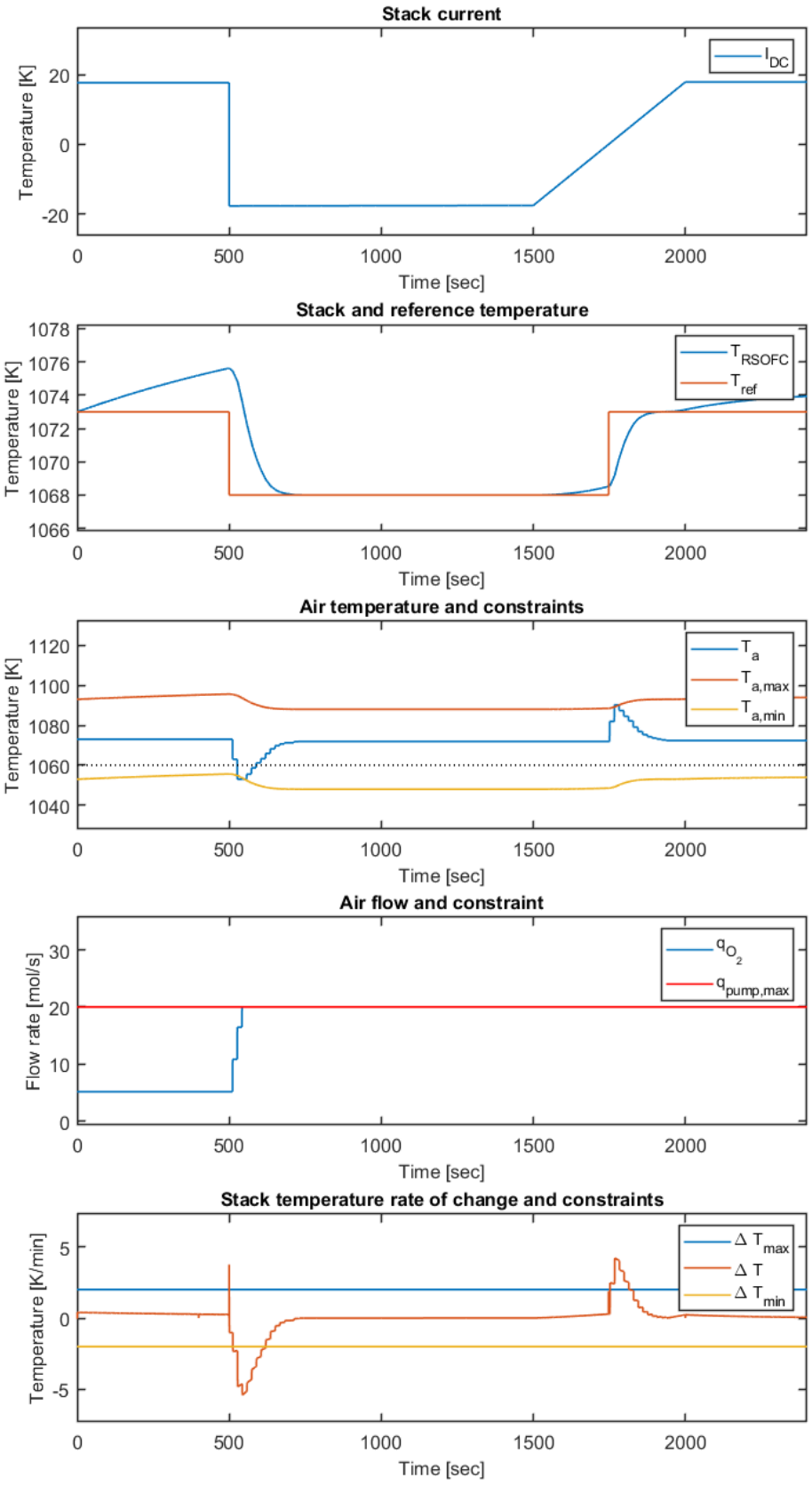

Figure A-4: Control results without adaptive control

Bibliography

[1] N. Mahato, A. Banerjee, A. Gupta, S. Omar, and K. Balani, "Progress in material selection for solid oxide fuel cell technology: A review," *Progress in Materials Science*, vol. 72, pp. 141 – 337, 2015.

[2] Koyama, "Solid oxide fuel cells." http://www.aki.che.tohoku.ac.jp/ koyama/html/research/SOFC.html, 2003. (Accessed on 12/10/2018).

[3] h2e Power Systems Inc, NEW YORK, NY, "Solid oxide fuel cell technology, webpage." http://h2epower.net/technology/, 2019. (Accessed on 01/21/2019).

[4] J. Ren, "Modelling and optimisation of the dynamic performance of a reversible solid oxide fuel cell system for the grid integration of renewables, university of strathclyde electronic and electrical engineering department," Jan 2013.

[5] Y. Hajimolana, "rSOC system design and operation, handout thesis kick-off meeting," 2018.

[6] N. Amin, "Single phase full h-bridge inverter simplified, slideshare," p. 1, 08 2017. (Accessed on 01/10/2019).

[7] Haitham Abu-Rub, Atif Iqbal, and Jaroslaw Guzinski., "Pulse width modulation of power electronic dc-ac converter," in *High Performance Control of AC Drives with MATLAB/Simulink Models, First Edition,John Wiley & Sons, Ltd.*, vol. 1, pp. 1–44, Sep. 2012.

[8] J. Padulles, G. Ault, and J. McDonald, "An integrated sofc plant dynamic model for power systems simulation," *Journal of Power Sources*, vol. 86, no. 1, pp. 495 – 500, 2000.

[9] M. Ni, M. K. Leung, and D. Y. Leung, "Parametric study of solid oxide fuel cell performance," *Energy Conversion and Management*, vol. 48, no. 5, pp. 1525 – 1535, 2007.

[10] M. Ni, M. K. Leung, and D. Y. Leung, "A modeling study on concentration overpotentials of a reversible solid oxide fuel cell," *Journal of Power Sources*, vol. 163, no. 1, pp. 460 – 466, 2006. Special issue including selected papers presented at the Second International Conference on Polymer Batteries and Fuel Cells together with regular papers.

[11] J. Ren, A. J Roscoe, S. Gamble, and G. Burt, "Modeling a reversible solid oxide fuel cell as a storage device within ac power networks," vol. 12, pp. 1 – 6, 05 2010.

[12] O. Z. Sharaf and M. F. Orhan, "An overview of fuel cell technology: Fundamentals and applications," *Renewable and Sustainable Energy Reviews*, vol. 32, pp. 810 – 853, 2014.

[13] W. Ostwald, *Electrochemistry: history and theory*. Electrochemistry: History and Theory, Published for the Smithsonian Institution and the National Science Foundation by Amerind Pub. Co., 1980.

[14] H. Behret, "Fuel cells and their applications, vch, weinheim, 1996. isbn 3-527-28579-2, dm 248," *Berichte der Bunsengesellschaft fur physikalische Chemie*, vol. 100, no. 11, pp. 1922–1922.

[15] J. M. G. Hacker, Barton C, *On the Shoulders of Titans: a history of Project Gemini, NASA Special Publication-4203*. 1977.

[16] M. M. Mench, *Fuel Cell Engines - Matthew M. Mench - Google Boeken*. John Wiley and Sons, April 2008. (Accessed on 11/19/2018).

[17] K. A. Adamson, G. Crawley, and D. Jollie, "Fuel cell today 2004 worldwide survey," Fuel Cell Today, 2004.

[18] X. Huang, Z. Zhang, and J. Jiang, "Fuel cell technology for distributed generation: An overview," in *2006 IEEE International Symposium on Industrial Electronics*, vol. 2, pp. 1613–1618, July 2006.

[19] "Review of state-of-the-art fuel cell technologies for distributed generation, a technical and marketing analysis," *Wisconsin, USA: Energy Center of Wisconsin*.

[20] C. Polat, "Market opportunities for hydrogen solid oxide fuel cells (SOFC): A review of the literature and the future market trends.," p. 6, 06 2008.

[21] M. W. Ellis, M. R. V. Spakovsky, and D. J. Nelson, "Fuel cell systems: efficient, flexible energy conversion for the 21st century," *Proceedings of the IEEE*, vol. 89, pp. 1808–1818, Dec 2001.

[22] Office of energy efficiency and renewable energy, "FCTO Comparison of Fuel Cell Technologies," p. 1, US Department Of Energy, 04 2016.

[23] J. M. p. Fuel Cell Today Limited, "Fuel cell technologies, overview," p. 1, 01 2019.

[24] Z. Binti Awang Mat, M. , B. K. Yap, S. Hasmady, and N. Talik, "Proton exchange membrane (pem) and solid oxide (sofc) fuel cell based vehicles-a review," pp. 123–126, 09 2017.

[25] J. Boyd, "Home fuel cells to sell in japan," *IEEE Spectrum*, vol. 45, pp. 14–14, 10 2008.

[26] Office of energy efficiency and renewable energy, "Fuel Cell Technologies Program, Types of Fuel Cells," p. 23, US Department Of Energy, 06 2009.

[27] UTC Power, a United Technologies Company, "PureCell 400 system specifications," p. 14, UTC Power, a United Technologies Company, 05 2011.

[28] T. Elmer and S. B Riffat, "State of the art review: Fuel cell technologies in the domestic built environment," 08 2012.

[29] A. Hawkes, I. Staffell, D. Brett, and N. Brandon, "Fuel cells for micro-combined heat and power generation," *Energy and Environmental Science - ENERGY ENVIRON SCI*, vol. 2, 01 2009.

[30] S. Mukerjee, R. Leah, M. Selby, G. Stevenson, and N. P. Brandon, "Chapter 9 - life and reliability of solid oxide fuel cell-based products: A review," in *Solid Oxide Fuel Cell Lifetime and Reliability* (N. P. Brandon, E. Ruiz-Trejo, and P. Boldrin, eds.), pp. 173 – 191, Academic Press, 2017.

[31] H. Ono, T. Sonoda, Y. Ohtani, H. Kuraseko, M. Noda, and S. Hasebe, "Optimal start-up operation for fuel cell systems," *KAGAKU KOGAKU RONBUNSHU*, vol. 29, 07 2003.

[32] M. L. M. Zuo, Chendong Liu, "Solid oxide fuel cells. sol-gel processing for conventional and alternative energy.," 2012.

[33] E. A. Guggenheim, *Thermodynamics, Classical and Statistical*, pp. 1–118. Berlin, Heidelberg: Springer Berlin Heidelberg, 1959.

[34] D. T. Hawthorn, "Chemistry, third edition (zumdahl, steven s.)," *Journal of Chemical Education*, vol. 71, no. 3, p. A82, 1994.

[35] M. A. Matthews, "A to z of thermodynamics by pierre perrot (universitat des sciences et technologies de lille). oxford university press: Oxford, new york, and tokyo. 1998. vi + 329 pp.," *Journal of the American Chemical Society*, vol. 122, no. 15, pp. 3799–3800, 2000.

[36] R. E. J.H. Hirschenhofer, D.B. Stauffer and M. Klett, *Fuel Cell Handbook, 4th Edition*. Parsons Corporation, 1998.

[37] M. Hauck, S. Herrmann, and H. Spliethoff, "Simulation of a reversible sofc with aspen plus," *International Journal of Hydrogen Energy*, vol. 42, no. 15, pp. 10329 – 10340, 2017.

[38] A. M. Sharaf and A. A. A. El-Gammal, "A smart dynamic electric energy conservation vsc-self regulating controller for micro hydro-fuel cell green scheme," *2010 Fourth Asia International Conference on Mathematical/Analytical Modelling and Computer Simulation*, pp. 424–430, 2010.

[39] Y. Sun, Y. Liu, M. Su, X. Wenjing, and J. Yang, "Review of active power decoupling topologies in single-phase systems," *IEEE Transactions on Power Electronics*, vol. 31, pp. 1–1, 01 2015.

[40] K. Mertens, "Photovoltaics: Fundamentals, technology, and practice, 2nd edition," pp. 233–339, May, 2018.

[41] Unknown Author, "Chapter 3, Cascaded H-Bridge Multilevel Inverter.," p. 1, 01 2018.

[42] S. J. Lee, H. S. Bae, and B. H. Cho, "Modeling and control of the single-phase photovoltaic grid-connected cascaded h-bridge multilevel inverter," in *2009 IEEE Energy Conversion Congress and Exposition*, pp. 43–47, Sep. 2009.

[43] D. G. Holmes and T. A. Lipo, *Modulation of Three Phase Voltage Source Inverters*. IEEE, 2003.

[44] Guillaume Dubois, *Modeling and Simulation : Challenges and Best Practices for Industry, First edition*. CRC Press, 2018.

[45] S. A. Hajimolana and M. Soroush, "Dynamic behavior and control of a tubular solid-oxide fuel cell system," *2009 American Control Conference*, pp. 2660–2665, 2009.

[46] B. Tjaden, M. Gandiglio, A. Lanzini, M. Santarelli, and M. JÃČÂđrvinen, "Small-scale biogas-sofc plant: Technical analysis and assessment of different fuel reforming options," *Energy & Fuels*, vol. 28, no. 6, pp. 4216–4232, 2014.

[47] G. Botta, M. Romeo, A. Fernandes, S. Trabucchi, and P. Aravind, "Dynamic modeling of reversible solid oxide cell stack and control strategy development," *Energy Conversion and Management*, vol. 185, pp. 636 – 653, 2019.

[48] Y. Zhu and K. Tomsovic, "Development of models for analyzing the load-following performance of microturbines and fuel cells," *Electric Power Systems Research*, vol. 62, no. 1, pp. 1 – 11, 2002.

[49] J. Ren, A. J. Roscoe, S. Gamble, and G. Burt, "Modelling a reversible solid oxide fuel cell to be used as a storage device within ac power networks," in *5th IET International Conference on Power Electronics, Machines and Drives (PEMD 2010)*, pp. 1–6, April 2010.

[50] P. Kazempoor and R. Braun, "Model validation and performance analysis of regenerative solid oxide cells: Electrolytic operation," *International Journal of Hydrogen Energy*, vol. 39, no. 6, pp. 2669 – 2684, 2014.

[51] L. Sun, G. Wu, Y. Xue, J. Shen, D. Li, and K. Y. Lee, "Coordinated control strategies for fuel cell power plant in a microgrid," *IEEE Transactions on Energy Conversion*, vol. 33, pp. 1–9, March 2018.

[52] L. Sun, D. Li, G. Wu, K. Y. Lee, and Y. Xue, "A practical compound controller design for solid oxide fuel cells," *IFAC-PapersOnLine*, vol. 48, no. 30, pp. 445 – 449, 2015. 9th IFAC Symposium on Control of Power and Energy Systems CPES 2015.

[53] Y. Li, J. Shen, and J. Lu, "Constrained model predictive control of a solid oxide fuel cell based on genetic optimization," *Journal of Power Sources*, vol. 196, no. 14, pp. 5873 – 5880, 2011.

[54] K. Sedghisigarchi and A. Feliachi, "Dynamic and transient analysis of power distribution systems with fuel cells-part i: fuel-cell dynamic model," *IEEE Transactions on Energy Conversion*, vol. 19, pp. 423–428, June 2004.

[55] B. Huang, Y. Qi, and M. Murshed, "Solid oxide fuel cell: Perspective of dynamic modeling and control," *Journal of Process Control*, vol. 21, no. 10, pp. 1426 – 1437, 2011.

[56] S. Chan, K. Khor, and Z. Xia, "A complete polarization model of a solid oxide fuel cell and its sensitivity to the change of cell component thickness," *Journal of Power Sources*, vol. 93, no. 1, pp. 130 – 140, 2001.

[57] Y. Patcharavorachot, A. Arpornwichanop, and A. Chuachuensuk, "Electrochemical study of a planar solid oxide fuel cell: Role of support structures," *Journal of Power Sources*, vol. 177, no. 2, pp. 254 – 261, 2008.

[58] M. Ni, M. K. H. Leung, and D. Y. C. Leung, "An electrochemical model of a solid oxide steam electrolyzer for hydrogen production," *Chemical Engineering and Technology*, vol. 29, pp. 636–642, 5 2006.

[59] B. Poling, J. Prausnitz, and J. O'Connell, *The Properties of Gases and Liquids*. 11 2000.

[60] P. Mottaghizadeh, S. Santhanam, M. P. Heddrich, K. A. Friedrich, and F. Rinaldi, "Process modeling of a reversible solid oxide cell (r-soc) energy storage system utilizing commercially available soc reactor," *Energy Conversion and Management*, vol. 142, pp. 477 – 493, 2017.

[61] X. Wang, B. Huang, and T. Chen, "Data-driven predictive control for solid oxide fuel cells," *Journal of Process Control*, vol. 17, no. 2, pp. 103 – 114, 2007.

[62] A. Yahya, D. Ferrero, H. Dhahri, P. Leone, K. Slimi, and M. Santarelli, "Electrochemical performance of solid oxide fuel cell: Experimental study and calibrated model," *Energy*, vol. 142, pp. 932 – 943, 2018.

[63] K. Tseronis, I. Bonis, I. Kookos, and C. Theodoropoulos, "Parametric and transient analysis of non-isothermal, planar solid oxide fuel cells," *International Journal of Hydrogen Energy*, vol. 37, no. 1, pp. 530 – 547, 2012. 11th China Hydrogen Energy Conference.

[64] S. Campanari and P. Iora, "Definition and sensitivity analysis of a finite volume sofc model for a tubular cell geometry," *Journal of Power Sources*, vol. 132, no. 1, pp. 113 – 126, 2004.

[65] S. Campanari, "Thermodynamic model and parametric analysis of a tubular sofc module," *Journal of Power Sources*, vol. 92, no. 1, pp. 26 – 34, 2001.

[66] A. M. Murshed, B. Huang, and K. Nandakumar, "Control relevant modeling of planer solid oxide fuel cell system," *Journal of Power Sources*, vol. 163, no. 2, pp. 830 – 845, 2007.

[67] E. Reznicek and R. J. Braun, "Techno-economic and off-design analysis of stand-alone, distributed-scale reversible solid oxide cell energy storage systems," *Energy Conversion and Management*, vol. 175, pp. 263 – 277, 2018.

[68] B. Chen, Y. S. Hajimolana, V. Venkataraman, M. Ni, and P. Aravind, "Integration of reversible solid oxide cells with methane synthesis (resoc-ms) in grid stabilization: A dynamic investigation," *Applied Energy*, vol. 250, pp. 558 – 567, 2019.

[69] F. Zhao and A. V. Virkar, "Dependence of polarization in anode-supported solid oxide fuel cells on various cell parameters," *Journal of Power Sources*, vol. 141, no. 1, pp. 79 – 95, 2005.

[70] W. Bujalski, C. M. Dikwal, and K. Kendall, "Cycling of three solid oxide fuel cell types," *Journal of Power Sources*, vol. 171, no. 1, pp. 96 – 100, 2007. Scientific Advances in Fuel Cell Systems, Turin, Italy, 13-14 September 2006.

[71] R. Kandepu, L. Imsland, B. A. Foss, C. Stiller, B. Thorud, and O. Bolland, "Modeling and control of a SOFC-GT-based autonomous power system," *Energy*, vol. 32, no. 4, pp. 406 – 417, 2007.

[72] S. A. Taher and S. Mansouri, "Optimal pi controller design for active power in grid-connected sofc dg system," *International Journal of Electrical Power & Energy Systems*, vol. 60, pp. 268 – 274, 2014.

[73] Y. H. Li, S. S. Choi, and S. Rajakaruna, "An analysis of the control and operation of a solid oxide fuel-cell power plant in an isolated system," *IEEE Transactions on Energy Conversion*, vol. 20, pp. 381–387, June 2005.

[74] A. Chaisantikulwat, C. Diaz-Goano, and E. S. Meadows, "Dynamic modelling and control of planar anode-supported solid oxide fuel cell," *Computers & Chemical Engineering*, vol. 32, pp. 2365–2381, 2008.

[75] X. Zhang, S. Chan, H. Ho, J. Li, G. Li, and Z. Feng, "Nonlinear model predictive control based on the moving horizon state estimation for the solid oxide fuel cell," *International Journal of Hydrogen Energy*, vol. 33, no. 9, pp. 2355 – 2366, 2008.

[76] M. Sorrentino, C. Pianese, and Y. G. Guezennec, "A hierarchical modeling approach to the simulation and control of planar solid oxide fuel cells," *Journal of Power Sources*, vol. 180, no. 1, pp. 380 – 392, 2008.

[77] A. Sendjaja and V. Kariwala, "Decentralized control of solid oxide fuel cells," *IEEE Trans. Industrial Informatics*, vol. 7, pp. 163–170, 05 2011.

[78] Y. Lindberg, "A comparison between mpc and pid controllers for education and steam reformers," 2017.

[79] J. Ren, S. Gamble, A. J. Roscoe, and G. Burt, "Modelling interaction between solid oxide fuel cell, inverters and ac power networks," in *2009 44th International Universities Power Engineering Conference (UPEC)*, pp. 1–5, Sep. 2009.

[80] X. Lin, K. Sun, J. Lin, Z. Zhang, and W. Kong, "A multi-port bidirectional power conversion system for reversible solid oxide fuel cell applications," in *2018 International Power Electronics Conference (IPEC-Niigata 2018 -ECCE Asia)*, pp. 3460–3465, May 2018.

[81] C. Stiller, B. Thorud, O. Bolland, R. Kandepu, and L. Imsland, "Control strategy for a solid oxide fuel cell and gas turbine hybrid system," *Journal of Power Sources*, vol. 158, no. 1, pp. 303 – 315, 2006.

[82] S. A. Taher and S. Mansouri, "Optimal PI controller design for active power in grid-connected SOFC DG system," *International Journal of Electrical Power and Energy Systems*, vol. 60, pp. 268 – 274, 2014.

[83] S. A. Hajimolana and M. Soroush, "Dynamics and control of a tubular solid-oxide fuel cell," *Industrial & Engineering Chemistry Research*, vol. 48, no. 13, pp. 6112–6125, 2009.

[84] M. L. Ferrari, "Solid oxide fuel cell hybrid system: Control strategy for stand-alone configurations," *Journal of Power Sources*, vol. 196, no. 5, pp. 2682 – 2690, 2011.

[85] A. Gebregergis and P. Pillay, "The development of solid oxide fuel cell (sofc) emulator," in *2007 IEEE Power Electronics Specialists Conference*, pp. 1232–1238, June 2007.

[86] M. Carre, R. Brandenburger, W. Friede, F. Lapicque, U. Limbeck, and P. da Silva, "Feed-forward control of a solid oxide fuel cell system with anode offgas recycle," *Journal of Power Sources*, vol. 282, pp. 498 – 510, 2015.

[87] H. Camblong, S. Baudoin, I. Vechiu, and A. Etxeberria, "Design of a sofc/gt/scs hybrid power system to supply a rural isolated microgrid," *Energy Conversion and Management*, vol. 117, pp. 12 – 20, 2016.

[88] P. Song, Y. Zhou, Y. Zhang, W. Liu, X. Wang, H. Chen, and X. Le, "The study on the role of reversible solid oxide cell (rsoc) in sector-coupling of energy systems," in *2018 International Conference on Power System Technology (POWERCON)*, pp. 2210–2215, Nov 2018.

[89] R. Ma, F. Gao, E. Breaz, Y. Huangfu, and P. Briois, "Multidimensional reversible solid oxide fuel cell modeling for embedded applications," *IEEE Transactions on Energy Conversion*, vol. 33, pp. 692–701, June 2018.

[90] K. Wei, Q. Keqing, L. Xiang, S. Kai, M. Shujun, and Z. You, "Loss comparison of two bidirectional isolated dc/dc converters for reversible solid oxide fuel cell systems," in *2018 IEEE International Power Electronics and Application Conference and Exposition (PEAC)*, pp. 1–6, Nov 2018.

[91] L. Barelli, G. Bidini, G. Cinti, and A. Ottaviano, "Study of sofc-soe transition on a rsofc stack," *International Journal of Hydrogen Energy*, vol. 42, no. 41, pp. 26037 – 26047, 2017.

[92] S. Srikanth, M. Heddrich, S. Gupta, and K. Friedrich, "Transient reversible solid oxide cell reactor operation: An experimentally validated modeling and analysis," *Applied Energy*, vol. 232, pp. 473 – 488, 2018.

[93] L. Zhang, X. Li, J. Jiang, S. Li, J. Yang, and J. Li, "Dynamic modeling and analysis of a 5-kw solid oxide fuel cell system from the perspectives of cooperative control of thermal safety and high efficiency," *International Journal of Hydrogen Energy*, vol. 40, no. 1, pp. 456 – 476, 2015.

[94] W. Qi, J. Liu, and P. D. Christofides, "A distributed control framework for smart grid development: Energy/water system optimal operation and electric grid integration," *Journal of Process Control*, vol. 21, no. 10, pp. 1504 – 1516, 2011.

[95] X.-J. Wu, X.-J. Zhu, G.-Y. Cao, and H.-Y. Tu, "Nonlinear modeling of a sofc stack based on anfis identification," *Simulation Modelling Practice and Theory*, vol. 16, no. 4, pp. 399 – 409, 2008.

[96] F. A. Rolf Findeisen, "An introduction to nonlinear model predictive control," *Allgower*, 2007.

[97] A. Bemporad, N. L. Ricker, and J. G. Owen, "Model predictive control - new tools for design and evaluation," in *Proceedings of the 2004 American Control Conference*, vol. 6, pp. 5622–5627 vol.6, June 2004.

[98] "Matlab optimization problem." https://nl.mathworks.com/help/mpc/ug/optimization-problem.html. Accessed: 2019-10-10.

[99] M. H. Weik, *Nyquist theorem*, pp. 1127–1127. Boston, MA: Springer US, 2001.

[100] C. A. Vincent, "2 - theoretical background," in *Modern Batteries (Second Edition)* (C. Vincent and B. Scrosati, eds.), pp. 18 – 64, Oxford: Butterworth-Heinemann, second edition ed., 1997.

[101] "Simulink simplified model of a small scale micro-grid." https://nl.mathworks.com/help/physmod/sps/examples/simplified-model-of-a-small-scale-micro-grid.html. Accessed: 2019-10-10.

[102] C. Wendel, P. Kazempoor, and R. Braun, "Novel electrical energy storage system based on reversible solid oxide cells: System design and operating conditions," *Journal of Power Sources*, vol. 276, pp. 133 – 144, 2015.

Glossary

List of Acronyms

RSOFC	reversible solid oxide fuel cell
SOFC	solid oxide fuel cell
SOEC	solid oxide electrolyser cell
PEMFC	proton-exchange membrane fuel cell
PAFC	phosphoric acid fuel cell
MCFC	molten carbonate fuel cell
DMFC	mirect methanol fuel cell
AFC	alkaline fuel cell
CHP	combined heat and power
PCU	power conditioning units
THD	total harmonic distortion
IGBT	insulated-gate bipolar transistor
CB-PWM	carrier based PWM
SV-PWM	space vector PWM
PCBT	pulverised coal boiler turbine
PV	photo-voltaic
FCFI	fuel cell follows inverter
IFFC	inverter follows fuel cell
AC	Alternating Current

DC Direct current

NiYSZ nickel and yttrium stabilised zirconia